

N 84 - 3433 1

DOE/NASA/0324-1
NASA CR-174728

High Temperature Ceramic Interface Study

L.J. Lindberg
Garrett Turbine Engine Company
A Division of The Garrett Corporation

August 1984

Prepared for
NATIONAL AERONAUTICS AND SPACE ADMINISTRATION
Lewis Research Center
Under Contract DEN 3-324

for
U.S. DEPARTMENT OF ENERGY
Conservation and Renewable Energy
Office of Vehicle and Engine R&D

NOTICE

This report was prepared to document work sponsored by the United States Government. Neither the United States nor its agent, the United States Department of Energy, nor any Federal employees, nor any of their contractors, subcontractors or their employees, makes any warranty, express or implied, or assumes any legal liability or responsibility for the accuracy, completeness, or usefulness of any information, apparatus, product or process disclosed, or represents that its use would not infringe privately owned rights.

DOE/NASA/0324-1
NASA CR-174728

High Temperature Ceramic Interface Study

L.J. Lindberg
Garrett Turbine Engine Company
A Division of The Garrett Corporation

August 1984

Prepared for
National Aeronautics and Space Administration
Lewis Research Center
Cleveland, Ohio 44135
Under Contract DEN 3-324

for
U.S. DEPARTMENT OF ENERGY
Conservation and Renewable Energy
Office of Vehicle and Engine R&D
Washington, D.C. 20545
Under Interagency Agreement DE-A101-80CS50194

TABLE OF CONTENTS

	<u>Page</u>
1.0 SUMMARY	1
2.0 INTRODUCTION	3
3.0 TECHNICAL PROGRESS SUMMARY	9
3.1 Baseline Flexure Testing	9
3.2 Microstructural Examination of TTZ	17
3.3 Stress Rupture Testing	19
3.4 Contact Stress Testing	27
4.0 CONCLUSIONS	49
REFERENCES	109

1.0 SUMMARY

Monolithic SiC and Si₃N₄ are susceptible to contact stress damage at static and sliding interfaces.

The objective of this study program was to evaluate transformation-toughened zirconia (TTZ) under realistic contact conditions. Measurements of coefficient of friction and material strength retention as a function of normal load, contact geometry and temperature was accomplished for sliding contact conditions. Material characteristics such as baseline room temperature and elevated temperature flexure strength, and stress rupture properties, also were measured.

Four TTZ materials were evaluated in this study. The materials evaluated included:

- o Nilsen TS Grade (thermal shock resistant) MgO stabilized TTZ
- o NGK Z-191 Y₂O₃ stabilized TTZ
- o Coors TT-ZrO₂ MgO stabilized TTZ
- o Feldmühle TTZ MgO stabilized TTZ

Contact stress tests were conducted at normal loads ranging from 0.455 to 22.7 kg (1 to 50 pounds) at temperatures ranging from room temperature to 1204°C (2200°F). Static and dynamic friction were measured as a function of temperature.

Flexural strength measurements after these tests determined that the contact stress exposure did not reduce the strength of TTZ at contact loads of 0.455, 4.55, and 11.3 kg (1, 10, and 25 pounds). Prior testing with SiC and Si₃N₄ materials resulted in a substantial strength reduction at loads of only 4.55 and 11.3 kg (10 and 25 pounds).

Baseline material flexure strength was established and the stress rupture capability of TTZ was evaluated. Stress rupture tests have determined that TTZ materials are susceptible to deformation due to creep and that aging of TTZ materials at elevated temperatures results in a reduction of material strength.

These evaluations will provide guidelines for material selection, contact design, load limitations, temperature limitations, and further development needs for ceramics for advanced heavy duty diesel applications.

2.0 INTRODUCTION

Ceramic materials have the potential for substantially improving the performance of heat engines by permitting uncooled operation at increased temperatures. In addition, ceramics potentially have lower cost and are lighter in weight.

Transformation-toughened zirconia (TTZ) has been selected as one of the current materials most likely to benefit advanced heavy diesel engines (ref. 1, 2). Zirconia has a low thermal conductivity that makes it a very good insulator. By fabricating the piston cap, cylinder head, cylinder liner, and exhaust ports from TTZ, thermal energy normally lost to cooling water and exhaust gas can be recycled and converted to useful power through turbocompounding. Turbocompounding is accomplished by compressing the engine inlet air with a turbocharger. Combustion occurs in the insulated combustion chamber, and useful energy is extracted from the pistons. The high-temperature, high-pressure exhaust gas is expanded through two high-temperature turbines. The first turbine is used to drive the turbocharger. The second turbine is connected by gears to the engine crankshaft to further increase the useful power output of the engine. Turbocompounding increases engine efficiency and power, and eliminates the water cooling system. Another advantage of TTZ is that the thermal expansion coefficient is very close to that of steel. The close expansion match will make TTZ easier to interface with metallic components and minimizes contact and thermal stresses. The transformation toughening provides much higher toughness than is available in typical ceramics and should make this material less sensitive to contact stress damage. Diesel engine manufacturers as well as companies that manufacture TTZ have been working together to successfully introduce TTZ into diesel engines.

In recent years much work has been done on introducing ceramic materials, such as Si_3N_4 and SiC in gas turbine engines (ref. 3). Because of their brittle nature, contact stresses at ceramic-to-ceramic and ceramic-to-metal interfaces cause unique design problems. High localized stresses in contact regions do not redistribute in ceramics as in metals. The use of finite-element analysis computer techniques including zoom modeling has been used to calculate the complex state-of-stress at contact interfaces (ref. 4, 5). The analysis has shown that when ceramics are in contact and a tangential load component is added (such as results during sliding), a sharp tensile stress spike is present at the trailing edge of the contact (Figure 1) (ref. 6, 7). Some of the key parameters affecting the magnitude of the tensile stress spike are the contact load, the coefficient of friction, and geometry of the contact interface (ref. 8).

Contact stress damage resulting from the tensile stress spike has caused ceramic turbine engine components to fracture

unpredictably and prematurely (ref. 3). Much testing has been performed using reaction bonded Si_3N_4 , hot-pressed Si_3N_4 and sintered alpha SiC to determine experimentally the threshold coefficients of friction, temperatures and normal contact loads that lead to contact stress damage in these materials (ref. 9, 10).

Determining the contact stress behavior of TTZ is an important and necessary task if TTZ is to be introduced in advanced heat engines. The following paragraphs describe the evolution of pure zirconium oxide to the strong and tough TTZ materials considered for heat engine use.

Zirconia

Pure zirconia (ZrO_2) exhibits the following transformations between room temperatures and its melting point:

1170°C (2138°F)	2370°C (4298°F)	2680°C (4856°F)	
monoclinic	≡ tetragonal	≡ cubic	≡ liquid

The cubic phase is stable from 2370°C (4298°F) to the melting point of 2680 ±15°C (4856 ±27°F). This phase is identified by Smith and Cline (ref. 11) by high-temperature X-ray diffraction. The cubic phase has a fluorite-type crystal structure in which each Zr atom is coordinated by eight equidistant oxygen atoms and each oxygen atom is tetrahedrally coordinated by four zirconium atoms.

From 1170 to 2370°C (2138 to 4298°F) the stable phase is tetragonal in structure. Teufer (ref. 12) has shown that each Zr atom is surrounded by eight oxygen atoms, four at a distance of 0.2455 nm and four at 0.2065 nm.

The monoclinic phase is stable below 1170°C (2138°F). The crystal structure of monoclinic ZrO_2 was analyzed by X-ray diffraction by McCullough and Trueblood (ref. 13), Smith and Newkirk (ref. 14) and others. The structure has sevenfold coordination of Zr atoms with various bond lengths and bond angles, triangular coordinated $\text{O}_I\text{-Zr}_3$ and tetrahedral coordinated $\text{O}_{II}\text{-Zr}_4$, and layers of Zr atoms parallel to the (100) planes separated by layers of O atoms.

The monoclinic ≡ tetragonal transformation was first detected in 1929 by Ruff and Ebert (ref. 15) using high-temperature X-ray diffraction. A major problem associated with pure ZrO_2 is

the three-percent volume expansion that occurs when cooling through the tetragonal to monoclinic transformation at 1170°C (2138°F). This volume expansion leads to extensive macrocracking which causes the zirconia to crumble. Wolten (ref. 16) suggested that the tetragonal to monoclinic transformation was martensitic, for the following reasons:

- o The high-temperature tetragonal phase cannot be quenched to room temperature
- o The thermal expansion of monoclinic ZrO_2 is strongly anisotropic. The \bar{b} axis exhibits negligible expansion and the \bar{a} and \bar{c} axis exhibit substantial expansion
- o The transformation is athermal. The transformation does not take place at a fixed temperature but over a range of temperatures
- o The transformation exhibits a large thermal hysteresis. The forward transition occurs at 1170°C (2138°F) and the reverse at between 850 to 1000°C (1562 to 1832°F)
- o The transformation occurs at a velocity approaching the speed of sound

The disastrous effects of the volume expansion in pure zirconia can be avoided by doping the zirconia with additions of CaO , MgO , or Y_2O_3 . These additions stabilize ZrO_2 in its high-temperature form, the cubic crystal structure. This material is known as fully stabilized zirconia (FSZ). FSZ can be cycled from room temperature to its melting point without any destructive phase transformations. Fully stabilized zirconia has a coarse grain structure, low strength, low toughness, and a high thermal expansion coefficient.

Many problems associated with pure and fully stabilized zirconia can be eliminated by partially stabilizing the zirconia with additions of CaO , MgO , or Y_2O_3 . Partially stabilized zirconia (PSZ) has a lower thermal expansion coefficient, making it more resistant to thermal shock than fully stabilized zirconia. Also, PSZ has a higher strength and toughness than FSZ. Microstructural evaluation of PSZ has shown the major phase to be cubic ZrO_2 solid solution with monoclinic or tetragonal ZrO_2 as the minor precipitate phase (ref. 17 through 20). The tetragonal or monoclinic phase may precipitate at the grain boundaries or within the cubic matrix grains depending on the processing and heat treatments. With correct processing the tetragonal precipitates in PSZ are held (in a metastable condition) within the cubic matrix at room temperature. Though normally the martensitic transformation from tetragonal to monoclinic occurs at 1100°C

(2012^{OF}). The metastable tetragonal phase in the cubic matrix will transform to the monoclinic phase with the application of stress. The importance of this stress induced transformation on toughening of PSZ was first noted by Garvie (ref. 21). Porter (ref. 17) demonstrated this by showing that all precipitate particles within several microns of a crack were monoclinic and all others remained tetragonal. The stress near the crack tip caused the precipitates to transform from tetragonal to monoclinic, which stopped crack propagation. The stress induced martensitic transformation of metastable tetragonal particles to the stable monoclinic phase is the mechanism which stops crack propagation. This transformation strengthens and toughens the PSZ. PSZ with the metastable tetragonal phase became known as transformation-toughened zirconia (TTZ).

One or more of the following mechanisms are believed to contribute the high toughness and strength of TTZ materials.

The mechanisms are:

- o The advancing crack front is deflected by interaction with the compressive stress fields surrounding the transformed areas
- o Transformation induced microcracking leads to crack branching and an increase in energy necessary to continue crack propagation
- o Energy absorption by the tetragonal to monoclinic phase transformation process itself
- o The tetragonal to monoclinic transformation places the material at the crack tip in compression, therefore, requiring higher applied tensile stresses for crack propagation

Program Scope

The objective of this study program was to evaluate TTZ under realistic contact conditions. Measurements of coefficient of friction and material strength retention as a function of normal load, contact geometry and temperature was accomplished for sliding contact conditions. Material characteristics such as baseline room temperature and elevated temperature flexure strength, and stress rupture properties, also were measured. These evaluations will provide guidelines for material selection, contact design, load limitations, temperature limitations, and further development needs for ceramics for advanced heavy duty diesel applications.

Four TTZ materials were evaluated in this study. The materials evaluated included:

- o Nilsen TS grade (thermal shock resistant) MgO stabilized TTZ
- o NGK Z-191 Y₂O₃ stabilized TTZ
- o Coors TT-ZrO₂ MgO stabilized TTZ
- o Feldmühle TTZ MgO stabilized TTZ

3.0 TECHNICAL PROGRESS SUMMARY

3.1 Baseline Flexure Testing

3.1.1 Baseline Flexure Testing Procedure

Sufficient specimens of the four transformation-toughened zirconia (TTZ) materials were procured to conduct the study.

The baseline four-point flexure strength of all four TTZ materials was measured. The quantities of specimens tested and test temperatures are listed in Table I. The test specimen size was 0.3175 x 0.627 x 4.90 cm (0.125 x 0.247 x 1.930 inches). A self-aligning metal four-point flexure fixture with an outer span of 3.81 cm (1.5 inches) and an inner span of 1.91 cm (0.75 inch) was used for room temperature testing. A silicon carbide (SiC) test fixture of the same dimensions was used for the elevated temperature flexure testing. An Instron test machine was used at a crosshead speed of 0.05 cm (0.02 inch) per minute to apply the load.

TABLE I. BASELINE STRENGTH TEST MATRIX

Material	Temperature °C (°F)				
	Room Temperature	760 (1400)	982 (1800)	1093 (2000)	1204 (2200)
Coors TTZ	10	10	10	10	10
Nilsen TTZ	10	5	5	5	5
NGK TTZ	10	5	5	5	5
Feldmuhle TTZ	5	5	5	5	5

3.1.2 Baseline Flexure Strength Results

Nilsen TTZ. - The baseline flexure strength of Nilsen's TTZ is summarized in Table II in terms of average strength, characteristic strength, and Weibull modulus. It should be recognized that 5 or 10 data points are insufficient to determine an accurate Weibull slope. Therefore, the Weibull slopes reported can be considered only as rough approximations.

The fracture surfaces of the specimens were visually inspected at 10X to 40X magnification. Fracture origins were

TABLE II. BASELINE FLEXURE STRENGTH SUMMARY OF NILSEN TTZ

Parameters	Temperature °C (°F)				
	Room Temperature	760 (1400)	982 (1800)	1093 (2000)	1204 (2200)
Mean Flexure Strength, MPa (ksi)	604.0 (87.6)	368.2 (53.4)	329.6 (47.8)	287.5 (41.7)	254.4 (36.9)
Standard Deviation, MPa (ksi)	29.0 (4.2)	13.8 (2.0)	44.1 (6.4)	39.3 (5.7)	13.8 (2.0)
Characteristic Flexure Strength, MPa (ksi)	617.8 (89.6)	375.1 (54.4)	349.6 (50.7)	306.8 (44.5)	264.8 (38.4)
Weibull Modulus	21.6	27.5	7.4	6.8	18.4
Data Points	9	5	5	5	5

identified to determine the types of flaws distributed through the material and to correlate the fracture strength to the fracture initiating flaws (Table III). Scanning electron microscopy (SEM) was performed on several specimens that had fractured at the tensile face. At the higher magnifications, small irregularly-shaped pores open to the surface are visible as shown in Figures 2 through 4. This type of flaw appears to be typical of the majority of Nilsen baseline fracture origins.

The mean flexure strength of baseline Nilsen TTZ versus temperature is shown graphically in Figure 5. Figures 6 and 7 include Weibull plots of individual data points for each temperature.

NGK Z-191 TTZ. - A summary of baseline flexure testing results on NGK Z-191 TTZ are tabulated in Table IV. The mean flexure strength is 993.5 MPa (144.1 ksi) at room temperature, 427.5 MPa (62 ksi) at 760°C (1400°F), 301.3 MPa (43.7 ksi) at 982°C (1800°F), 254.4 MPa (36.9 ksi) at 1093°C (2000°F), and 1020 MPa (14.8 ksi) at 1204°C (2200°F). The baseline flexure strengths are plotted as a function of temperature in Figure 8. Visual inspection of the fracture surfaces at 10X to 40X was performed and the fracture origins are listed in Table V. At room temperature the fractures appeared to originate from the tensile surface. No flaws could be detected visually. At 760 and 982°C (1400 and 1800°F) the predominant flaws are internal pores. At 1093 and 1204°C (2000 and 2200°F) most flaws appeared to originate at the test bar surface.

TABLE III. FLEXURE STRENGTH OF NILSEN TTZ

Specimen Number	Four-Point Flexure Strength, MPa (ksi)	Fracture Origin Identified by Visual Inspection (10X - 40X)
Room Temperature		
11873	630.2 (91.4)	Tensile Face (TF)
11874	550.9 (79.9)	Internal, near chamfer
11875	593.0 (86.0)	TF
11876	593.0 (86.0)	TF
11877	566.1 (82.1)	TF
11878	626.0 (90.8)	Missing, appears to be TF
11879	628.1 (91.1)	TF
11881	620.5 (90.0)	TF
11893	622.6 (90.3)	TF
760°F (1400°F)		
11882	374.4 (54.3)	TF
11883	353.0 (51.2)	TF
11884	358.5 (52.0)	TF
11885	368.2 (53.4)	TF
11886	387.5 (56.2)	TF
982°C (1800°F)		
11887	348.9 (50.6)	TF
11888	343.4 (49.8)	TF surface irregularity
11889	312.3 (45.3)	TF
11890	379.9 (55.1)	Missing, appears to be TF
11891	264.1 (38.3)	Internal, pore
1093°C (2000°F)		
11953	317.9 (46.1)	TF
11954	322.0 (46.7)	TF
11955	224.1 (32.5)	TF
11956	288.2 (41.8)	TF
11957	286.1 (41.5)	TF
1204°C (2200°F)		
11892	244.1 (35.4)	Internal, pore
11894	269.6 (39.1)	TF
11895	269.6 (39.1)	Internal, near TF
11896	264.8 (38.4)	TF
11897	244.1 (35.4)	TF

TABLE IV. BASELINE FLEXURE STRENGTH SUMMARY OF NGK TTZ

Parameters	Temperature °C (°F)				
	Room Temperature	760 (1400)	982 (1800)	1093 (2000)	1204 (2200)
Mean Flexure Strength, MPa (ksi)	993.5 (144.1)	427.5 (62.0)	301.3 (43.7)	254.4 (36.9)	102.0 (14.8)
Standard Deviation, MPa (ksi)	75.8 (11.0)	37.9 (5.5)	31.7 (4.6)	51.0 (7.4)	6.9 (1.0)
Characteristic Flexure Strength, MPa (ksi)	1030.1 (149.4)	445.4 (64.6)	315.8 (45.8)	277.2 (40.2)	105.5 (15.3)
Weibull Modulus	13.5	10.8	9.6	4.9	15.0
Data Points	10	4	5	5	5

Typical NGK baseline flexure fracture origins were characterized by SEM. The predominant mode of failure was caused by internal clusters of small irregular-shaped pores or larger single irregular-shaped pores. Figures 9 through 11 reveal that room temperature, 760°C (1400°F), and 982°C (1800°F) fractures originated at porosity. As shown in Figures 12 and 13, 1093°C (2000°F) and 1204°C (2200°F) fractures originated at porosity, and evidence of slow crack growth was visible surrounding the fracture origins.

Weibull plots of the baseline flexure data are presented in Figures 14 and 15.

Coors TTZ. - Baseline flexure testing of Coors magnesia stabilized TTZ is summarized in Table VI. The flexure strength at room temperature is 446.1 MPa (64.7 ksi); this drops to 199.3 MPa (28.9 ksi) at 760°C (1400°F) and gradually drops to 130.3 MPa (18.9 ksi) at 1204°C (2200°F) (Figure 16). The individual test bar strengths and fracture origins are listed in Table VII. Figures 17 and 18 display the Weibull plots for Coors baseline flexure strength data. Visual inspection of the fracture surfaces under a 10 to 40X optical microscope revealed that a majority of the fractures appeared to originate at the chamfer and tensile face of the test bar. Coors has many large pores but only a few specimens failed at these pores.

Scanning electron microscopy (SEM) examination of Coors TTZ baseline flexure specimens was performed to characterize typical fracture initiating flaws. A 760°C (1400°F) fracture, which

TABLE V. FLEXURE STRENGTH OF NGK TTZ

Specimen Number	Four-Point Flexure Strength, MPa (ksi)	Fracture Origin Identified by Visual Inspection (10X - 40X)
Room Temperature		
12384	1034.9 (150.1)	Tensile face (TF)
12385	1065.2 (154.5)	Missing, appears to be TF
12386	1043.2 (151.3)	2 Origins, TF and chamfer
12387	944.6 (137.0)	TF
12388	902.5 (130.9)	TF
12389	1014.9 (147.2)	TF
12390	904.6 (131.2)	Missing, appears to be TF
12391	884.6 (128.3)	TF
12392	1075.6 (156.0)	TF
12393	1065.2 (154.5)	Missing, appears to be TF
760°C (1400°F)		
12394	452.3 (65.6)	Internal pore
12395	134.4 (19.5)*	TF
12396	402.0 (58.3)	Subsurface pore near TF
12397	466.1 (67.6)	TF
12398	388.2 (56.3)	Internal pore
982°C (1800°F)		
12399	315.8 (45.8)	Internal pore
12400	293.7 (42.6)	Pore at chamfer
12401	347.5 (50.4)	Missing
12402	285.4 (41.4)	Missing
12403	263.4 (38.2)	Internal pore
1093°C (2000°F)		
12404	257.2 (37.3)	Missing
12405	337.2 (48.9)	Chamfer linear pore, SCG**
12406	215.1 (31.2)	TF linear pore, SCG
12407	208.9 (30.3)	TF linear pore, SCG
12408	255.1 (37.0)	TF linear pore, SCG
1204°C (2200°F)		
12409	98.6 (14.3)	Chamfer, SCG
12410	106.2 (15.4)	Chamfer, SCG
12411	108.2 (15.7)	Chamfer, SCG
12412	106.2 (15.4)	Chamfer, SCG
12413	92.4 (13.4)	Chamfer, SCG

* Data Point Omitted

** Slow Crack Growth

originated at the chamfer, is shown in Figure 19. A fracture which originated near the tensile face at a subsurface cluster of porosity is shown in Figure 20. These two fracture origins are typical of the majority of Coors fracture origins. Specimen 13106 baseline flexure tested at 1204°C (2200°F), fractured through a large irregular-shaped internal pore (Figure 21).

TABLE VI. BASELINE FLEXURE STRENGTH SUMMARY OF COORS TTZ

Parameters	Temperature °C (°F)				
	Room Temperature	760 (1400)	982 (1800)	1093 (2000)	1204 (2200)
Mean Flexure Strength, MPa (ksi)	446.1 (64.7)	199.3 (28.9)	143.9 (20.8)	144.8 (21.0)	130.3 (18.9)
Standard Deviation, MPa (ksi)	37.2 (5.4)	16.5 (2.4)	14.5 (2.1)	33.8 (4.9)	19.3 (2.8)
Characteristic Flexure Strength, MPa (ksi)	463.3 (67.2)	207.5 (30.1)	149.6 (21.7)	159.3 (23.1)	138.6 (20.1)
Weibull Modulus	12.7	12.3	10.5	4.5	7.4
Data Points	10	10	10	10	10

Feldmühle TTZ. - Baseline strength tests were conducted on Feldmühle TTZ at room temperature, 760, 982, 1093, and 1204°C (1400, 1800, 2000, and 2200°F).

Table VIII and Figure 22 summarize the flexure test results. Flexure strength at room temperature is 377.8 MPa (54.8 ksi), which reduces to 192.4 MPa (27.9 ksi) at 760°C (1400°F) and gradually reduces to 139.3 MPa (20.2 ksi) at 1204°C (2200°F).

Weibull plots for the baseline strength are shown in Figures 23 and 24.

Visual inspection of the fracture surfaces was performed to determine the predominant mode of failure (Table IX). No material flaws could be detected by visual inspection at 10 to 40X. All fractures appeared to originate from the surface at the chamfer, or tensile face.

Typical baseline flexure fracture surfaces are shown in Figures 25 and 26. The exact location of the Feldmühle TTZ frac-

TABLE VII. FLEXURE STRENGTH OF COORS TTZ

Specimen Number	Four-Point Flexure Strength, MPa (ksi)	Fracture Origin Identified by Visual Inspection (10X - 40X)
Room Temperature		
13059	402.7 (58.4)	Internal pore
13060	470.2 (68.2)	Chamfer
13061	484.7 (70.3)	Chamfer
13062	454.4 (65.9)	Tensile Face (TF)
13063	442.6 (64.2)	TF
13064	402.7 (58.4)	Internal pore
13065	496.4 (72.0)	Chamfer
13066	478.5 (69.4)	Chamfer
13067	440.6 (63.9)	TF
13068	390.2 (56.6)	TF
760°C (1400°F)		
13069	206.2 (29.9)	Chamfer
13070	188.2 (27.3)	TF
13071	177.9 (25.8)	Chamfer
13072	199.9 (29.0)	Chamfer
13073	188.2 (27.3)	Chamfer
13074	194.4 (28.2)	Chamfer
13075	199.9 (29.0)	Chamfer
13076	192.4 (27.9)	Chamfer
13077	239.9 (34.8)	Chamfer
13078	208.2 (30.2)	Chamfer
982°C (1800°F)		
13079	146.2 (21.2)	Chamfer
13080	137.9 (20.0)	Chamfer
13081	142.0 (20.6)	TF
13082	144.1 (20.9)	Chamfer
13083	154.4 (22.4)	Chamfer
13084	126.2 (18.3)	Chamfer
13085	150.3 (21.8)	Chamfer
13086	174.4 (25.3)	Chamfer
13087	132.4 (19.2)	TF
13088	124.1 (18.0)	Chamfer
1093°C (2000°F)		
13089	214.4 (31.1)	TF
13090	115.8 (16.8)	Chamfer
13091	132.4 (19.2)	Chamfer

TABLE VII. FLEXURE STRENGTH OF COORS TTZ (Contd)

Specimen Number	Four-Point Flexure Strength, MPa (ksi)	Fracture Origin Identified by Visual Inspection (10X - 40X)
1093°C (2000°F) 13092 13093 13094 13095 13096 13097 13098	120.0 (17.4) 134.4 (19.5) 128.2 (18.6) 142.0 (20.6) 120.0 (17.4) 142.0 (20.6) 196.5 (28.5)	Chamfer Chamfer Chamfer Chamfer Chamfer Chamfer Chamfer
1204°C (2200°F) 13099 13100 13101 13102 13103 13104 13105 13106 13107 13108	132.4 (19.2) 135.8 (19.7) 106.2 (15.4) 157.9 (22.9) 164.1 (23.8) 110.3 (16.0) 117.9 (17.1) 132.4 (19.2) 117.9 (17.1) 128.2 (18.6)	Chamfer Chamfer Chamfer Chamfer Chamfer Chamfer Chamfer Internal pore Chamfer Chamfer

TABLE VIII. BASELINE FOUR-POINT FLEXURE STRENGTH
SUMMARY OF FELDMÜHLE TTZ

Parameters	Temperature °C (°F)				
	Room Temperature	760 (1400)	982 (1800)	1093 (2000)	1204 (2200)
Mean Flexure Strength, MPa (ksi)	377.8 (54.8)	192.4 (27.9)	162.0 (23.5)	120.0 (17.4)	139.3 (20.2)
Standard Deviation, MPa (ksi)	28.3 (4.1)	27.6 (4.0)	23.4 (3.4)	6.9 (1.0)	23.4 (3.4)
Characteristic Flexure Strength, MPa (ksi)	391.6 (56.8)	205.5 (29.8)	173.1 (25.1)	123.4 (17.9)	150.3 (21.9)
Weibull Modulus	12.9	6.4	6.3	17.1	5.4
Data Points	5	4	4	5	4

ture origins are difficult to determine although the area where the fracture initiated is visible. Arrows point to the areas where the fractures originated.

3.2 Microstructural Examination of TTZ

A microstructural examination of as-received TTZ was performed. Photographs of the microstructures at 200X of Nilsen, Coors, and NGK TTZ are shown in Figure 27. Nilsen and Coors, both magnesia stabilized TTZ, have a large grain structure. The grain size ranges from 6 to 10 microns. The light area surrounding the grains of Nilsen material is reported (ref. 1) to be monoclinic phase. The yttria stabilized NGK material has a much finer (0.2 to 3 microns) grain structure.

Further microstructural examination was performed using the SEM. The microstructure of Nilsen TTZ at 2000X is shown in Figure 28. Visible in this photograph is the irregular shaped porosity as well as large grains typical of Nilsen TTZ. At 20,000X the grain boundary structure is visible. Energy dispersive X-ray (EDX) analysis identified the presence of zirconium and minor amounts of silicon. At 50,000X the individual tetragonal or monoclinic precipitates* embedded in the cubic stabilized zirconia matrix (ref. 1) are visible.

*The difference between tetragonal and monoclinic precipitates cannot be distinguished by SEM. Since the application of a stress can cause the tetragonal phase to spontaneously transform to monoclinic it is possible that transformation from tetragonal to monoclinic occurred during sample preparation.

TABLE IX. FLEXURE STRENGTH OF FELDMÜHLE TTZ

Specimen Number	Four-Point Flexure Strength, MPa (ksi)	Fracture Origin Identified by Visual Inspection (10X - 40X)
Room Temperature		
13791	352.3 (51.1)	Chamfer
13792	387.5 (56.2)	Tensile Face (TF)
13793	359.9 (52.2)	Chamfer
13794	366.1 (53.1)	TF
13795	422.0 (61.2)	Chamfer
760°C (1400°F)		
13796	187.5 (27.2)	Chamfer
13798	232.4 (33.7)	Chamfer
13799	172.4 (25.0)	Chamfer
13800	177.2 (25.7)	Chamfer
982°C (1800°F)		
13801	195.8 (28.4)	Chamfer
13803	148.9 (21.6)	Chamfer
13804	144.8 (21.0)	Chamfer
13805	157.2 (22.8)	Chamfer
1093°C (2000°F)		
13806	113.1 (16.4)	Chamfer
13807	121.3 (17.6)	Chamfer
13808	127.6 (18.5)	Chamfer
13809	125.5 (18.2)	Chamfer
13810	113.1 (16.4)	Chamfer
1204°C (2200°F)		
13811	146.9 (21.3)	Chamfer
13812	140.7 (20.4)	Chamfer
13813	162.0 (23.5)	Chamfer
13814	106.2 (15.4)	Chamfer

Figure 29 shows the typical microstructure of Coors TTZ. The tetragonal or monoclinic precipitates of Coors TTZ are visible in this 50,000X SEM photograph.

The microstructure of NGK TTZ is shown in Figure 30. Woods and Oda (ref. 2) have shown from X-ray diffraction that the major phases are tetragonal and cubic with a trace of monoclinic. The larger 1 to 3 μm grains are cubic and the smaller 0.2 to 0.5 μm grains are tetragonal in structure.

3.3 Stress Rupture Testing

3.3.1 Stress Rupture Test Procedure

Stress rupture tests were conducted using silicon carbide four-point flexure fixtures with an outer span of 3.81 cm (1.5 inches) and an inner span of 1.91 cm (0.75 inch). The ceramic specimen size was 0.3175 x 0.627 x 4.90 cm (0.125 x 0.247 x 1.930 inches).

Two types of stress rupture tests were conducted. Stepped stress rupture tests were initiated at a stress level approximately one-half the baseline flexure strength at the temperature of interest. The specimen was held at that stress level and temperature for 24 hours. If no failure occurred the stress level was increased by 68.9 MPa (10 ksi) while the temperature was held constant. This sequence was repeated until the specimen either deformed or fractured.

The second type of stress rupture test was conducted at a constant stress level and temperature for 500 hours. Subsequent to the stress rupture testing the specimens were broken in four-point flexure to measure the retained strength.

3.3.2 Stress Rupture Results

Nilsen TTZ. - Stepped stress rupture tests were conducted on Nilsen TS (thermal-shock resistant grade) specimens at constant temperatures of 760, 982, 1093, and 1204°C (1400, 1800, 2000, and 2200°F). Figure 31 shows the stepped stress rupture test data for Nilsen.

At 760°C (1400°F) the specimen failed at 344.7 MPa (50 ksi) after 5 hours. At 982°C (1800°F) and above, the specimens deformed but did not fracture. These tests were conducted to determine appropriate stress levels and temperatures for subsequent 500-hour stress rupture tests.

Temperatures of 982, 1038, and 1093°C (1800, 1900, and 2000°F) were selected at respective stress levels of 137.9,

103.4, and 103.4 MPa (20, 15, and 15 ksi) for the 500-hour stress rupture tests. On completion of the 500-hour tests all specimens had deformed under the load. Test results are summarized in Table X. The three stress rupture specimens were flexure tested at room temperature to measure retained strength after the 500-hour static exposure under stress. The specimens were tested in such a manner as to apply tensile stress to the concave side of the test bar. The retained strength after 500 hours at 982°C (1800°F) is 235.8 MPa (34.2 ksi), which dropped to 164.1 MPa (23.8 ksi) at 1038°C (1900°F), and to 135.1 MPa (19.6 ksi) at 1093°C (2000°F).

NGK TTZ. - Stepped stress rupture test results for NGK at 760, 871, 982, 1093, and 1204°C (1400, 1600, 1800, 2000, and 2200°F) are shown in Figure 32. Unlike the Nilsen TTZ, which deformed during stress rupture testing at the higher temperatures, the NGK specimens always fractured.

At 760°C (1400°F) the stepped stress rupture test was started at a load of 137.9 MPa (20 ksi). The load was increased every 24 hours until a stress level of 413.7 MPa (60 ksi) was attained. The specimen failed after 53 minutes at this load. At 871°C (1600°F) the specimen failed at 344.7 MPa (50 ksi) after 1.5 hours. This test was initially started at a 137.9 MPa (20 ksi) stress level. At 982 and 1093°C (1800 and 2000°F) both specimens failed at 137.9 MPa (20 ksi) after 7.3 hours and 10 minutes, respectively. At 1204°C (2200°F) the specimen failed after 15 minutes at 68.9 MPa (10 ksi).

Five-hundred hour stress rupture tests were conducted at 760, 871, and 982°C (1400, 1600, and 1800°F) at constant loads of 137.9, 137.9, and 68.9 MPa (20, 20, and 10 ksi), respectively. Results of these tests are reported in Table XI. Little deformation was detected at 760 and 871°C (1400 and 1600°F) but 0.76 mm (0.030 inch) was measured at 982°C (1800°F). Retained strength after stress rupture testing was measured and compared to the baseline room temperature strength. Strength reductions of 36.5, 57.7, and 64.5 percent after stress rupture testing at 760, 871, and 982°C (1400, 1600, and 1800°F), respectively, were measured.

Coors TTZ. - Stepped stress rupture results are shown in Figure 33. At 760°C (1400°F) the specimen was started at an initial stress level of 68.9 MPa (10 ksi); every 24 hours the level was increased until it failed at 206.8 MPa (30 ksi) after three minutes at load. At 982°C (1800°F) the specimen failed after reaching 344.7 MPa (50 ksi) after 2.5 hours. The 1093°C (2000°F) test specimen failed after 18 minutes at 310.3 MPa (45 ksi). The 1204°C (2200°F) stepped stress rupture test was ini-

TABLE X. NILSEN TTZ 500-HOUR STRESS RUPTURE TEST RESULTS

Temperature, °C (°F)	Load, MPa (ksi)	Deflection, mm (in)	Flexure Strength, MPa (ksi)	Baseline Strength, MPa (ksi)
982 (1800)	137.9 (20)	0.13 (0.005)	235.8 (34.2)	604.0 (87.6)
1038 (1900)	103.4 (15)	0.51 (0.020)	164.1 (23.8)	604.0 (87.6)
1093 (2000)	103.4 (15)	1.14 (0.045)	135.1 (19.6)	604.0 (87.6)

TABLE XI. NGK TTZ 500-HOUR STRESS RUPTURE TEST RESULTS

Temperature, °C (°F)	Load, MPa (ksi)	Deflection, mm (in)	Room Temperature Flexure Strength After 500-Hour Stress-Rupture, MPa (ksi)	Baseline Room Temperature Flexure Strength, MPa (ksi)
760 (1400)	137.9 (20)	0.03 (0.001)	630.9 (91.5)	993.5 (144.1)
871 (1600)	137.9 (20)	0.05 (0.002)	420.6 (61.0)	993.5 (144.1)
982 (1800)	68.9 (10)	0.76 (0.030)	352.3 (51.1)	993.5 (144.1)

tially started at a stress level of 68.9 MPa (10 ksi). The specimen fractured after being at a 206.8 MPa (30 ksi) stress level for 1.2 hours.

Five-hundred hour constant temperature and stress, stress rupture tests were conducted at 760, 871, and 982°C (1400, 1600, and 1800°F) at a constant load of 137.9 MPa (20 ksi). Upon completion of 500 hours, each specimen was measured to determine the deflection and four-point flexure tested to measure the retained strength. The results are listed in Table XII. At 760°C (1400°F) the specimen exhibited no loss in strength. At 871°C (1600°F) the specimen retained 78 percent of the room temperature baseline strength. However, at 982°C (1800°F) the specimen deflected 0.84 mm (0.033 inch) under the 137.9 MPa (20 ksi) load and retained only 33 percent of the baseline strength.

Feldmühle. - Stepped stress rupture results of Feldmühle TTZ are presented in Figure 34. Tests were conducted at 760 and 871°C (1400 and 1600°F). At both temperatures the specimens fractured on application of a 275.8 MPa (40 ksi) load after surviving 24 hours at both 137.9 and 206.9 MPa (20 and 30 ksi).

Five-hundred hour stress rupture tests were conducted at 760, 871, and 982°C (1400, 1600, and 1800°F) at a constant stress level of 137.9 MPa (20 ksi) as summarized in Table XIII. At 760 and 871°C (1400 and 1600°F) little or no creep was noted. After completion of 500 hours, no reduction in room-temperature strength was measured compared to the baseline strength. At 982°C (1800°F) and 137.9 MPa (20 ksi) the Feldmühle specimen deformed 0.015 cm (0.006 inch) after 500 hours and had retained 79 percent of its strength.

3.3.3 Stress Rupture Tests Discussion

Stress rupture test results illustrate much about material behavior at temperatures under load for an extended period of time. These tests provide information on creep deformation and aging effects on the material, which cannot be obtained from elevated temperature fast fracture test results.

~~Stepped stress rupture testing on Nilsen's TTZ revealed that at 982°C (1800°F) and above, specimens deformed severely so that the test had to be stopped at loads lower than measured during fast fracture. This limits the use of Nilsen TTZ to stress levels considerably lower than both the fast fracture strength and the stepped stress rupture loads if deformation is a concern.~~

The results of the 500-hour constant stress rupture tests indicate that there is an aging effect which significantly reduces the room temperature flexure strength when Nilsen's TTZ

TABLE XII. COORS TTZ 500-HOUR STRESS RUPTURE TEST RESULTS

Temperature, °C (°F)	Load, MPa (ksi)	Deflection, mm (in)	Room Temperature Flexure Strength After 500-Hour Stress-Rupture, MPa (ksi)	Baseline Room Temperature Flexure Strength, MPa (ksi)
760 (1400)	137.9 (20)	0.03 (0.001)	442.6 (64.2)	446.1 (64.7)
871 (1600)	137.9 (20)	0.05 (0.002)	347.5 (50.4)	446.1 (64.7)
982 (1800)	137.9 (20)	0.84 (0.033)	146.9 (21.3)	446.1 (64.7)

TABLE XIII. 500-HOUR STRESS RUPTURE TESTING OF FELDMÜHLE TTZ

Temperature, °C (°F)	Load, MPa (ksi)	Deflection, mm (in)	Flexure Strength, MPa (ksi)	Baseline Flexure Strength, MPa (ksi)
760 (1400)	137.9 (20)	None	397.2 (57.6)	377.8 (54.8)
871 (1600)	137.9 (20)	<0.025 (<0.001)	403.4 (58.5)	377.8 (54.8)
982 (1800)	137.9 (20)	0.152 (0.006)	297.9 (43.2)	377.8 (54.8)

is exposed to a constant elevated temperature under a constant load. The reduction of room temperature strength from 604.0 MPa (87.6 ksi) to 135.1 MPa (19.6 ksi), a 77-percent reduction, after 500 hours at 1093°C (2000°F) under a 103.4 MPa (15 ksi) load limits the use of Nilsen TTZ to <1093°C (<2000°F) if high strength is required.

NGK stepped-stress rupture specimens fractured, unlike the Nilsen TTZ specimens which deformed at the higher temperatures. At 760°C (1400°F) the NGK specimen fractured at a stress level very close in value to the fast fracture baseline flexure strength. At 982 and 1093°C (1800 and 2000°F) the stepped stress rupture specimens fractured at stress levels approximately one-half the value obtained during fast fracture baseline testing.

NGK TTZ also experiences an aging effect that results in reduced strength after exposure at elevated temperatures for 500 hours. The excellent NGK room temperature strength of 993.5 MPa (144.1 ksi) is reduced to 352.3 MPa (51.1 ksi) after 500 hours at 982°C (1800°F). The strength reduction as well as the excessive creep at 982°C (1800°F) limit NGK's use in heat engines to temperatures less than 982°C (1800°F).

Comparisons of stress rupture results between Nilsen and NGK TTZ materials show that both materials creep at elevated temperatures but that creep occurs more readily in NGK TTZ. For instance, a Nilsen specimen deformed 0.13 mm (0.005 inch) after 500 hours at 982°C (1800°F) under a 137.9-MPa (20-ksi) load. NGK tested for the same time and temperature under a 68.9-MPa (10-ksi) load deformed 0.76 mm (0.030 inch).

Results of Coors TTZ stepped-stress rupture tests conducted at 760, 982, 1093, and 1204°C (1400, 1800, 2000, and 2200°F) yielded results very different than both NGK and Nilsen. The initial stress level of 68.9 MPa (10 ksi) was selected because the baseline fast fracture strengths reported here and by Larsen and Adams (ref. 22) are relatively low 130.1 to 199.3 MPa (18.9 to 28.9 ksi). The stepped-stress rupture specimens ultimately failed at loads greater than the fast fracture strengths measured. At 982 and 1093°C (1800 and 2000°F) the stress rupture specimens failed at 344.7 and 310.3 MPa (50 and 45 ksi), respectively. Results of stepped temperature stress rupture testing conducted on Coors MgO stabilized TTZ by Schioler, Quinn, and Katz (ref. 23) showed that specimens ultimately failed at loads of 296.5 MPa (43 ksi) at 1100°C (2012°F) and 248.2 MPa (36 ksi) at 1200°C (2200°F). No elevated temperature baseline flexure strength values were available to compare to the stress rupture data. Similar stress rupture results were obtained in both studies.

3.4 Contact Stress Testing

3.4.1 Contact Stress Test Procedure

The contact test apparatus used for room temperature and high-temperature tests is shown in Figures 35 and 36. The apparatus consists of a furnace, a dead-weight loading system for applying a normal force, and an Instron test machine for applying relative motion and recording the resulting tangential force.

The contact test apparatus, which is very versatile, can be operated from room temperature to 1400°C (2550°F) over a broad loading range. The test bar contact configuration allows for point, line, or area contact, although the line contact condition was used for this study since it best simulates a typical heat engine configuration.

The specimens were machined to close tolerances as shown in Figure 37, to allow the specimens to expand during high-temperature testing without breaking the contact stress fixtures. Specimen B was held stationary during the test, and the 0.635 cm (0.250 inch) radius surface was held in contact with Specimen A. Specimen A was tangentially moved during the test, and the 0.630 cm (0.248 inch) flat surface was used as the test surface.

The contact test sequence consisted of the following steps:

- (a) Mount specimens in fixture.
- (b) Heat specimens to test temperature.
- (c) Apply normal load and zero load cell.
- (d) Hold under load at temperature 30 minutes.
- (e) Apply relative motion with Instron crosshead and record the friction-induced tangential breakaway and sliding loads.
- (f) Remove the specimen from the contact apparatus and conduct a four-point flexure strength test to measure retained strength after contact.
- (g) Examine the contact surface and fracture surface by optical microscopy and scanning electron microscopy (SEM); calculate the static and dynamic friction coefficients; calculate the strength after contact exposure; and correlate this data to determine if the specimen received contact damage and to determine the extent of the damage.

The contact test quantities, temperatures, and normal loads applied for the four TTZ materials are shown in Table XIV.

3.4.2 Contact Stress Test Results

Nilsen TTZ. - Contact stress tests were conducted at room temperature, 760, 982, 1093, and 1204°C (1400, 1800, 2000, and 2200°F) with contact loads of 0.455, 4.55, and 11.3 kg (1.0, 10, and 25 pounds). Static and dynamic coefficients of friction and forces as well as retained strength after contact are tabulated in Table XV. The static and dynamic coefficients of friction are plotted as a function of temperature in Figures 38 and 39. At a temperature of 982°C (1800°F) and below the load has a negligible effect on the coefficient of friction of Nilsen TTZ. Above 982°C (1800°F) the dynamic and static coefficients of friction are significantly greater with the 4.55- and 11.3-kg (10- and 25-pound) normal contact load than with a 0.455-kg (1.0-pound) normal load. This is opposite from what was found with SASC, of which the lower normal loads had the higher coefficients of friction at higher temperature. The high friction of SASC at low loads was attributed to a viscous oxide layer that forms on the surface of the material at high temperatures (ref. 9). In the case of Nilsen TTZ, the increased friction above 982°C (1800°F) for 4.55- and 11.4-kg (10- and 25-pound) contact loads may be a result of creep deformation. The stress rupture testing at 982°C (1800°F) and above has shown that Nilsen TTZ readily creeps. During contact testing at high temperatures the material may be deforming at the contact point. This may cause a depression in the material surface, which results in higher friction at the 4.55- and 11.4-kg (10- and 25-pound) contact loads but not at 0.45-kg (1.0-pound) loads.

Subsequent to the retained strength tests, visual inspection of contact stress test specimens revealed that several specimens under 4.5- and 11.4-kg (10- and 25-pound) contact loads fractured in the contact areas. Specimens that failed in the contact area did not appear to have a significantly lower strength than those that failed elsewhere. SEM evaluation revealed that none of the fractures were caused by contact stress. Figure 40 shows the fracture origin of specimen 11927, which was contact tested at 760°C (1400°F) with a 11.4-kg (25-pound) normal contact load and fractured through the contact area. The fracture origin was due to a linear pore and agglomerate located in the contact area.

SEM photographs of the contact area of the moving Nilsen contact specimens are shown in Figure 41 for room temperature, 760, 982, 1093, and 1204°C (1400, 1800, 2000, and 2200°F). Little evidence of contact is visible from room temperature to 982°C (1800°F). The contact area is visible on specimen frac-

TABLE XIV. CONTACT TEST MATRIX

Normal Load, kg (lb)	Temperature °C (°F)									
	Room Temperature	316 (600)	538 (1000)	760 (1400)	871 (1600)	982 (1800)	1093 (2000)	1204 (2200)		
<u>Nilisen TTZ</u>										
0.455 (1)	3	-	-	3	-	3	3	3	3	3
4.55 (10)	3	-	-	3	-	3	3	3	3	3
11.3 (25)	3	-	-	3	-	3	3	3	3	3
<u>NGK TTZ</u>										
4.55 (10)	3	3	3	3	3	3	3	3	3	3
11.3 (25)	3	3	3	3	3	3	3	3	3	3
22.7 (50)	3	-	3	3	3	3	3	3	3	3
<u>Coors TTZ</u>										
4.55 (10)	3	-	3	3	3	3	3	3	3	3
11.3 (25)	3	-	3	3	3	3	3	3	3	3
22.7 (50)	3	3	3	3	3	3	3	3	3	3
<u>Feldmühle TTZ</u>										
4.55 (10)	3	-	-	-	-	-	-	-	-	-
11.3 (25)	3	-	-	-	-	-	-	-	-	-
22.7 (50)	3	3	3	3	3	3	3	3	3	3

TABLE XV. NILSEN TTZ FRICTION DATA

Specimen Number	Normal Load, kg (lb)	Static Friction Coefficient	Dynamic Friction Coefficient	Retained Strength, MPa (ksi)	Contact Stress Fracture
Room Temperature					
11911	4.5 (10)	0.100	0.120	316.5 (45.9)	No
11912	4.5 (10)	0.125	0.120	686.7 (99.6)	No
11913	4.5 (10)	0.135	0.130	522.6 (75.8)	No
		x = 0.120	x = 0.120		
11908	11.4 (25)	0.128	0.122	574.3 (83.3)	No
11909	11.4 (25)	0.134	0.130	574.3 (83.3)	No
11910	11.4 (25)	0.136	0.128	492.3 (71.4)	No
		x = 0.130	x = 0.130		
760°C (1400°F)					
11933	0.45 (1)	0.40	0.40	473.0 (68.6)	No
11932	0.45 (1)	0.30	0.30	448.9 (65.1)	No
11931	0.45 (1)	0.30	0.30	430.2 (62.4)	No
		x = 0.33	x = 0.33		
11930	4.5 (10)	0.32	0.34	430.2 (62.4)	No
11929	4.5 (10)	0.36	0.38	442.0 (64.1)	No
11928	4.5 (10)	0.36	0.38	401.3 (58.2)	No
		x = 0.35	x = 0.37		
11927	11.4 (25)	0.38	0.40	417.8 (60.6)	No
11926	11.4 (25)	0.39	0.43	466.1 (67.6)	No
11925	11.4 (25)	0.35	0.42	451.6 (65.5)	No
		x = 0.37	x = 0.42		

TABLE XV. NILSEN TTZ FRICTION DATA (Contd)

Specimen Number	Normal Load, kg (lb)	Static Friction Coefficient	Dynamic Friction Coefficient	Retained Strength, MPa (ksi)	Contact Stress Fracture
982°C (1800°F)					
11924	0.45 (1)	0.60	0.60	430.2 (62.4)	NO
11923	0.45 (1)	0.30	0.50	466.1 (67.6)	NO
11922	0.45 (1)	--	$\frac{0.50}{x = 0.53}$	437.1 (63.4)	NO
11921	4.5 (10)	0.52	0.52	437.1 (63.4)	NO
11920	4.5 (10)	0.55	0.53	458.5 (66.5)	NO
11919	4.5 (10)	$\frac{0.56}{x = 0.54}$	$\frac{0.55}{x = 0.53}$	401.3 (58.2)	NO
11918	11.4 (25)	0.57	0.54	422.7 (61.3)	NO
11917	11.4 (25)	0.54	0.53	501.3 (72.7)	NO
11916	11.4 (25)	$\frac{0.52}{x = 0.54}$	$\frac{0.53}{x = 0.53}$	437.1 (63.4)	NO
1093°C (2000°F)					
11952	0.45 (1)	0.50	0.50	391.6 (56.8)	NO
11950	0.45 (1)	0.50	0.50	422.7 (61.3)	NO
11949	0.45 (1)	$\frac{0.50}{x = 0.50}$	$\frac{0.60}{x = 0.53}$	308.2 (44.7)	NO
11948	4.5 (10)	0.60	0.66	346.1 (50.2)	NO
11947	4.5 (10)	0.74	0.64	442.0 (64.1)	NO
11946	4.5 (10)	$\frac{0.74}{x = 0.69}$	$\frac{0.65}{x = 0.65}$	466.1 (67.6)	NO
11945	11.4 (25)	0.78	0.62	396.5 (57.5)	NO
11944	11.4 (25)	0.80	0.65	334.4 (48.5)	NO
11943	11.4 (25)	$\frac{0.74}{x = 0.77}$	$\frac{0.65}{x = 0.64}$	473.0 (68.6)	NO

TABLE XV. NILSEN TTZ FRICTION DATA (Contd)

Specimen Number	Normal Load, kg (lb)	Static Friction Coefficient	Dynamic Friction Coefficient	Retained Strength, MPa (ksi)	Contact Stress Fracture
12040C (2200OF)					
11942	0.45 (1)	0.60	0.70	511.6 (74.2)	NO
11941	0.45 (1)	0.50	0.70	632.9 (91.8)	NO
11940	0.45 (1)	0.50	0.60	391.6 (56.8)	NO
		x = 0.53	x = 0.67		
11939	4.5 (10)	0.86	0.75	391.6 (56.8)	NO
11938	4.5 (10)	0.85	0.75	523.3 (75.9)	NO
11938	4.5 (10)	0.92	0.78	435.1 (63.1)	NO
		x = 0.88	x = 0.76		
11936	11.4 (25)	0.83	0.76	501.9 (72.8)	NO
11935	11.4 (25)	0.84	0.74	477.8 (69.3)	NO
11934	11.4 (25)	0.87	0.79	348.9 (50.6)	NO
		x = 0.85	x = 0.76		

tured at 1093 and 1204°C (2000 and 2200°F), but no damage is visible. The lack of contact damage was verified by the high retained strengths of the Nilsen bars after contact stress testing.

NGK TTZ. - Contact stress test results are tabulated in Table XVI. Static and dynamic coefficients of friction are plotted as a function of temperature in Figures 42 and 43. The static and dynamic coefficients of friction measured at 11.4- and 22.7-kg (25- and 50-pound) normal loads are close in value over the entire temperature range. The relationship between the static coefficient of friction and temperature appears to be increasing linearly with increasing temperature. The 4.5-kg (10-pound) normal load data also follows fairly close to this trend, although there is more scatter. The dynamic friction increases with temperature to 760°C (1400°F). Between 760°C (1400°F) and 1204°C (2200°F) the coefficient of friction is constant at a value of 0.7.

After contact stress testing was completed, the specimens were flexure tested to measure the retained strength after contact. None of the specimens failed at contact loads of 4.5 Kg (10 pounds). At 11.4 kg (25 pounds), one specimen tested failed due to contact damage at 760°C (1400°F). At contact loads of 22.7 kg (50 pounds) all three test specimens failed due to contact at 760 and 1204°C (1400 and 2200°F). At 871, 982, and 1093°C (1600, 1800, and 2000°F) and at a contact load of 22.7 kg (50 pounds), several specimens did fail in the contact area. These specimens were inspected by SEM to determine if the fracture was caused by contact damage. One specimen tested at 871 and 982°C (1600 and 1800°F) did fail as a result of contact damage.

Selected contact stress test specimens, which fractured through the contact area, were photographed by SEM to characterize the fracture origins. Both the moving and stationary contact areas typically have shallow grooves where the material appears to have been pushed by the moving contact specimen and then deposited back on the specimen surface. Figure 44 shows the contact area and fracture origin of specimen 12365, which was contact tested at 1093°C (2000°F) with a 22.7-kg (50-pound) normal contact load. The contact did not reduce specimen strength.

The contact area and fracture origin for specimen 12347 is shown in Figure 45. This specimen was contact tested at 871°C (1600°F) under a 22.7-kg (50-pound) load. The fracture originated at an area where material had been removed and deposited on the surface. This flaw reduced the strength by only 20 percent of that of a specimen without contact damage.

TABLE XVI. NGK TTZ FRICTION DATA

Specimen Number	Normal Load, kg (lb)	Static Friction Coefficient	Dynamic Friction Coefficient	Retained Strength, MPa (ksi)	Contact Stress Fracture
Room Temperature					
12312	4.5 (10)	0.16	0.14	972.2 (141.0)	NO
12313	4.5 (10)	0.11	0.13	957.7 (138.9)	NO
12314	4.5 (10)	0.14	0.14	1020.4 (148.0)	NO
		x = 0.14	x = 0.14		
12315	11.4 (25)	0.17	0.14	1027.3 (149.0)	NO
12316	11.4 (25)	0.12	0.12	943.9 (136.9)	NO
12317	11.4 (25)	0.13	0.14	1070.1 (155.2)	NO
		x = 0.14	x = 0.13		
12318	22.7 (50)	0.13	0.13	1034.2 (150.7)	NO
12319	22.7 (50)	0.13	0.13	912.9 (132.4)	NO
12320	22.7 (50)	0.13	0.14	707.4 (102.6)	NO
		x = 0.13	x = 0.13		
316°C (600°F)					
12378	4.5 (10)	0.16	0.19	740.5 (107.4)	NO
11279	4.5 (10)	0.12	0.16	908.0 (131.7)	NO
12380	4.5 (10)	0.14	0.13	883.9 (128.2)	NO
		x = 0.14	x = 0.16		
12381	11.4 (25)	0.12	0.16	573.6 (83.2)	NO
12382	11.4 (25)	0.14	0.16	776.4 (112.6)	NO
12383	11.4 (25)	0.12	0.18	967.3 (140.3)	NO
		x = 0.13	x = 0.17		

TABLE XVI. NGK TTZ FRICTION DATA (Contd)

Specimen Number	Normal Load, kg (lb)	Static Friction Coefficient	Dynamic Friction Coefficient	Retained Strength, MPa (ksi)	Contact Stress Fracture
538°C (1000°F)					
12321	4.5 (10)	0.58	0.62	821.9 (119.2)	NO
12322	4.5 (10)	0.48	0.52	774.3 (112.3)	NO
12323	4.5 (10)	0.58	0.64	919.8 (133.4)	NO
		x = 0.55	x = 0.59		
12324	11.4 (25)	0.38	0.42	1008.0 (146.2)	NO
12325	11.4 (25)	0.42	0.44	864.6 (125.4)	NO
12326	11.4 (25)	0.43	0.50	774.3 (112.3)	NO
		x = 0.41	x = 0.45		
12327	22.7 (50)	0.40	0.49	893.6 (129.6)	NO
12328	22.7 (50)	0.36	0.36	912.9 (132.4)	NO
12329	22.7 (50)	0.38	0.48	883.9 (128.2)	NO
		x = 0.38	x = 0.44		
760°C (1400°F)					
12331	4.5 (10)	0.50	0.70	823.9 (119.5)	NO
12332	4.5 (10)	0.56	0.70	864.6 (125.4)	NO
		x = 0.53	x = 0.70		
12333	11.4 (25)	0.65	0.74	872.2 (126.5)	NO
12334	11.4 (25)	0.69	0.73	315.1 (45.7)	Yes
12335	11.4 (25)	0.62	0.70	699.8 (101.5)	NO
		x = 0.65	x = 0.72		
12336	22.7 (50)	0.68	0.72	341.3 (49.5)	Yes
12337	22.7 (50)	0.65	0.71	487.5 (70.7)	Yes
12338	22.7 (50)	0.64	0.74	329.6 (47.8)	Yes
		x = 0.66	x = 0.72		

TABLE XVI. NGK TTZ FRICTION DATA (Contd)

Specimen Number	Normal Load, kg (lb)	Static Friction Coefficient	Dynamic Friction Coefficient	Retained Strength, MPa (ksi)	Contact Stress Fracture
8710C (1600°F)					
12339	4.5 (10)	0.62	0.70	--	--
12340	4.5 (10)	0.63	0.70	657.1 (95.3)	No
12341	4.5 (10)	0.65	0.75	817.0 (118.5)	No
		x = 0.63	x = 0.72		
12342	11.4 (25)	0.62	0.69	852.9 (123.7)	No
12343	11.4 (25)	0.68	0.73	745.3 (108.1)	No
12344	11.4 (25)	0.62	0.71	525.4 (76.2)	No
		x = 0.64	x = 0.71		
12345	22.7 (50)	0.67	0.70	745.3 (108.1)	No
12346	22.7 (50)	0.63	0.70	850.8 (123.4)	No
12347	22.7 (50)	0.62	0.68	590.2 (85.6)	Yes
		x = 0.64	x = 0.69		
9820C (1800°F)					
12348	4.5 (10)	0.76	0.71	841.2 (122.0)	No
12349	4.5 (10)	0.75	0.76	--	--
12350	4.5 (10)	0.73	0.72	--	--
		x = 0.75	x = 0.73		
12351	11.4 (25)	0.68	0.70	846.0 (122.7)	No
12352	11.4 (25)	0.66	0.70	--	--
12353	11.4 (25)	0.68	0.70	792.9 (115.0)	No
		x = 0.67	x = 0.70		
12354	22.7 (50)	0.62	0.69	817.0 (118.5)	No
12355	22.7 (50)	0.64	0.68	494.9 (71.7)	Yes
12356	22.7 (50)	0.66	0.68	626.0 (90.8)	No
		x = 0.64	x = 0.68		

TABLE XVI. NGK TTZ FRICTION DATA (Contd)

Specimen Number	Normal Load, kg (lb)	Static Friction Coefficient	Dynamic Friction Coefficient	Retained Strength, MPa (ksi)	Contact Stress Fracture
10930C (2000OF)					
12357	4.5 (10)	0.75	0.73	836.3 (121.3)	No
12358	4.5 (10)	0.72	0.74	864.6 (125.4)	No
12359	4.5 (10)	0.78	0.76	781.2 (113.3)	No
		x = 0.75	x = 0.74		
12360	11.4 (25)	0.76	0.70	852.9 (123.7)	No
12361	11.4 (25)	0.72	0.68	544.7 (79.0)	No
12362	11.4 (25)	0.74	0.72	752.2 (109.1)	No
		x = 0.74	x = 0.70		
12363	22.7 (50)	0.70	0.69	728.8 (105.7)	No
12364	22.7 (50)	0.75	0.70	702.6 (101.9)	No
12365	22.7 (50)	0.69	0.68	707.4 (102.6)	No
		x = 0.71	x = 0.69		
12040C (2200OF)					
12366	4.5 (10)		0.64	728.8 (105.7)	No
12367	4.5 (10)		0.63	819.1 (118.8)	No
12368	4.5 (10)		0.60	728.8 (105.7)	No
			x = 0.62		
12369	11.4 (25)	0.72	0.68	859.8 (124.7)	No
12370	11.4 (25)	0.82	0.72	721.2 (104.6)	No
12371	11.4 (25)	0.83	0.74	748.1 (108.5)	No
		x = 0.79	x = 0.71		
12372	22.7 (50)	0.83	0.76	578.5 (83.9)	Yes
12373	22.7 (50)	0.85	0.74	585.4 (84.9)	Yes
12374	22.7 (50)	0.82	0.74	501.9 (72.8)	Yes
		x = 0.83	x = 0.75		

Specimen 12338 (Figure 46), which was contact tested at 760°C (1400°F) under a 22.7-kg (50-pound) normal contact load, also fractured at the contact area in a groove where parent material had been removed. This specimen experienced a 30-percent reduction in strength.

Coors TTZ. - The contact stress data is tabulated in Table XVII. The static and dynamic coefficients of friction are plotted versus temperature in Figures 47 and 48. The static and dynamic coefficient of friction were measured over the temperature range of room temperature to 1204°C (2200°F). The static coefficient of friction is 0.13 at room temperature, increases to 0.38-0.41 at 760°C (1400°F), increases to 0.59-0.61 at 982°C (1800°F), increases to 0.70-0.77 at 1093°C (2000°F), and increases further to 0.82-0.91 at 1204°C (2200°F). The dynamic coefficient of friction closely follows the static friction values measured, except at 1204°C (2200°F) where the dynamic coefficient of friction is 0.78.

After completion of the contact stress testing the Coors specimens were four-point flexure tested. The fracture location and the fracture surfaces were visually inspected with an optical microscope at magnifications of 10 to 40X. Only two of the Coors TTZ specimens, both at 22.7-kg (50-pound) normal contact loads, failed due to contact stress damage.

SEM examination of the contact areas was conducted on selected specimens tested under the 11.4-kg (25-pound) normal load. At room temperature and 760°C (1400°F) the contact surfaces revealed little evidence that the specimens had been in contact (Figure 49). At 982, 1093, and 1204°C (1800, 2000, and 2200°F) (Figures 50 through 52) the areas in contact can be clearly seen. Several items to note regarding the contact areas are no chipping or severe surface damage is visible and contact is complete over the area of contact. In comparison, under the same conditions, reaction bonded silicon nitride (RBSN) and sintered alpha SiC (SASC) has previously shown an uneven contact pattern covering only 30 to 50 percent of the surface, chipping or surface damage, and would fracture through the contact area (ref. 8, 9). The TTZ materials have more complete contact (usually 80 to 100 percent). This additional contact is probably due to the material deforming at the contact point. The increased amount of contact results in the contact load being more evenly distributed over the line contact area, thereby minimizing contact damage.

Feldmühle. - Feldmühle TTZ was contact tested at normal loads of 4.5, 11.4 and 22.7 kg (10, 25, and 50 pounds) at room temperature and at 22.7-kg (50-pound) loads at 316, 538, 760,

TABLE XVII. COORS TTZ FRICTION DATA

Specimen Number	Normal Load, kg (lb)	Static Friction Coefficient	Dynamic Friction Coefficient	Retained Strength, MPa (ksi)	Contact Stress Fracture
Room Temperature					
12282	4.5 (10)	0.14	0.13	489.5 (71.0)	NO
12283	4.5 (10)	0.13	0.13	501.9 (72.8)	NO
12224	4.5 (10)	0.05	0.12	549.5 (79.7)	NO
		x = 0.13	x = 0.13		
12285	11.4 (25)	0.13	0.12	539.9 (78.3)	NO
12286	11.4 (25)	0.13	0.12	566.1 (82.1)	NO
12287	11.4 (25)	0.12	0.12	582.6 (84.5)	NO
		x = 0.13	x = 0.12		
13143	22.7 (50)	0.11	0.12	466.1 (67.6)	NO
13144	22.7 (50)	0.08	0.12	446.8 (64.8)	NO
13145	22.7 (50)	0.11	0.11	539.9 (78.3)	NO
		x = 0.10	x = 0.12		
3160C (6000F)					
13176	22.7 (50)	0.14	0.18	489.5 (71.0)	NO
13177	22.7 (50)	0.20	0.26	494.4 (71.7)	NO
13178	22.7 (50)	0.10	0.12	504.0 (73.1)	NO
		x = 0.15	x = 0.19		
5380C (10000F)					
13146	4.5 (10)	0.36	0.42	492.3 (71.4)	NO
13147	4.5 (10)	0.34	0.38	444.0 (64.4)	NO
13148	4.5 (10)	0.34	0.39	537.8 (78.0)	NO
		x = 0.35	x = 0.40		
13149	11.4 (25)	0.36	0.44	497.1 (72.1)	NO
13150	11.4 (25)	0.35	0.40	370.3 (53.7)	NO
13151	11.4 (25)	0.38	0.41	537.8 (78.0)	NO
		x = 0.36	x = 0.42		

TABLE XVII. COORS T1Z FRICTION DATA (Contd)

Specimen Number	Normal Load, kg (lb)	Static Friction Coefficient	Dynamic Friction Coefficient	Retained Strength, MPa (ksi)	Contact Stress Fracture
5380C (1000OF) (Contd)					
13152	22.7 (50)	0.36	0.39	382.0 (55.4)	NO
13153	22.7 (50)	0.39	0.38	477.8 (69.3)	NO
13154	22.7 (50)	0.48	0.45	497.1 (72.1)	NO
		x = 0.36	x = 0.41		
7600C (1400OF)					
12288	4.5 (10)	0.39	0.44	525.4 (76.2)	NO
12289	4.5 (10)	0.39	0.44	504.0 (73.1)	NO
12290	4.5 (10)	0.37	0.46	537.8 (78.0)	NO
		x = 0.38	x = 0.45		
12291	11.4 (25)	0.50	0.48	497.1 (72.1)	NO
12292	11.4 (25)	0.38	0.41	525.4 (76.2)	NO
12293	11.4 (25)	0.34	0.35	497.1 (72.1)	NO
		x = 0.41	x = 0.41		
13155	22.7 (50)	0.43	0.49	470.9 (68.3)	NO
13156	22.7 (50)	0.52	0.52	439.9 (63.8)	NO
13157	22.7 (50)	0.46	0.50	513.7 (74.5)	NO
		x = 0.47	x = 0.50		
8710C (1600OF)					
13158	4.5 (10)	0.67	0.70	420.6 (61.0)	NO
13159	4.5 (10)	0.62	0.65	442.0 (64.1)	NO
13160	4.5 (10)	0.63	0.60	446.8 (64.8)	NO
		x = 0.64	x = 0.65		
13161	11.4 (25)	0.62	0.60	422.7 (61.3)	NO
13162	11.4 (25)	0.62	0.58	477.8 (69.3)	NO
13163	11.4 (25)	0.60	0.60	470.9 (68.3)	NO
		x = 0.61	x = 0.59		

TABLE XVII. COORS T1Z FRICTION DATA (Contd)

Specimen Number	Normal Load, kg (lb)	Static Friction Coefficient	Dynamic Friction Coefficient	Retained Strength, MPa (ksi)	Contact Stress Fracture
871°C (1600°F)					
13164	22.7 (50)	0.56	0.54	492.3 (71.4)	NO
13165	22.7 (50)	0.54	0.54	358.5 (52.0)	NO
13166	22.7 (50)	0.46	0.52	437.1 (63.4)	NO
		x = 0.52	x = 0.53		
982°C (1800°F)					
12294	4.5 (10)	0.56	0.60	492.3 (71.4)	NO
12295	4.5 (10)	0.56	0.64	468.2 (67.9)	NO
12296	4.5 (10)	0.64	0.64	533.0 (77.3)	NO
		x = 0.59	x = 0.63		
12297	11.4 (25)	0.60	0.64	542.6 (78.7)	NO
12298	11.4 (25)	0.58	0.58	515.7 (74.8)	NO
12299	11.4 (25)	0.60	0.62	470.9 (68.3)	NO
		x = 0.61	x = 0.61		
982°C (1800°F)					
13167	22.7 (50)	0.54	0.58	492.3 (71.4)	NO
13168	22.7 (50)	0.58	0.58	442.0 (64.1)	NO
13169	22.7 (50)	0.56	0.58	430.2 (62.4)	NO
		x = 0.56	x = 0.58		
1093°C (2000°F)					
12300	4.5 (10)	0.75	0.70	537.8 (78.0)	NO
12302	4.5 (10)	0.82	0.73	501.9 (72.8)	NO
12305	4.5 (10)	0.74	0.68	515.7 (74.8)	NO
		x = 0.77	x = 0.69		

TABLE XVII. COORS TTZ FRICTION DATA (Contd)

Specimen Number	Normal Load, kg (lb)	Static Friction Coefficient	Dynamic Friction Coefficient	Retained Strength, MPa (ksi)	Contact Stress Fracture
10930C (2000°F) (Contd)					
12303	11.4 (25)	0.68	0.70	468.2 (67.9)	No
12304	11.4 (25)	0.70	0.69	549.5 (79.7)	No
12301	11.4 (25)	<u>0.71</u>	<u>0.69</u>	525.4 (76.2)	No
		x = 0.70	x = 0.69		
13170	22.7 (50)	0.62	0.64	337.2 (48.9)	Yes
13171	22.7 (50)	0.60	0.66	382.0 (55.4)	No
13172	22.7 (50)	<u>0.60</u>	<u>0.62</u>	484.7 (70.3)	No
		x = 0.61	x = 0.64		
12040C (2200°F)					
12306	4.5 (10)	0.90	0.78	501.9 (72.8)	No
12308	4.5 (10)	<u>0.92</u>	<u>0.78</u>	461.3 (66.9)	No
		x = 0.91	x = 0.78		
12309	11.4 (25)	0.82	0.78	463.3 (67.2)	No
12310	11.4 (25)	0.82	0.81	539.9 (78.3)	No
12311	11.4 (25)	<u>0.82</u>	<u>0.76</u>	468.2 (67.9)	No
		x = 0.82	x = 0.78		
13173	22.7 (50)	0.70	0.74	239.2 (34.7)	Yes
13174	22.7 (50)	0.66	0.74	332.3 (48.2)	No
13175	22.7 (50)	<u>0.66</u>	<u>0.70</u>	126.9 (18.4)	No
		x = 0.67	x = 0.73		

871, 982, 1093, and 1204°C (600, 1000, 1400, 1600, 1800, 2000, and 2200°F). The static and dynamic coefficients of friction are plotted as a function of temperature in Figures 53 and 54. Feldmühle TTZ shows the same trends in coefficient of friction as the NGK, Nilsen and Coors materials. From room temperature to 316°C (600°F) the coefficient of friction is 0.35. The friction gradually increases until it reaches 0.66 at 1204°C (2200°F).

After contact testing was completed the specimens were flexure tested to determine if the specimens were damaged during contact. From room temperature to 982°C (1800°F) none of the specimens received contact damage (Table XVIII). One specimen, at 1093°C (2000°F), and all three specimens at 1204°C (2200°F) received contact damage.

Scanning electron microscopy was used to characterize specimen surfaces after contact testing at 22.7-kg (50-pound) normal contact loads. No indication of contact was visible at test temperatures below 760°C (1400°F). At 760°C (1400°F) (Figure 55) the contact area could be seen but contact did not damage the specimen surface. At 871°C (1600°F) and above the contact areas were clearly visible. Shallow grooves where TTZ material had been pushed and redeposited on the specimen surface are visible. At 1204°C (2200°F), under a 22.7-kg (50-pound) contact load, all three specimens were damaged due to contact and when flexure tested broke in the contact area (Figure 56).

3.4.3 Contact Stress Testing Discussion

Room temperature contact tests conducted on all four TTZ materials yielded relatively low static and dynamic coefficients of friction, 0.10 to 0.13. In comparison, the room temperature static and dynamic coefficients of friction for sintered alpha SiC (SASC) is in the range of 0.27 to 0.33 (ref. 9) and reaction-bonded Si₃N₄ (RBSN) has a range of 0.20 to 0.22 (ref. 8). The surface finish of the Nilsen specimens was measured and compared with the machined SASC and RBSN used for the above friction measurements. The surface finish of all four longitudinally-machined materials was in the range of 8 to 10 microinches rms. Therefore, the difference in room temperature coefficient of friction measurements does not appear to be due to surface finish.

3.4.4 Analytical Contact Stress Analysis of TTZ to TTZ Interfaces

A finite element stress analysis technique for evaluating the complex state of stress at ceramic-to-ceramic sliding inter-

TABLE XVIII. FELDMÜHLE TTZ FRICTION DATA

Specimen Number	Normal Load, kg (lb)	Static Friction Coefficient	Dynamic Friction Coefficient	Retained Strength, MPa (ksi)	Contact Stress Fracture
Room Temperature					
13816	4.5 (10)	0.13	0.12	424.7 (61.6)	NO
13817	4.5 (10)	0.13	0.12	344.7 (50.0)	NO
13818	4.5 (10)	0.13	0.13	331.6 (48.1)	NO
		x = 0.13	x = 0.12		
13819	11.4 (25)	0.11	0.13	411.6 (59.7)	NO
13820	11.4 (25)	0.12	0.13	353.0 (51.2)	NO
13821	11.4 (25)	0.12	0.12	377.1 (54.7)	NO
		x = 0.12	x = 0.13		
13822	22.7 (50)	0.11	0.12	358.5 (52.0)	NO
13823	22.7 (50)	0.10	0.12	377.1 (54.7)	NO
13824	22.7 (50)	0.11	0.12	377.1 (54.7)	NO
		x = 0.11	x = 0.12		
3160C (600°F)					
13825	22.7 (50)	0.14	0.17	353.0 (51.2)	NO
13826	22.7 (50)	0.14	0.18	427.5 (62.0)	NO
13827	22.7 (50)	0.18	0.18	355.8 (51.6)	NO
		x = 0.15	x = 0.18		
5380C (1000°F)					
13828	22.7 (50)	0.35	0.39	448.9 (65.1)	NO
13829	22.7 (50)	0.37	0.41	432.3 (62.7)	NO
13830	22.7 (50)	0.34	0.41	411.6 (59.7)	NO
		x = 0.35	x = 0.40		
7600C (1400°F)					
13831	22.7 (50)	0.39	0.40	297.2 (43.1)	NO
13832	22.7 (50)	0.42	0.49	427.5 (62.0)	NO
13833	22.7 (50)	0.40	0.48	424.7 (61.6)	NO
		x = 0.40	x = 0.46		

TABLE XVIII. FELDMÜHLE TTZ FRICTION DATA (Contd)

Specimen Number	Normal Load, kg (lb)	Static Friction Coefficient	Dynamic Friction Coefficient	Retained Strength, MPa (ksi)	Contact Stress Fracture
8710C (1600 ^{OF})					
13834	22.7 (50)	0.52	0.56	440.6 (63.9)	No
13835	22.7 (50)	0.54	0.56	411.6 (59.7)	No
13836	22.7 (50)	0.48	0.56	504.0 (73.1)	No
		$x = 0.51$	$x = 0.56$		
9820C (1800 ^{OF})					
13837	22.7 (50)	0.50	0.56	456.4 (66.2)	No
13838	22.7 (50)	0.56	0.60	527.5 (62.0)	No
13839	22.7 (50)	0.54	0.60	440.6 (63.9)	No
		$x = 0.53$	$x = 0.59$		
10930C (2000 ^{OF})					
13840	22.7 (50)	0.58	0.68	366.1 (53.1)	Yes
13841	22.7 (50)	0.54	0.64	448.9 (65.1)	No
13842	22.7 (50)	0.58	0.63	427.5 (62.0)	No
		$x = 0.57$	$x = 0.65$		
12040C (2200 ^{OF})					
13843	22.7 (50)	0.70	0.74	363.4 (52.7)	Yes
13844	22.7 (50)	0.64	0.68	347.5 (50.4)	Yes
13845	22.7 (50)	0.64	0.76	363.4 (52.7)	Yes
		$x = 0.66$	$x = 0.73$		

faces was developed by Finger (ref. 5). The model developed was for a cylinder contacting a semi-infinite plate, similar in configuration to the contact stress test specimens.

The model showed that when the cylinder and flat plate are held in contact under a normal load and at the same time a tangential load is applied, that a tensile stress is present at the trailing edge of the contact area. The magnitude of the tensile stress was found to be directly proportional to the coefficient of friction. If the friction was very high the tensile stress could actually exceed the strength of the material.

The analytical results compared favorably with actual room temperature contact stress tests conducted using Carborundum SASC (ref. 9). When the model predicted a high peak tensile stress due to the sliding contact, actual specimens contact stress tested at the same conditions had a significantly reduced strength due to contact stress damage.

The analytical model did not hold at elevated temperatures. Smyth (ref. 4) found that the model predicted contact damage should occur at elevated temperatures but actual SASC specimens tested did not receive contact damage. A viscous oxide layer which forms on SASC at elevated temperatures was thought to be responsible for preventing contact damage.

The analytical model developed by Finger was used to determine if it could accurately predict when contact damage would occur in TTZ. Table XIX lists the contact zone width and the minimum compressive stress due to contact specimens in contact without motion. Using the coefficients of friction measured during contact testing and the analytical model, the peak tensile stresses were calculated (Table XX). At elevated temperatures the calculated peak tensile stress due to contact exceeds the elevated temperature strength of the TTZ materials. Because contact damage was not observed for a majority of the specimens it can be concluded that the model does not hold at elevated temperatures for TTZ materials. The analytical model is based solely on linear elastic behavior. Parameters such as plastic deformation and toughness may need to be added to the model in order to more accurately predict the peak tensile stresses caused by sliding contact at elevated temperatures of TTZ.

TABLE XIX. COMPRESSIVE STRESS AND CONTACT ZONE WIDTH AT ROOM TEMPERATURE, LINE CONTACT, NO TANGENTIAL MOTION

	Normal Load kg (lb)	Contact Zone Width, mm (in.)	Compressive Stress, MPa (ksi)
Nilsen TTZ	0.455 (1)	0.015 (0.00057)	-61.4 (-8.9)
	4.55 (10)	0.046 (0.00181)	-194.4 (-28.2)
	11.3 (25)	0.072 (0.00285)	-307.5 (-44.6)
NGK TTZ	4.55 (10)	0.047 (0.00185)	-189.6 (-27.5)
	11.3 (25)	0.074 (0.00293)	-297.2 (-43.1)
	22.7 (50)	0.105 (0.00414)	-419.9 (-60.9)
Coors TTZ	4.55 (10)	0.047 (0.00187)	-187.5 (-27.2)
	11.3 (25)	0.075 (0.00296)	-297.2 (-43.1)
	22.7 (50)	0.106 (0.00418)	-419.9 (-60.9)

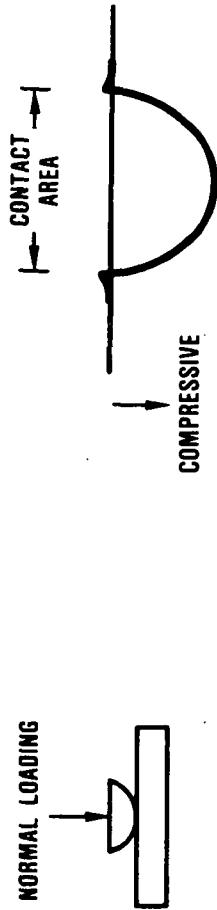
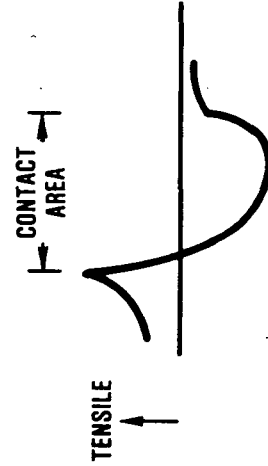
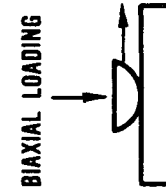


TABLE XX. CALCULATED PEAK TENSILE STRESS MPa (ksi),
LINE CONTACT

Normal Load (lb)	Temperature, °C (°F)				
	Room Temperature	760 (1400)	982 (1800)	1093 (2000)	1204 (2200)
<u>NGK TT2</u>					
10	49.6 (7.2)	195.1 (28.3)	277.9 (40.3)	277.9 (40.3)	-- --
25	79.3 (11.5)	382.0 (55.4)	393.7 (57.1)	435.1 (63.1)	464.7 (67.4)
50	104.8 (15.2)	550.2 (79.8)	533.7 (77.4)	592.3 (85.9)	692.9 (100.5)
<u>Coors TTZ</u>					
10	44.8 (6.5)	137.9 (20.0)	215.8 (31.3)	282.0 (40.9)	334.4 (48.5)
25	73.1 (10.6)	237.2 (34.4)	355.1 (51.5)	408.2 (59.2)	477.8 (69.3)
50	79.3 (11.5)	386.8 (56.1)	452.0 (67.0)	503.3 (73.0)	553.7 (80.3)
<u>Nilisen TTZ</u>					
1	-- --	37.9 (5.5)	-- --	57.9 (8.4)	61.4 (8.9)
10	42.7 (6.2)	131.0 (19.0)	204.1 (29.6)	261.3 (37.9)	334.4 (48.5)
25	75.1 (10.9)	221.3 (32.1)	324.7 (47.1)	464.7 (67.4)	513.7 (74.5)



4.0 CONCLUSIONS

There is a wide variation in four-point flexure strengths of the four TTZ materials tested. To compare the baseline flexure strengths as a function of temperature for the four TTZ materials, baseline strength is plotted as a function of temperature in Figure 57. NGK TTZ has the highest room temperature flexure strength, 993.6 MPa (144.1 ksi) of the four materials, but also shows the greatest decrease in flexure strength with increasing temperature. NGK has a 1204°C (2200°F) flexure strength of 102 MPa (14.8 ksi), a reduction of approximately 90 percent of the room temperature strength. NGK material that is stabilized with Y₂O₃ also contains 0.72 percent by weight of Si, which is in the form of SiO₂ (ref. 22). This glass is believed to be present in the grain boundaries, which accounts for the extremely low 1204°C (2200°F) flexure strength and slow crack growth visible on the 1093 to 1204°C (2000 to 2200°F) fracture surfaces.

Coors, Nilsen, and Feldmühle TTZ, which are MgO stabilized, show a more gradual decrease in flexure strength as a function of temperature. Nilsen decreases from 604.0 MPa (87.6 ksi) at room temperature to 254.4 MPa (36.9 ksi) at 1204°C (2200°F), a 58-percent decrease. Coors, which has a room temperature flexure strength of 446.1 MPa (64.7 ksi), decreases to 130.3 MPa (18.9 ksi) at 1204°C (2200°F), a 71-percent decrease in strength. Feldmühle decreases from 377.8 MPa (54.8 ksi) at room temperature to 139.3 MPa (20.2 ksi) at 1204°C (2200°F), 63-percent reduction. Although NGK TTZ has the highest strength from room temperature to 760°C (1400°F), Nilsen TTZ has the highest strength from 982 to 1204°C (1800 to 2200°F).

At room temperature all four TTZ materials tested appeared to have adequate strength for heat engine applications. The Y₂O₃ stabilized fine grained NGK material has much greater strength than the three large grained MgO stabilized Coors, Nilsen, and Feldmühle materials. The strength of all four TTZ materials drops rapidly at elevated temperatures. The NGK material has the most dramatic drop in strength at elevated temperature; again this is due to fine grain structure and SiO₂ at the grain boundaries. The relationship between grain size and strength is typical of most ceramic material (ref. 24).

TTZ materials experience degradation of strength when aged at elevated temperatures. The four TTZ materials tested experienced creep at temperatures of 760°C (1400°F) and above. The temperature where creep started and was the most severe varied with the different TTZ materials.

The coefficients of friction measured for the four TTZ materials were considerably lower than previously measured for SASC and RBSN over the entire temperature range measured. There

was no significant difference in friction coefficients between the four TTZ materials.

Contact did not cause damage at normal loads of 0.455, 4.55 and 11.3 kg (1, 10, and 25 pounds), but several specimens were contact damaged at 11.3 kg (50 pound) normal contact loads.

TTZ specimens that did sustain contact damage had retained strength approximately 70 to 90 percent of those specimens without contact damage. In comparison (Figure 58) all SASC and RBSN specimens contact tested with a 11.3-kg (25-pound) contact load sustained contact damage, which reduces the strength by as much as 50 percent when compared to samples without contact damage. At contact loads as low as 4.55 kg (10 pounds) many RBSN specimens have been damaged due to contact stress. TTZ specimens can survive contact loads much greater than can be tolerated by other structural ceramic materials such as RBSN and SASC.

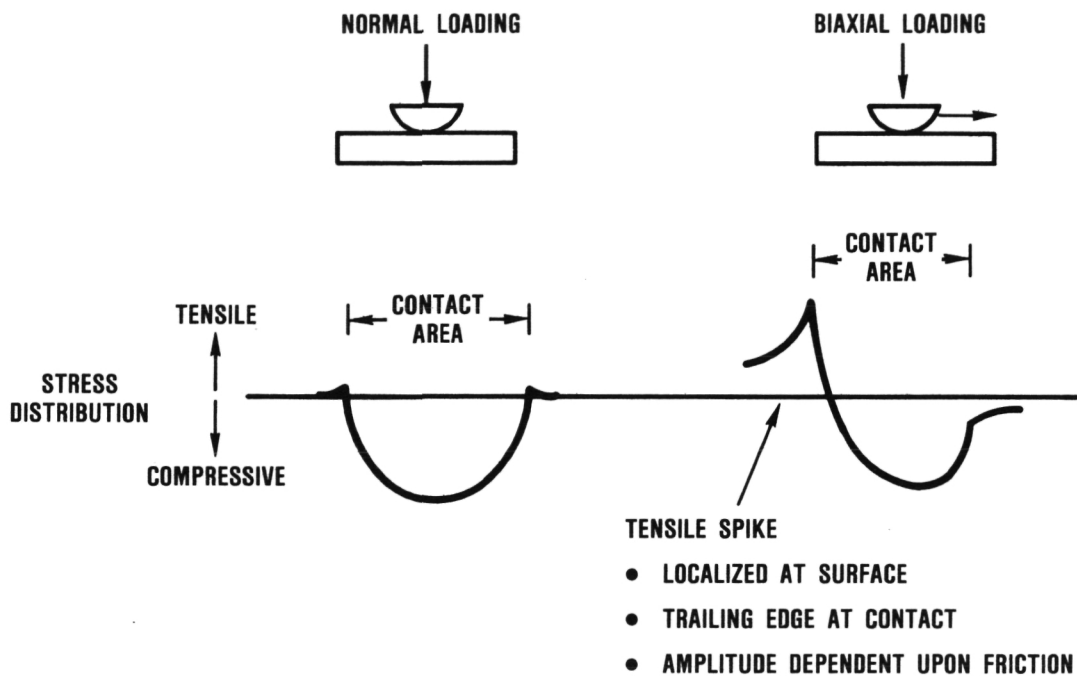
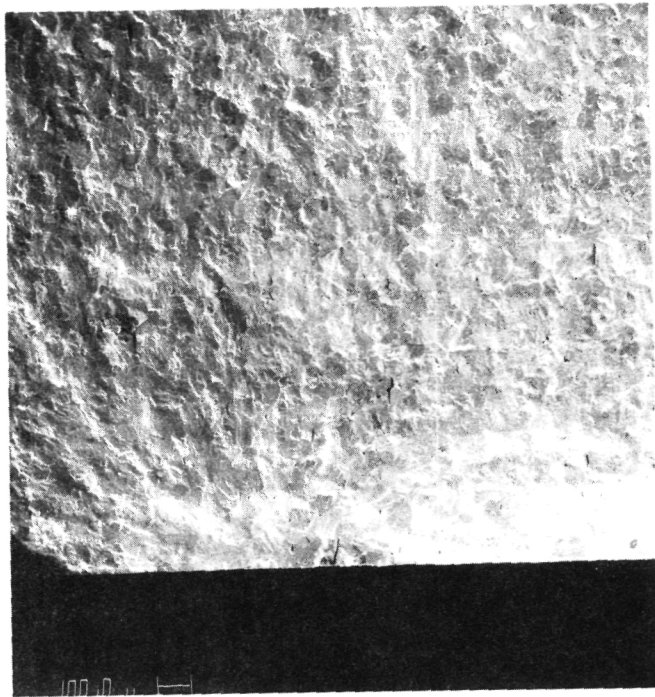
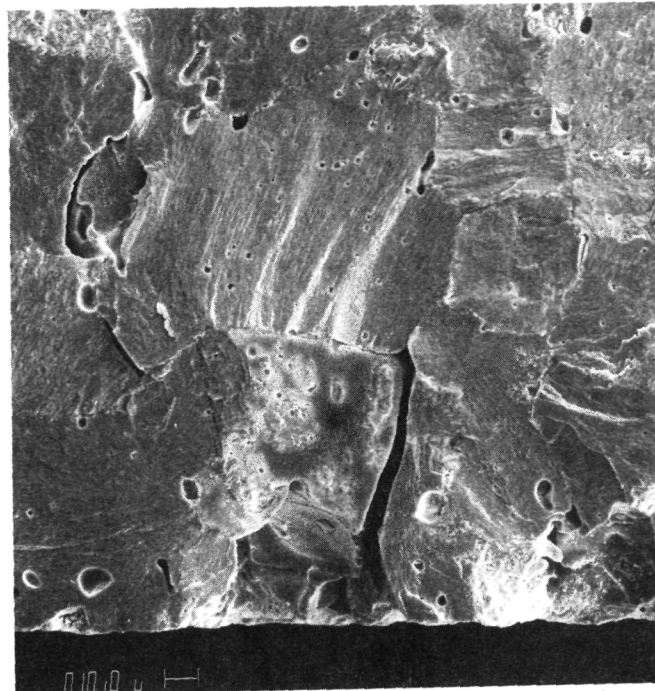


Figure 1. Schematic of Stress Distributions Resulting from Uniaxial and Biaxial Loading at a Contact Surface.

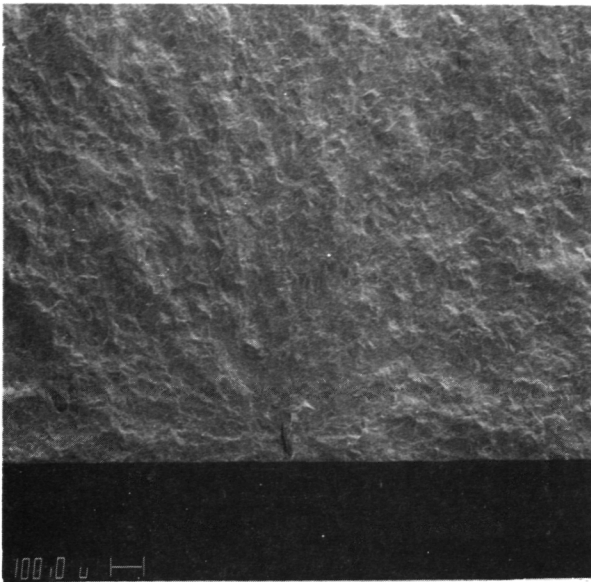


40x

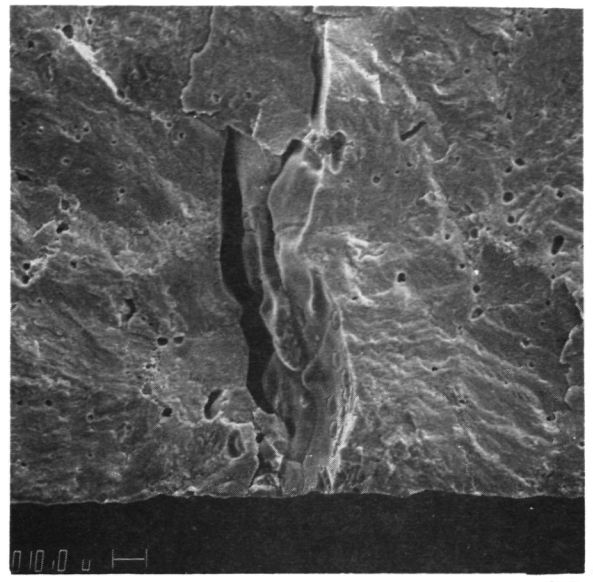


400x

Figure 2. Nilsen TTZ 1093°C (2000°F) Baseline
Flexure Fracture Origin, Specimen 11955.

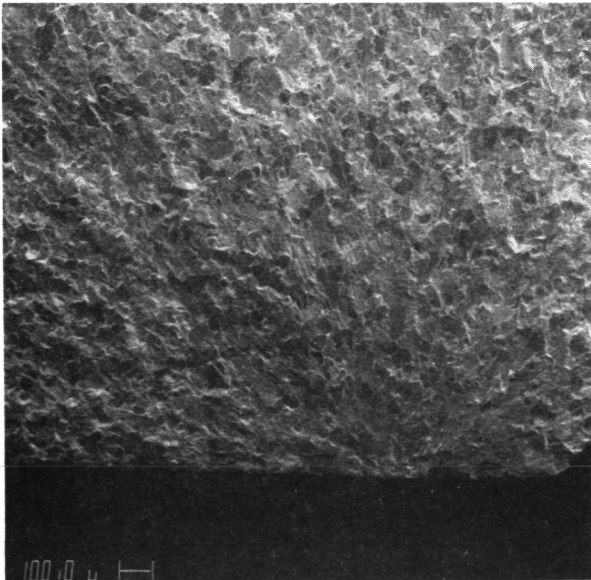


40x

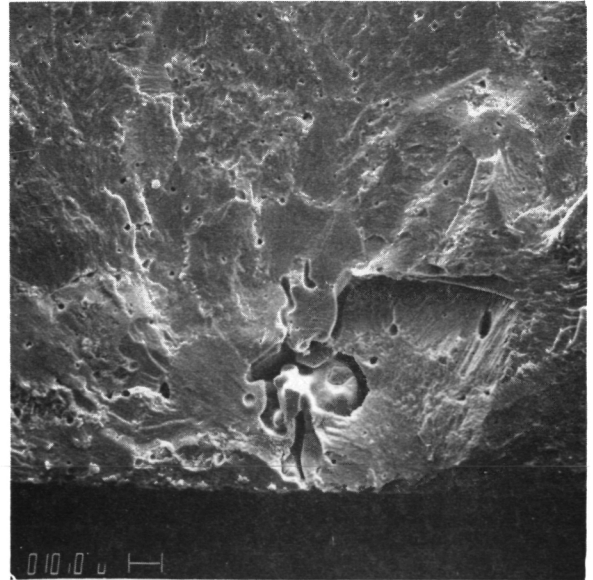


400x

S/N 11877



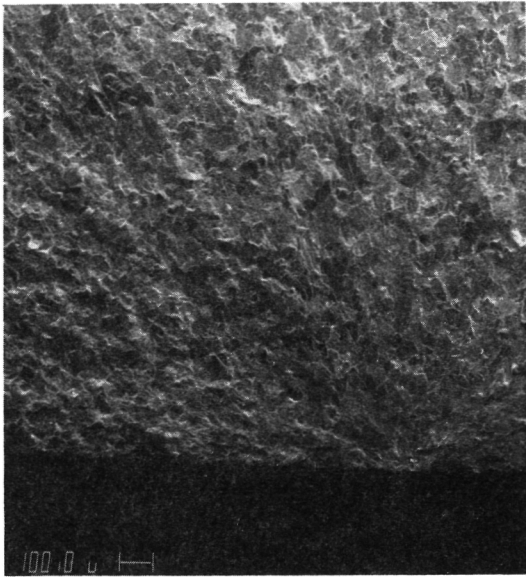
40x



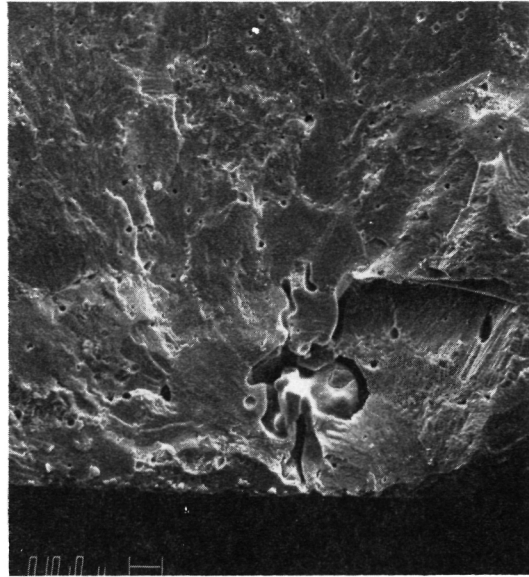
400x

S/N 11896

Figure 3. Nilsen TTZ Room Temperature Baseline Flexure Fracture Origin, Specimen 11877.

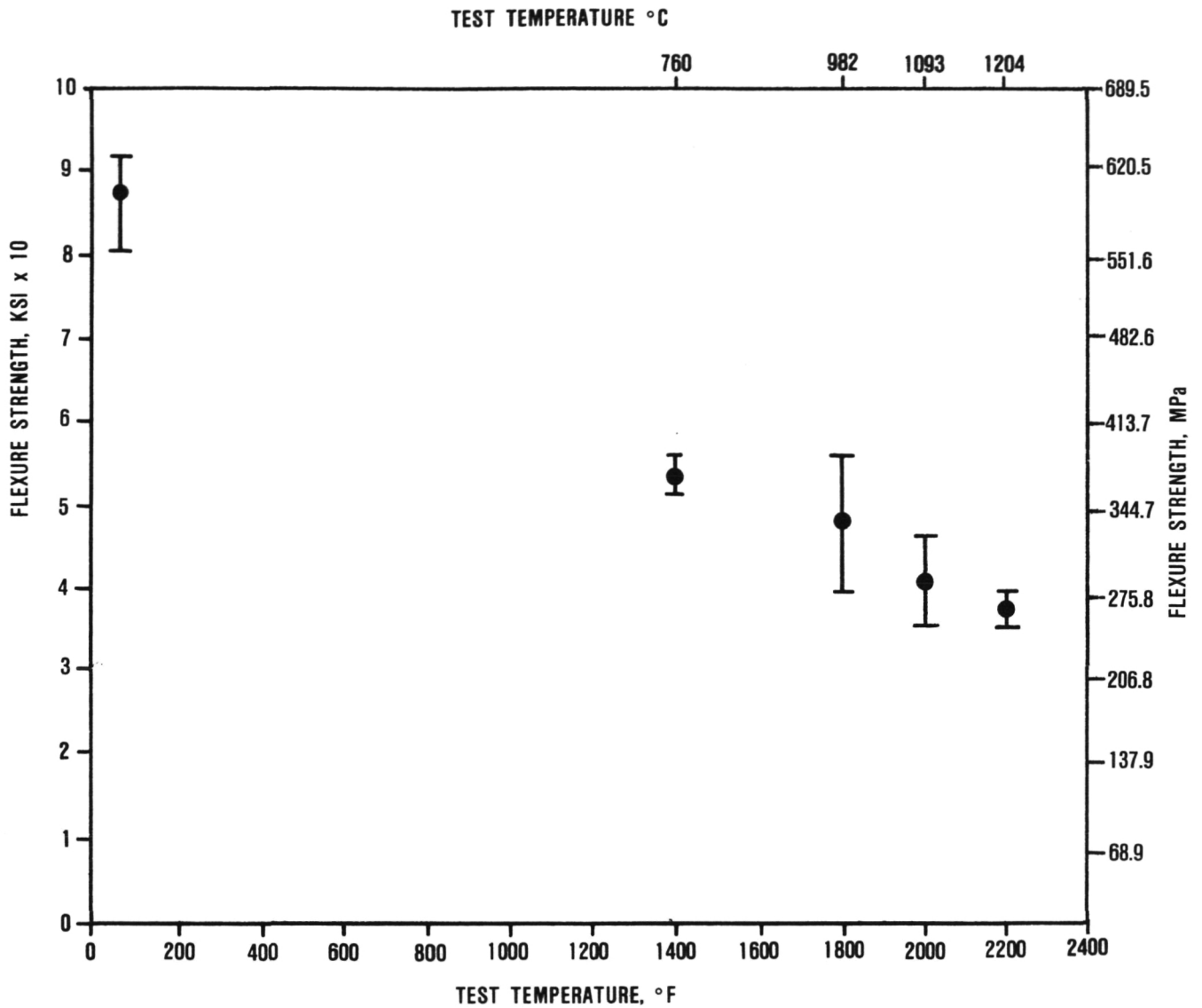


40x



400x

Figure 4. Nilsen TTZ 1204°C (2200°F) Baseline
Flexure Fracture Origin, Specimen 11896.



NOTE: BARS DENOTE RANGE OF STRENGTH VALUES

Figure 5. Baseline Flexure Strength of Nilsen TTZ.

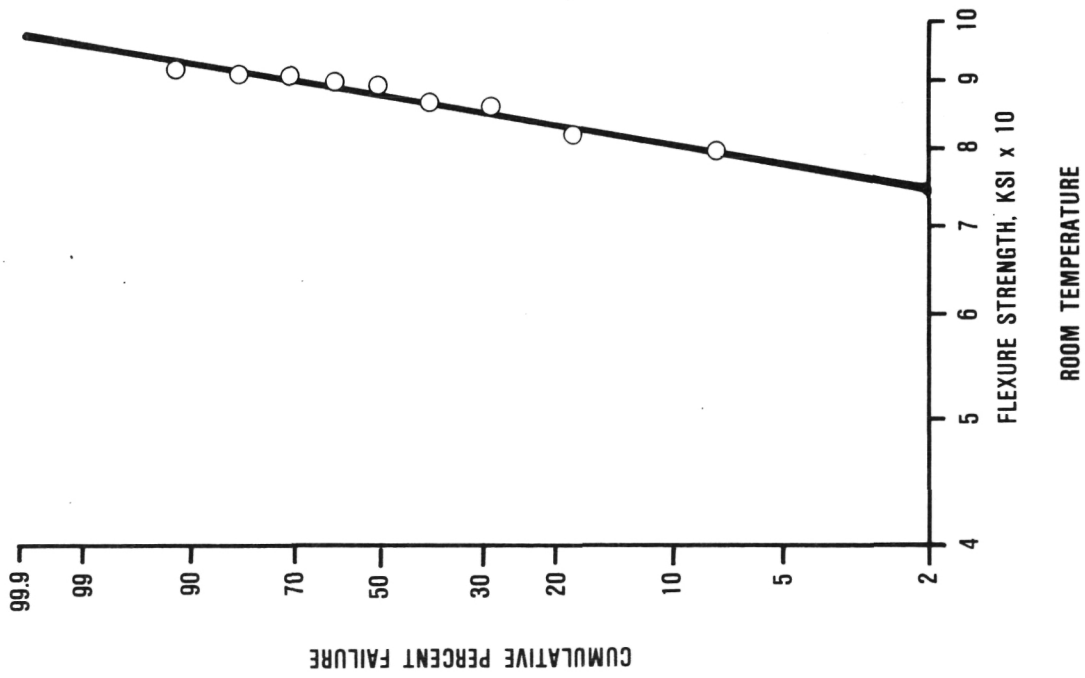
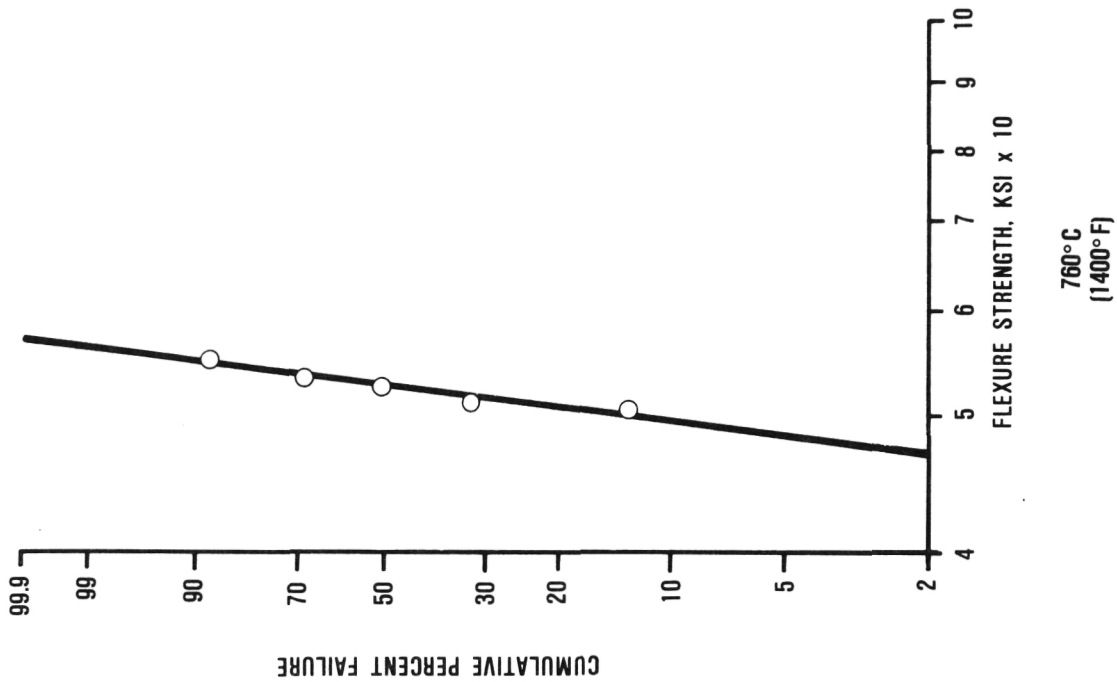


Figure 6. Nilsen TTZ Weibull Plots for Baseline Flexure Strength Data.

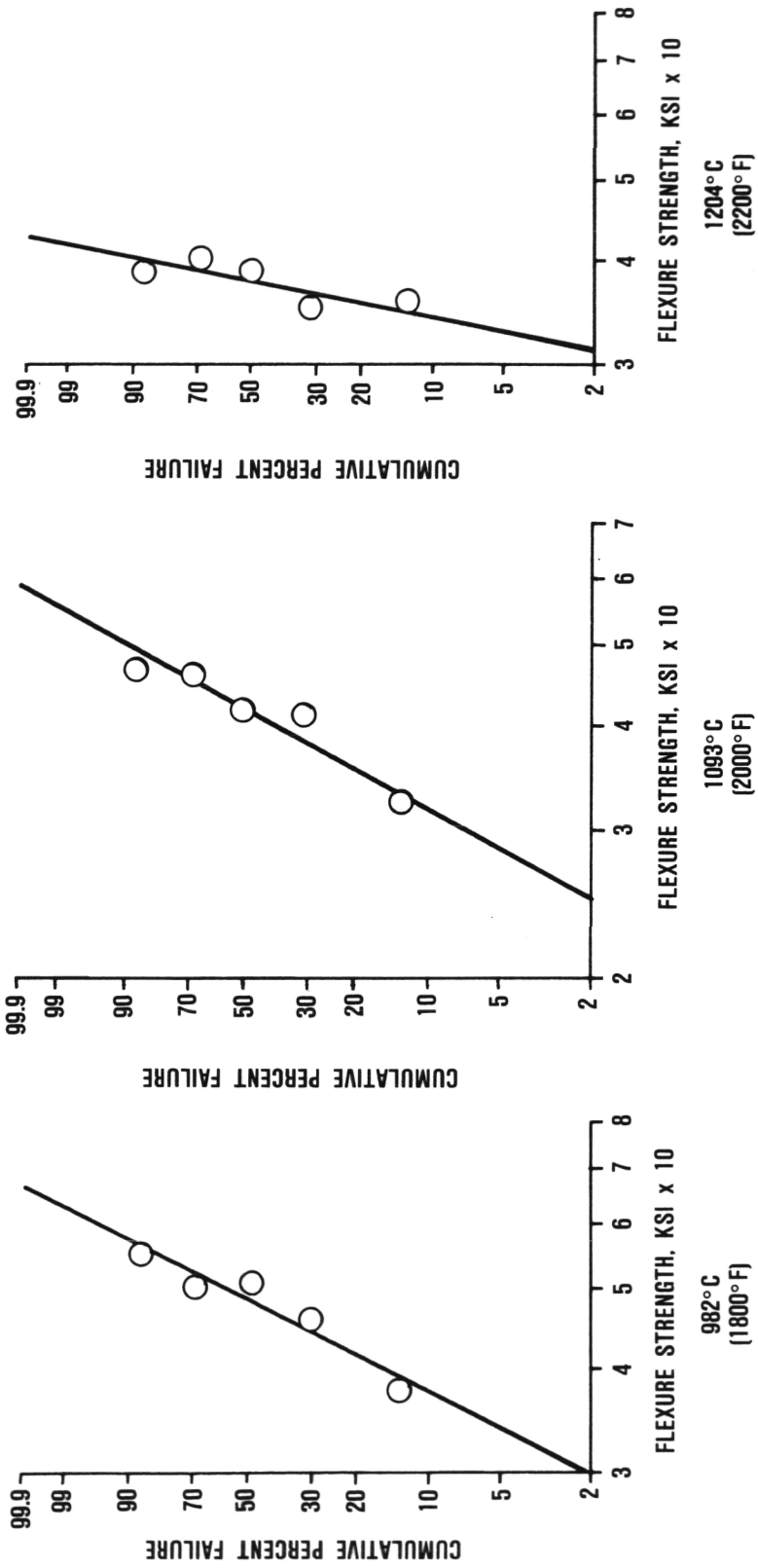
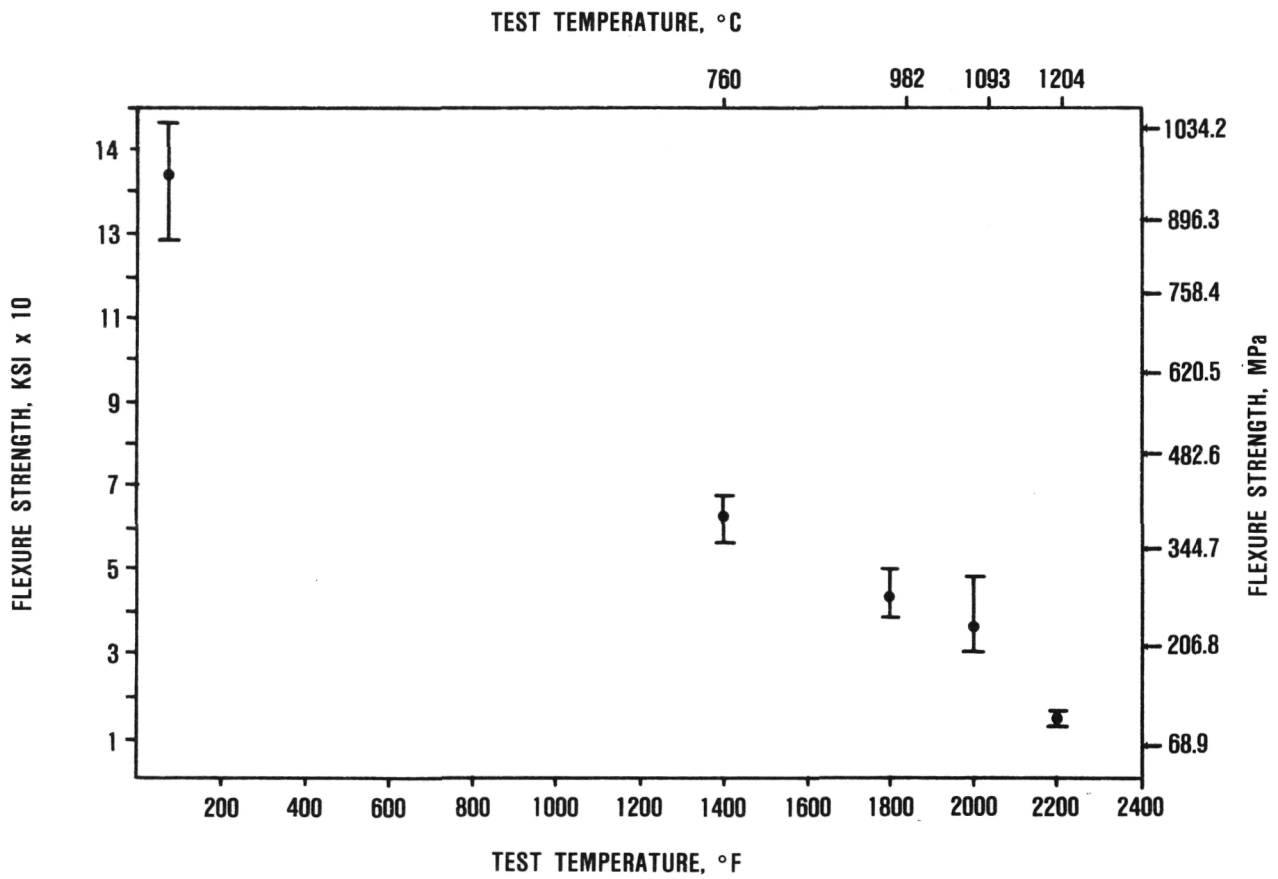
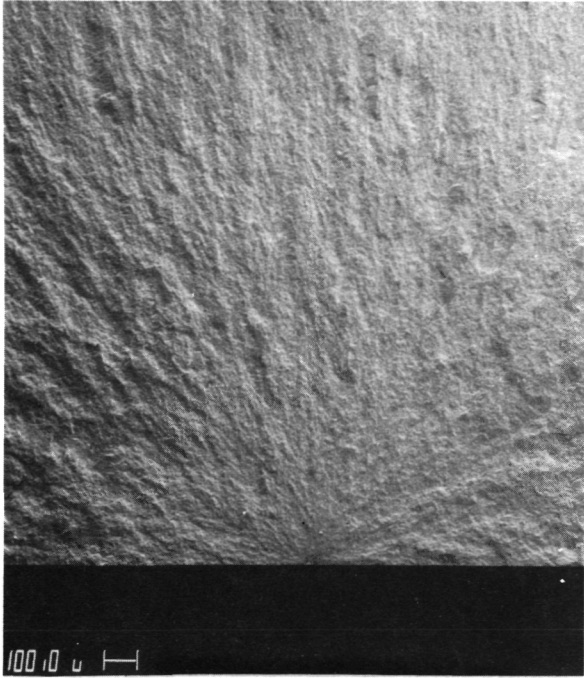


Figure 7. Nilsen TTZ Weibull Plots for Baseline Flexure Strength Data.

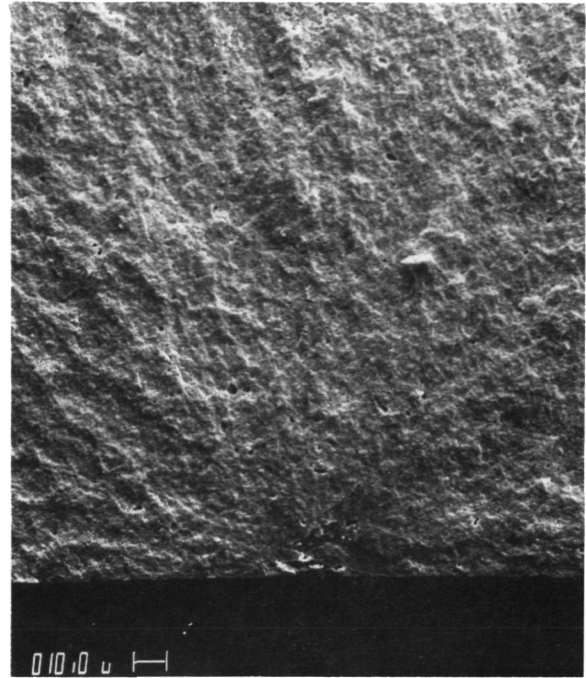


NOTE: BARS DENOTE RANGE OF STRENGTH VALUES

Figure 8. Baseline Flexure Strength of NGK TTZ.

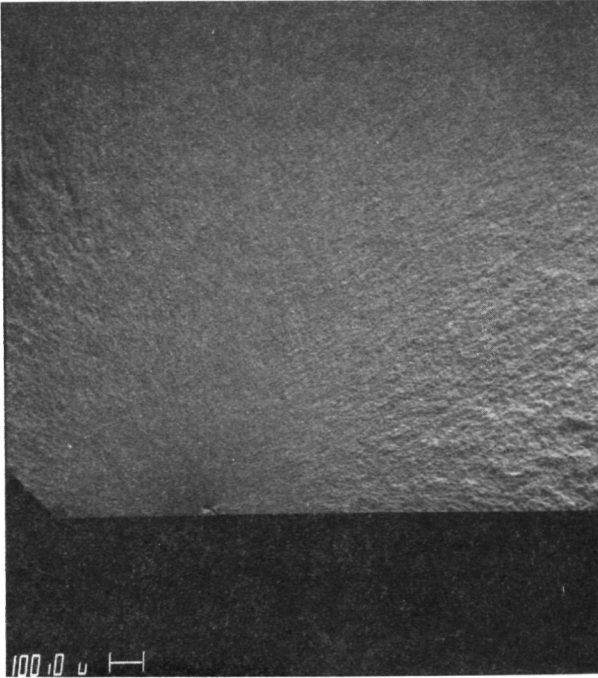


40X

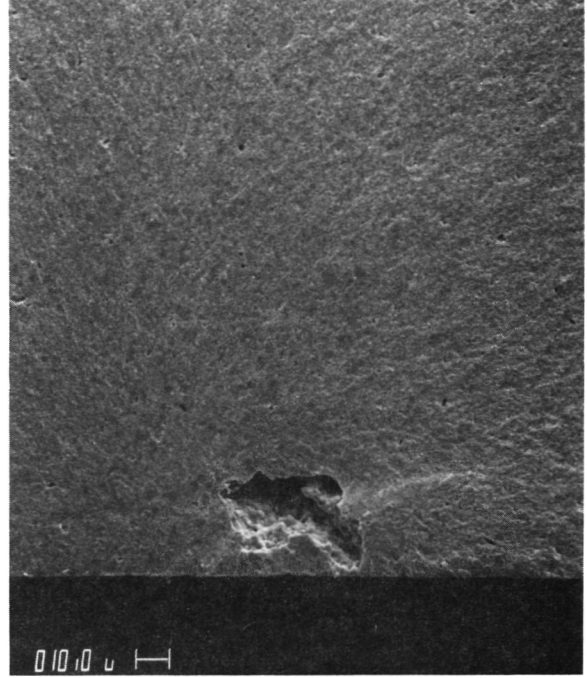


400X

Figure 9. NGK TTZ Room Temperature Baseline Flexure Fracture Origin, Specimen 12389.

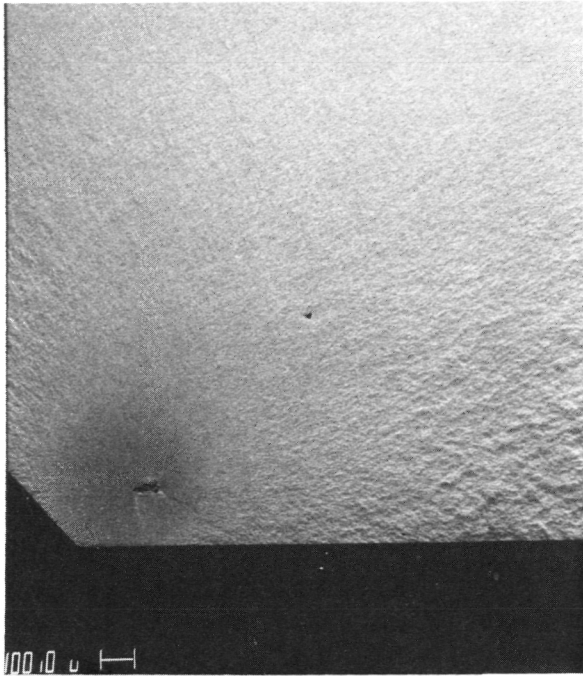


40X

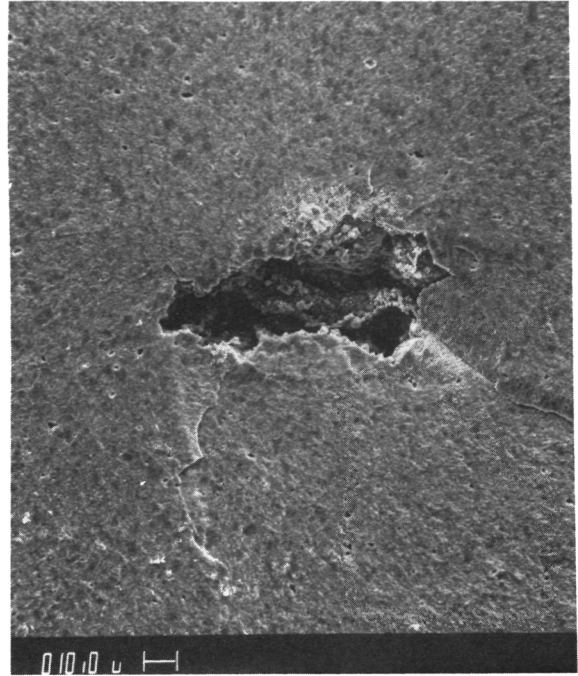


400X

Figure 10. NGK TTZ 760°C (1400°F) Baseline Flexure Fracture Origin, Specimen 12396.



40X

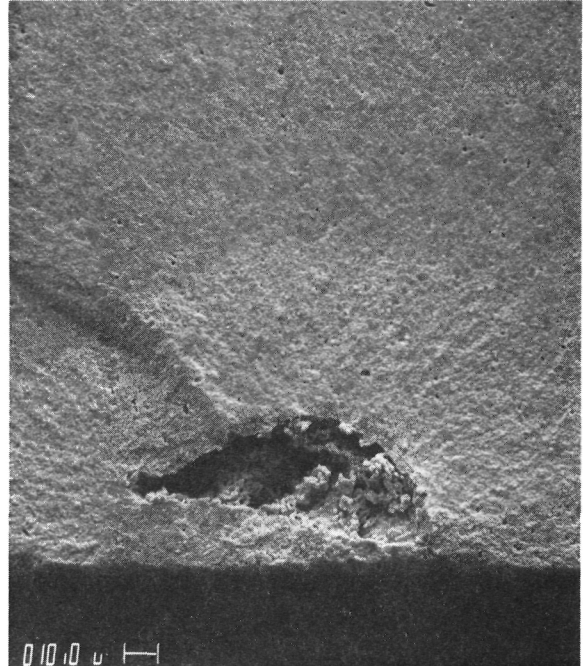


400X

Figure 11. NGK TTZ 982°C (1800°F) Baseline Flexure Fracture Origin, Specimen 12399.

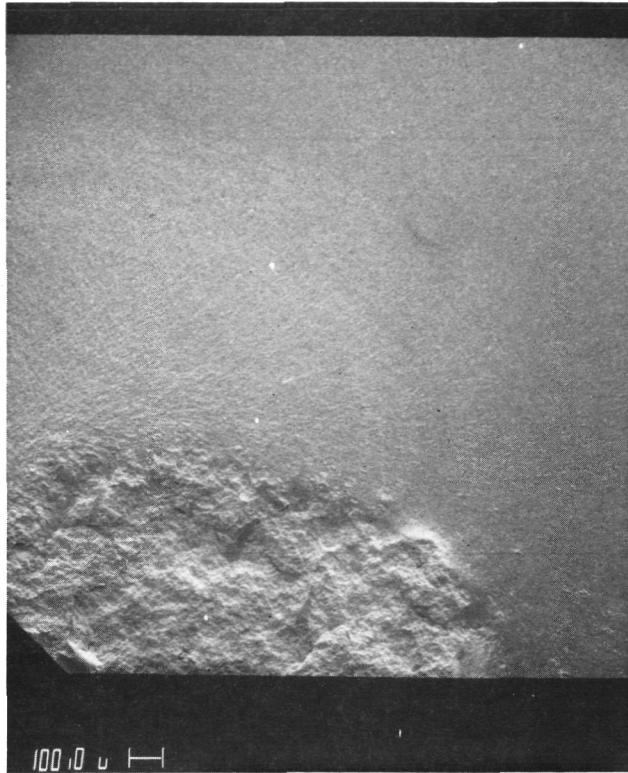


40X



400X

Figure 12. NGK TTZ 1093°C (2000°F) Baseline Flexure Fracture Origin, Specimen 12407.



40X

Figure 13. NGK TTZ 1204°C (2200°F) Baseline Flexure Fracture Origin, Specimen 12409.

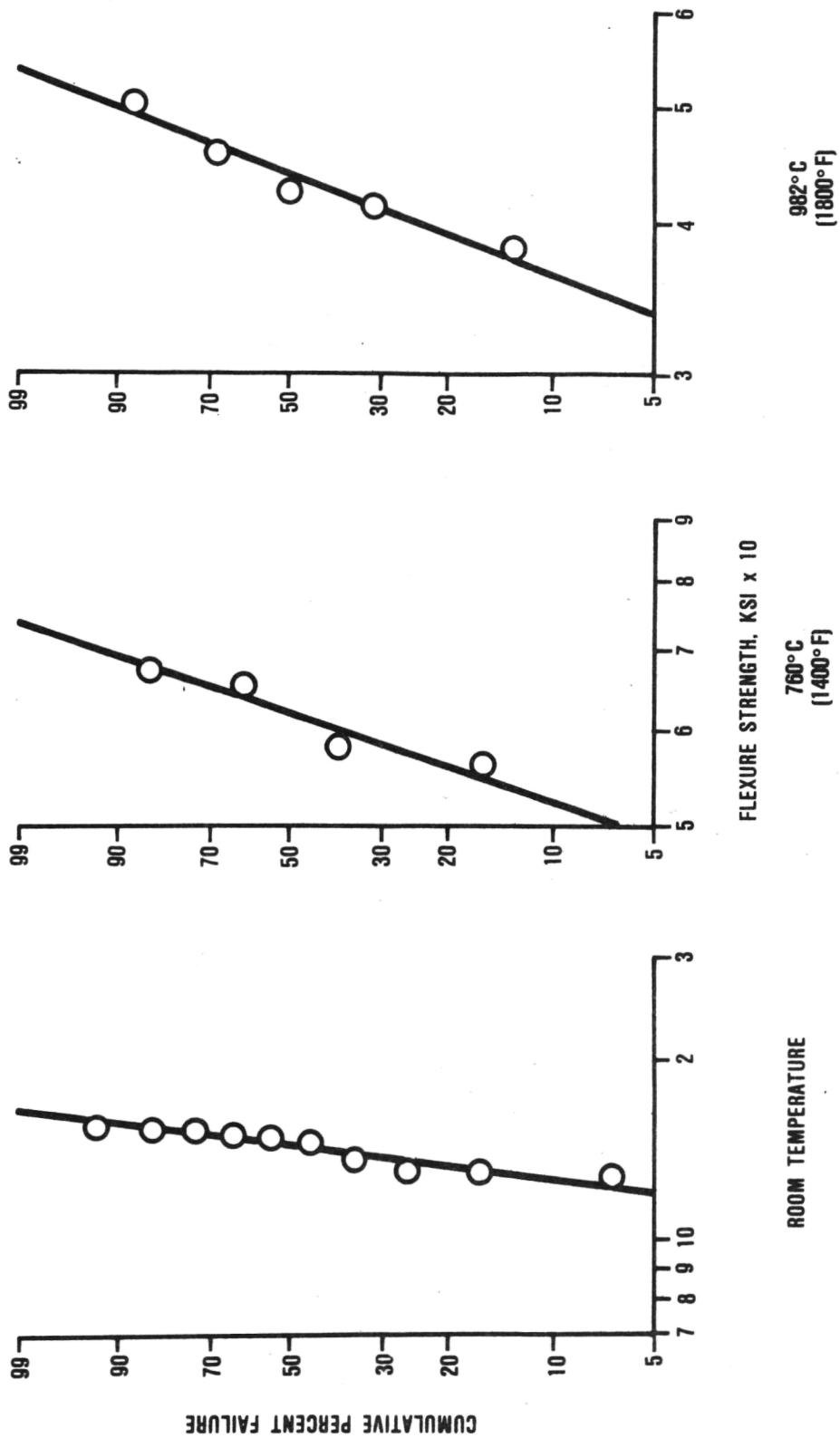


Figure 14. NGK TZT Weibull Plots for Baseline Flexure Strength Data.

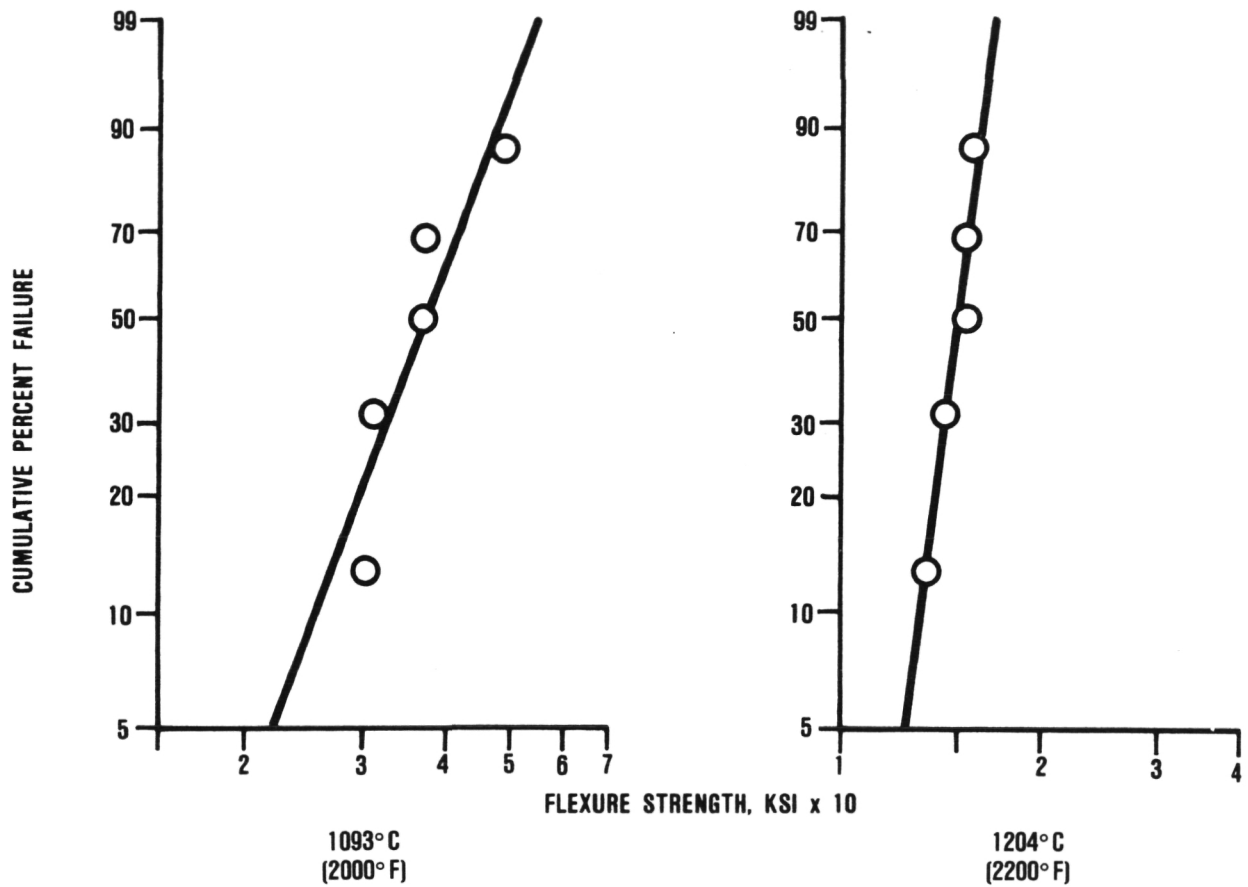
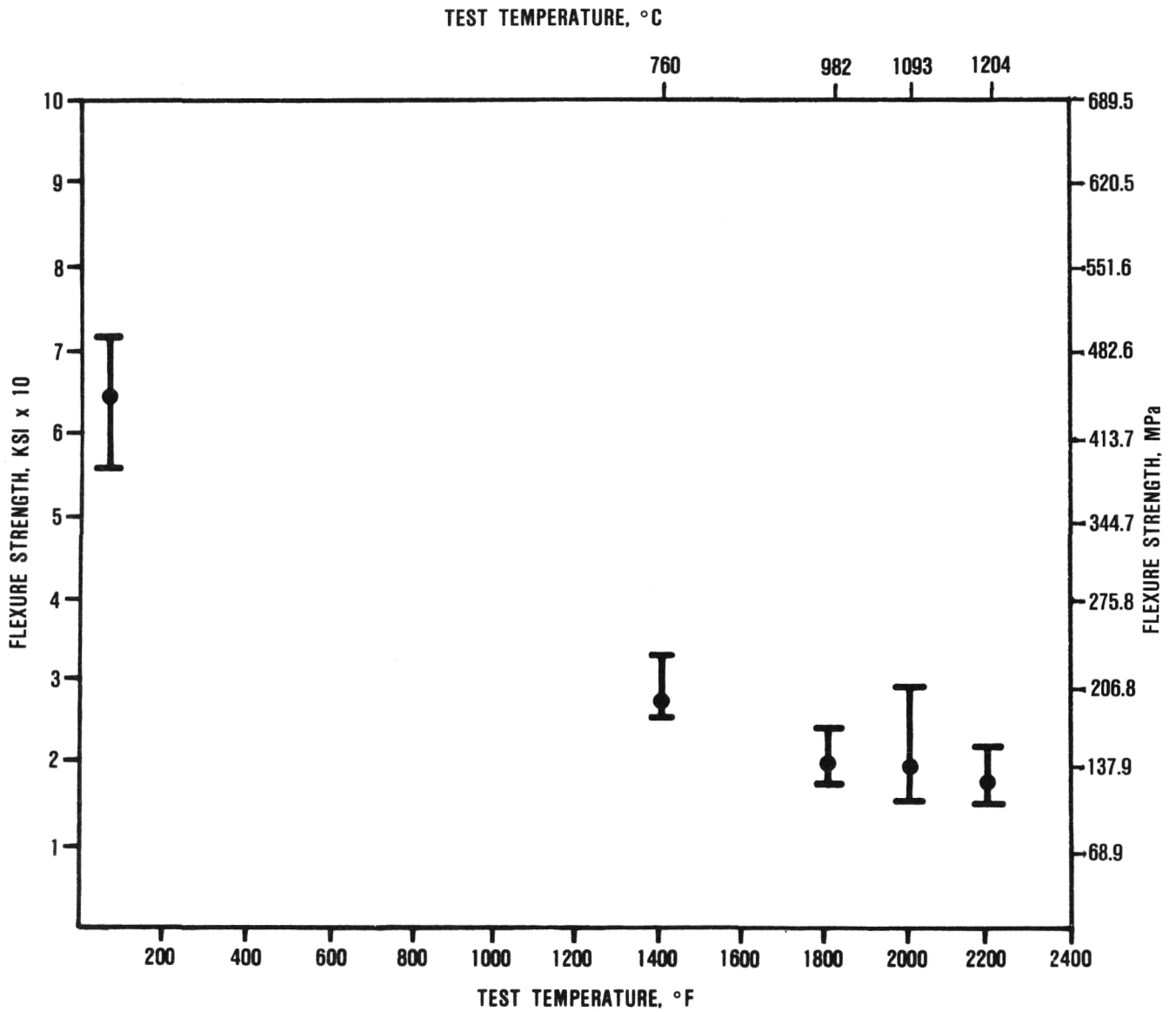


Figure 15. NGK TTZ Weibull Plots for Baseline Flexure Strength Data.



NOTE: BARS DENOTE RANGE OF STRENGTH VALUES

Figure 16. Baseline Flexure Strength of Coors TTZ.

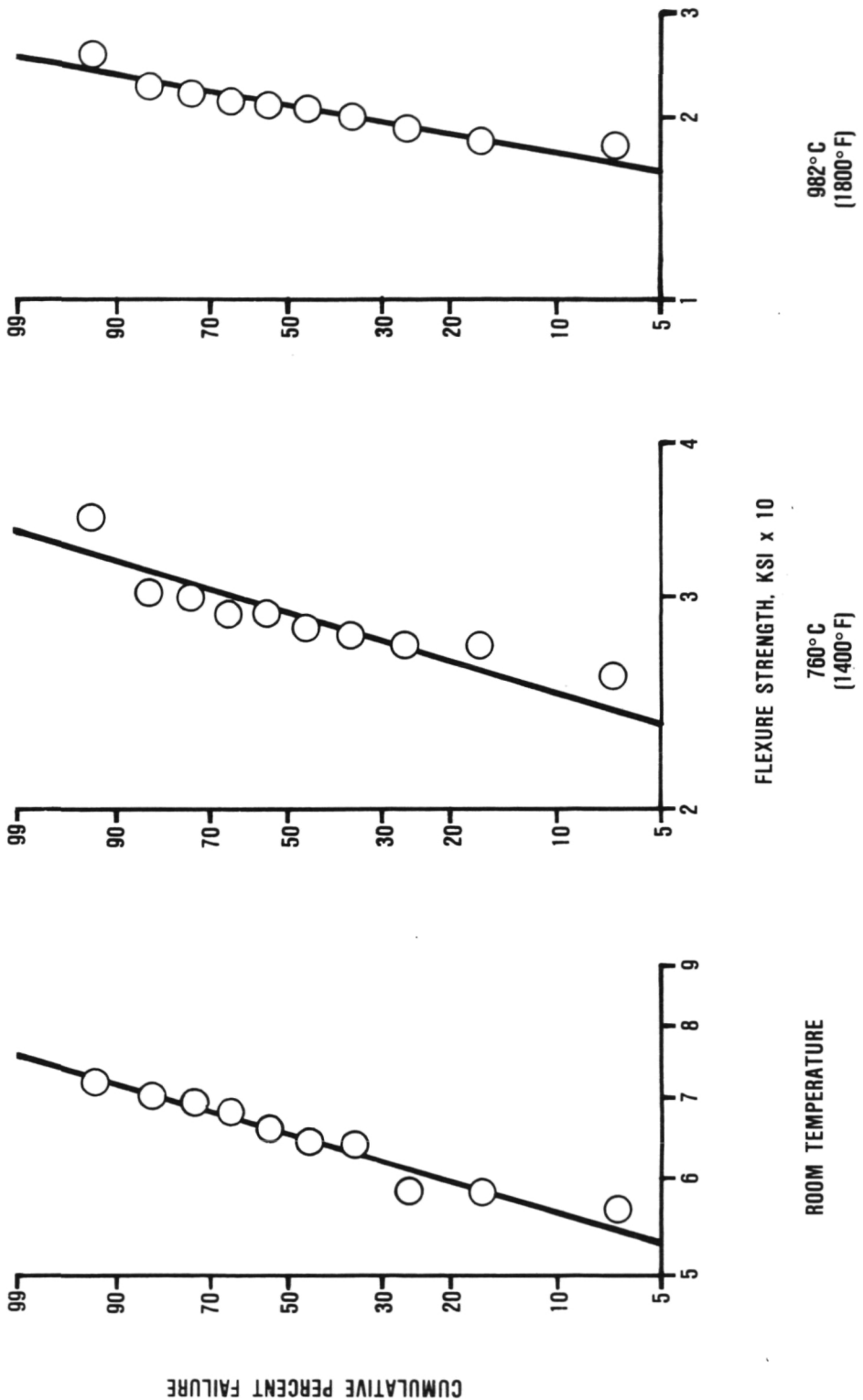


Figure 17. Coors TTZ Weibull Plots for Baseline Flexure Strength Data.

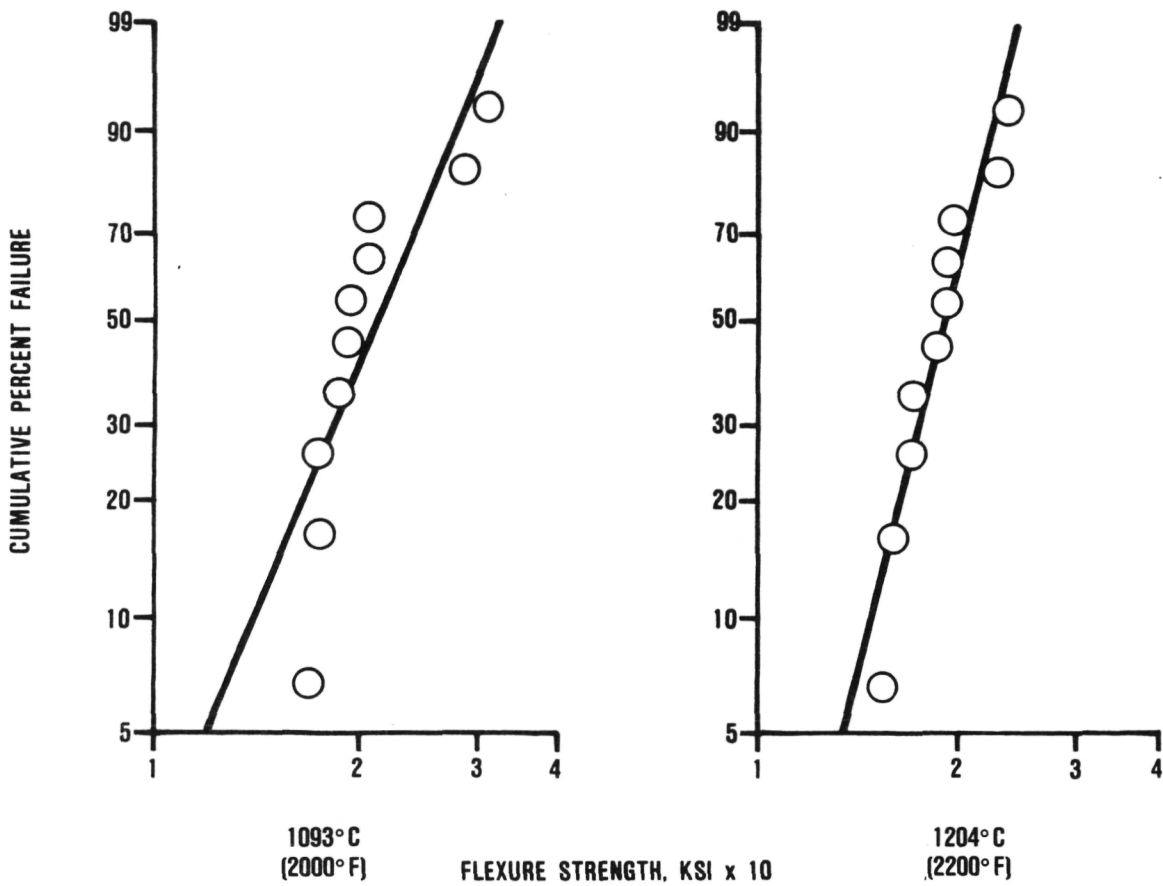
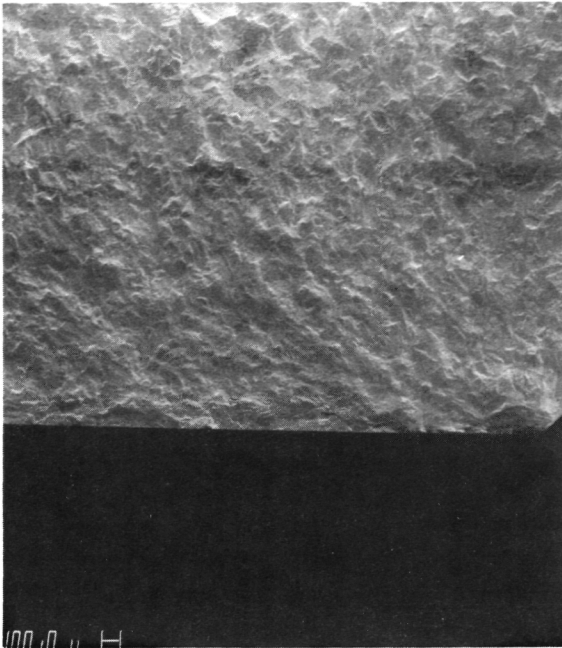
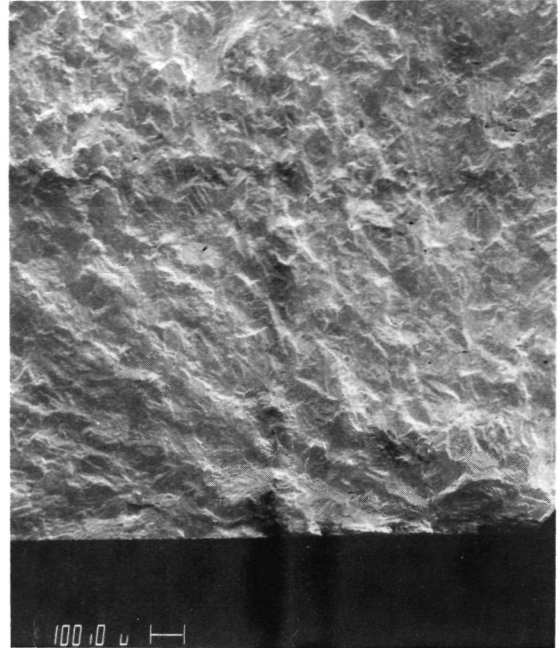


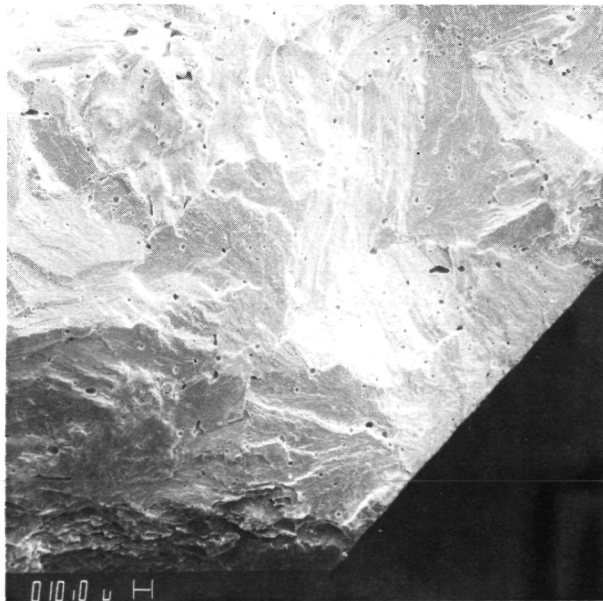
Figure 18. Coors TTZ Weibull Plots for Baseline Flexure Strength Data.



20x

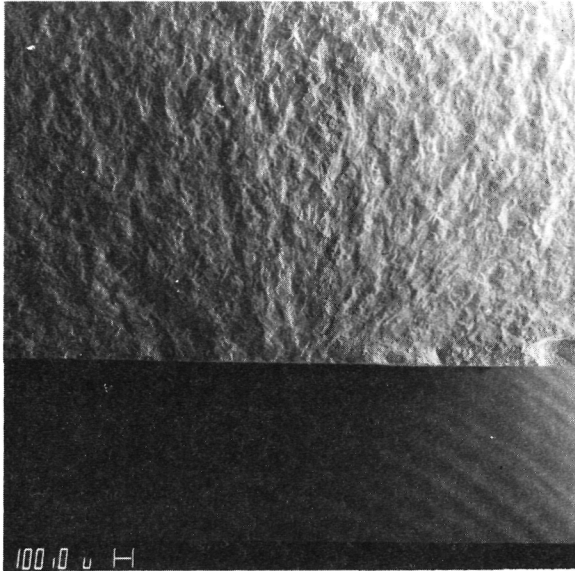


40x

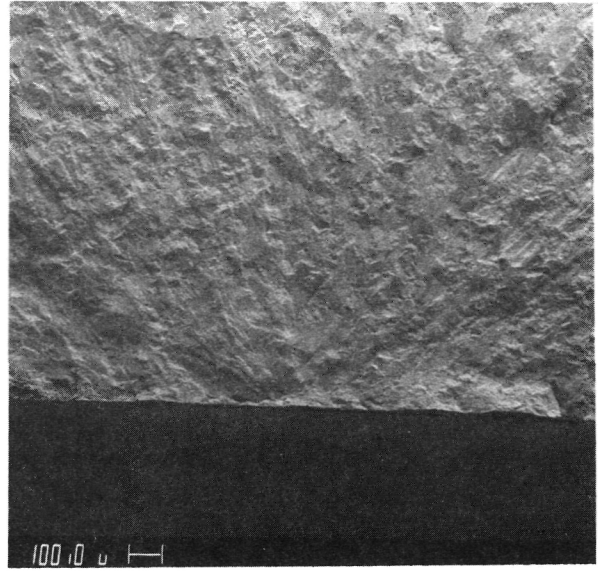


200x

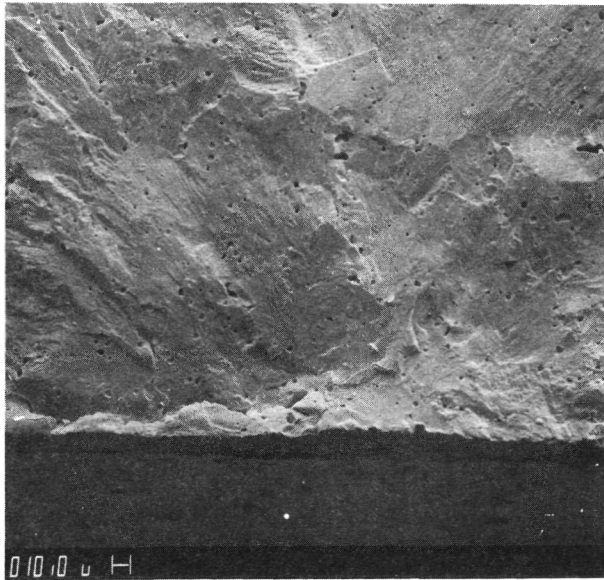
Figure 19. Coors TTZ 760°C (1400°F) Baseline Flexure Fracture Origin, Specimen 13074.



20x

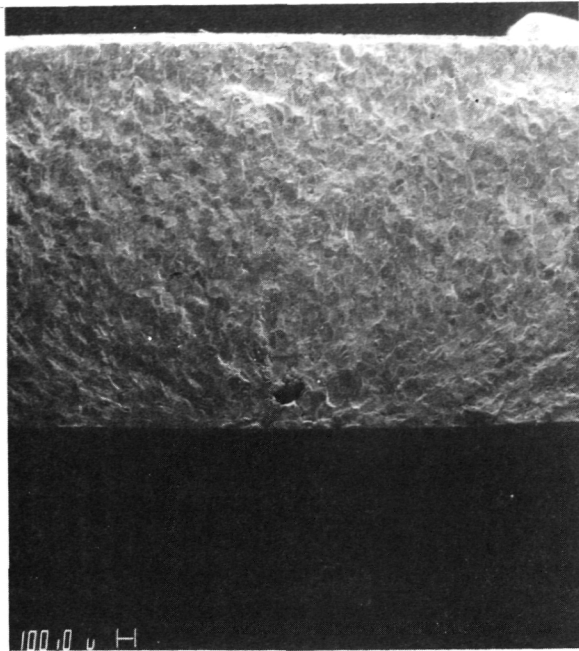


40x

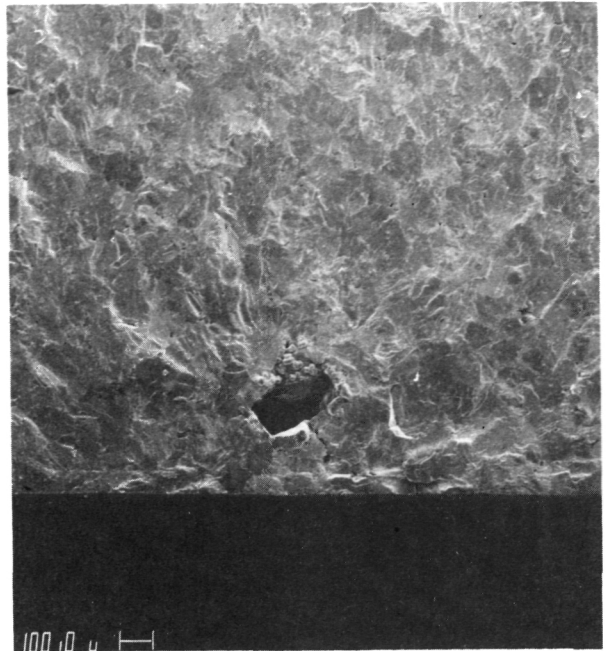


200x

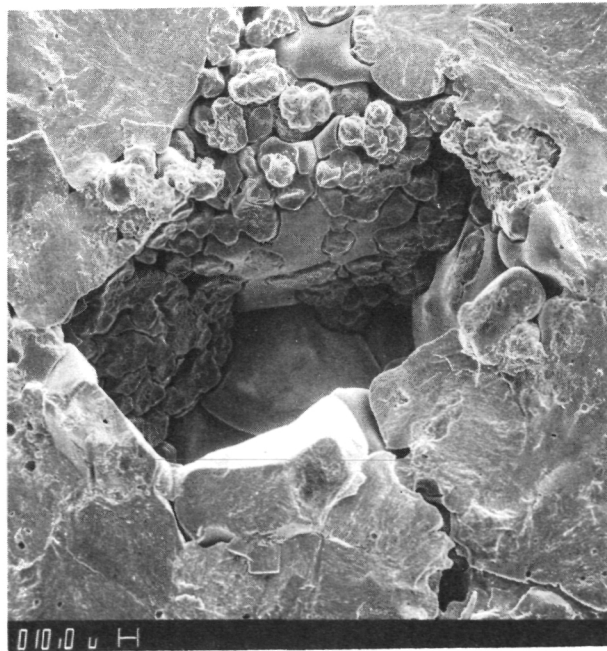
Figure 20. Coors TTZ 1093°C (2000°F) Baseline Flexure Fracture Origin, Specimen 13089.



20x



40x



200x

Figure 21. Coors TTZ 1204°C (2200°F) Baseline Flexure Fracture Origin, Specimen 13106.

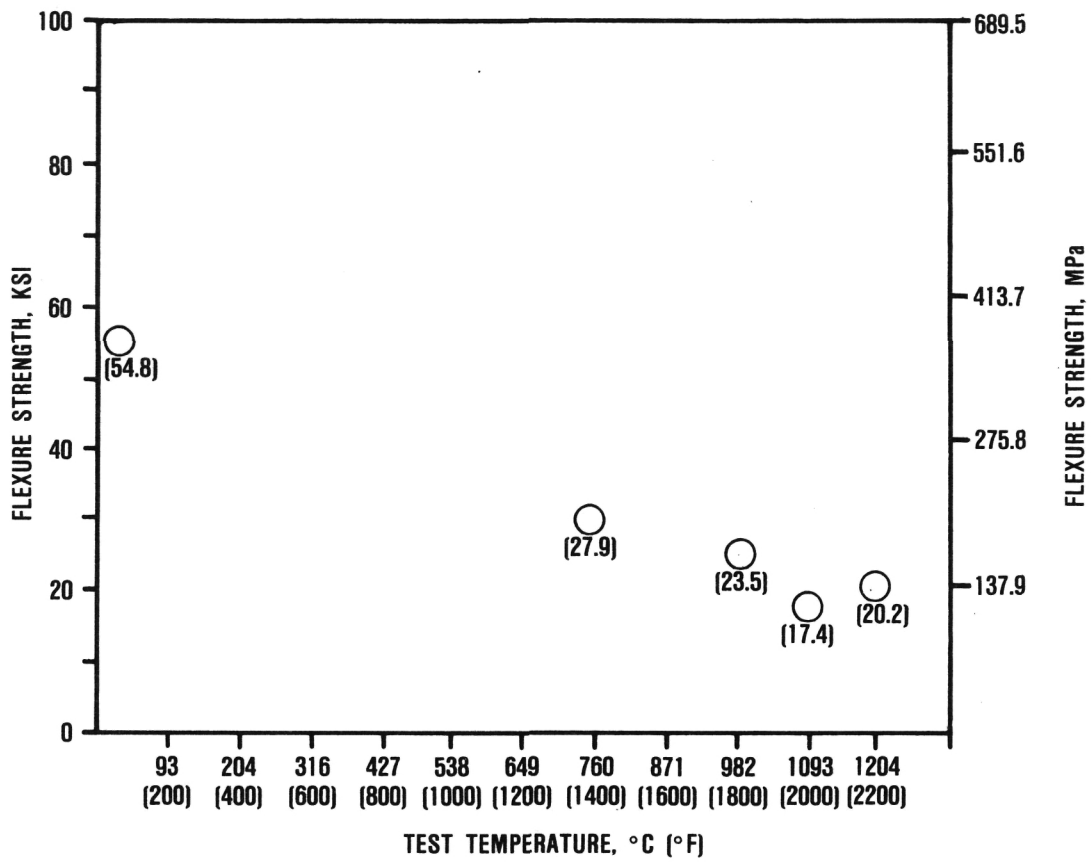


Figure 22. Baseline Four-Point Flexure Strength of Feldmühle TTZ.

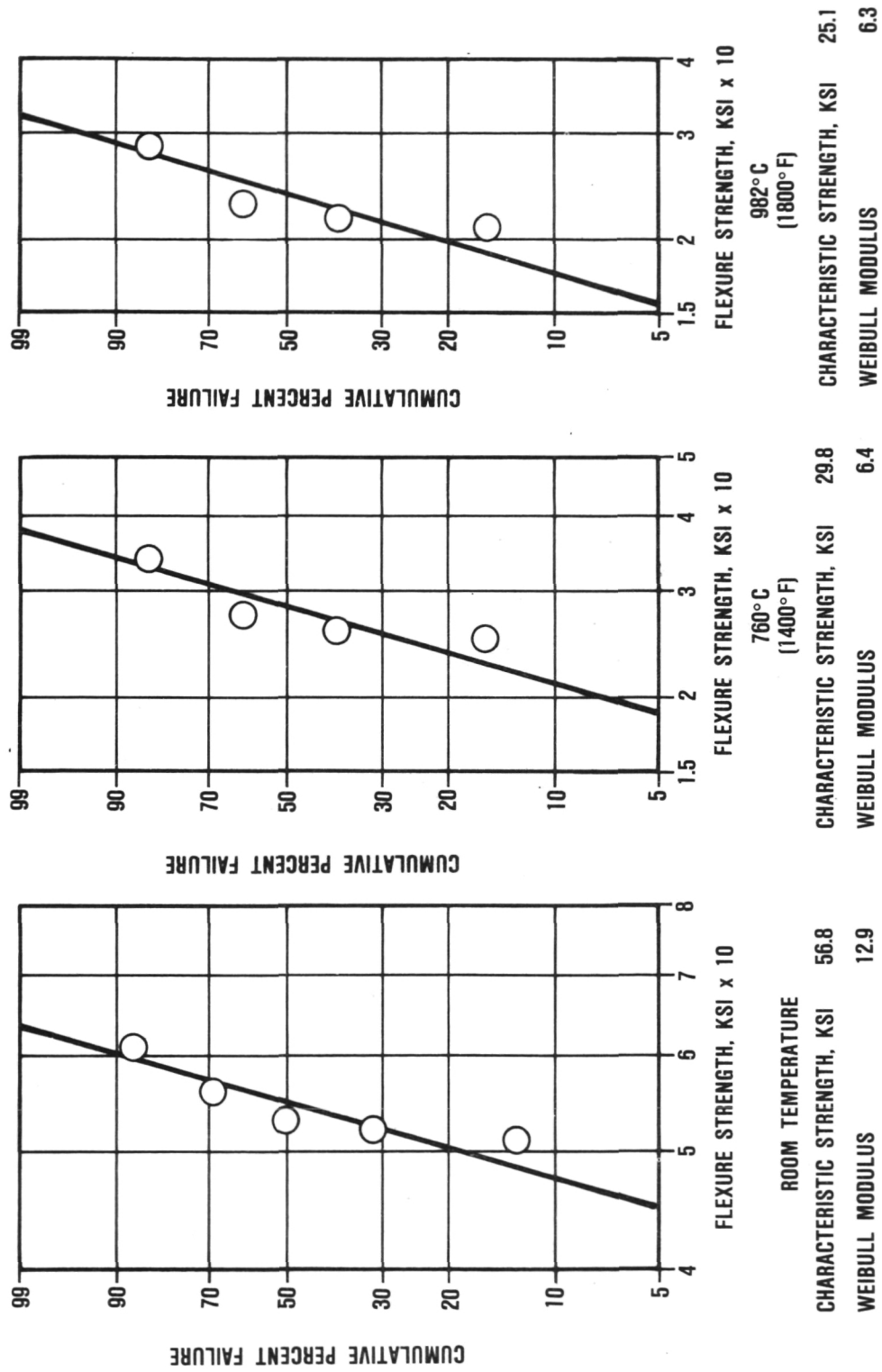


Figure 23. Feldmühle Baseline Weibull Plots.

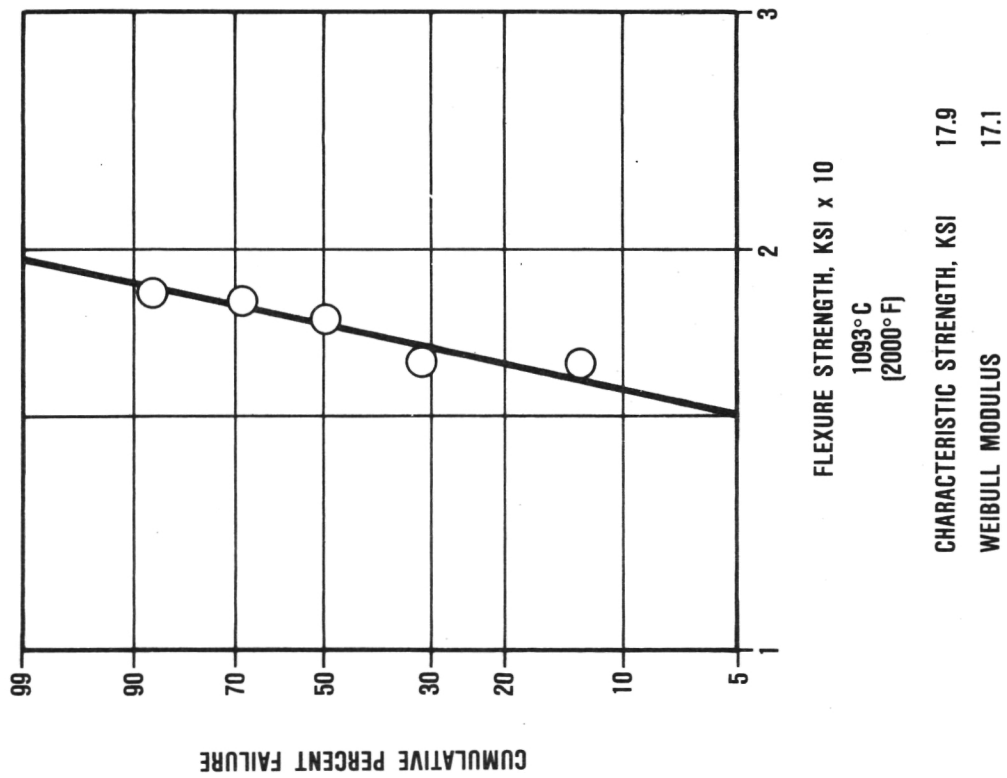
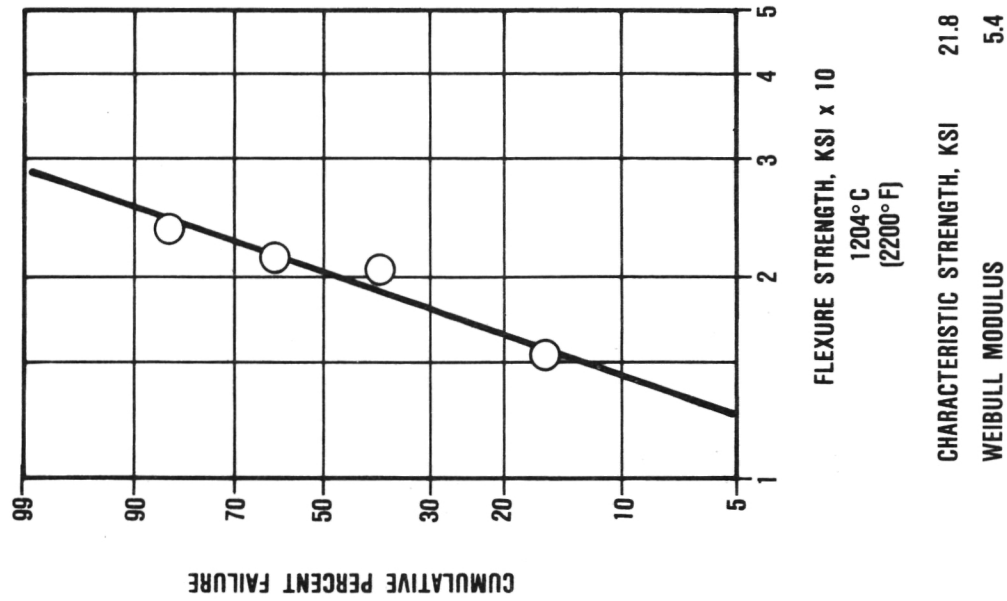
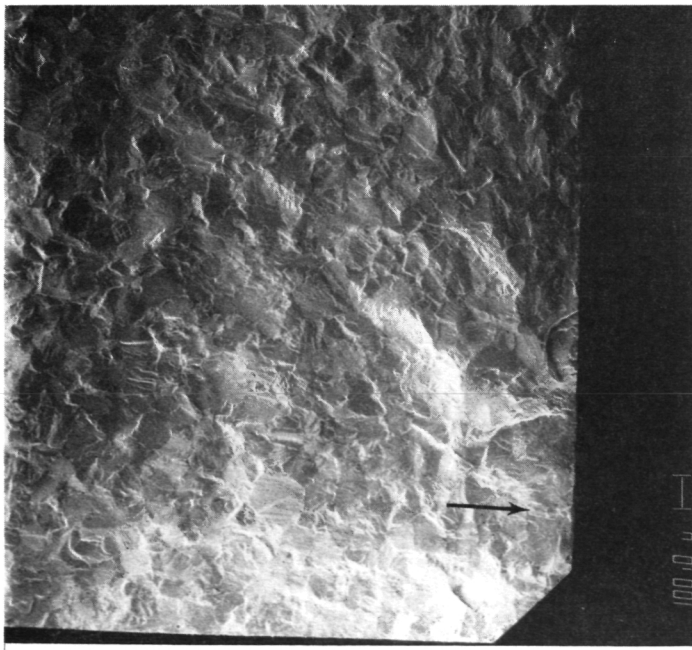
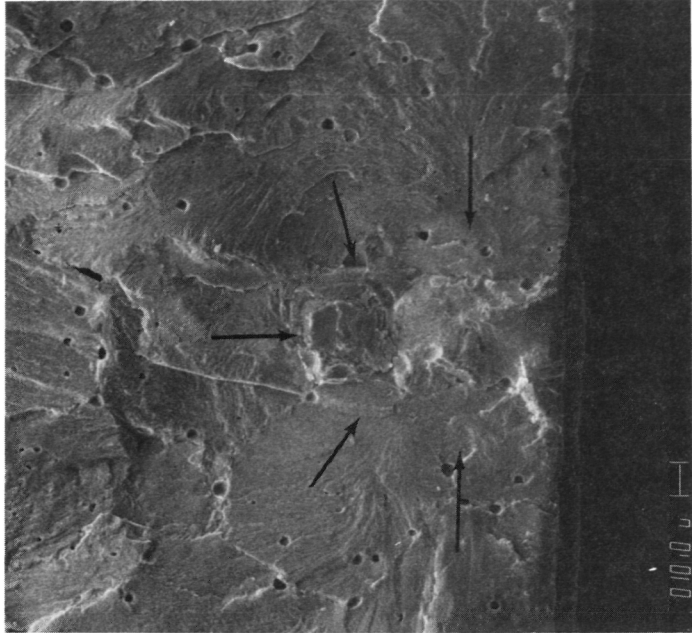


Figure 24. Feldmühle Baseline Weibull Plots.

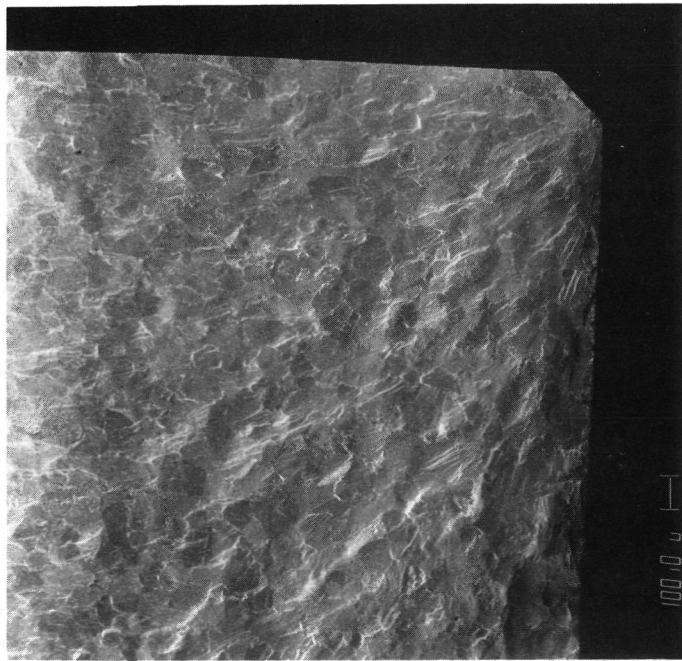


40x



400x

Figure 25. Feldmühle TTZ Baseline 7600C (14000F) Fracture Origin, Specimen 12796.

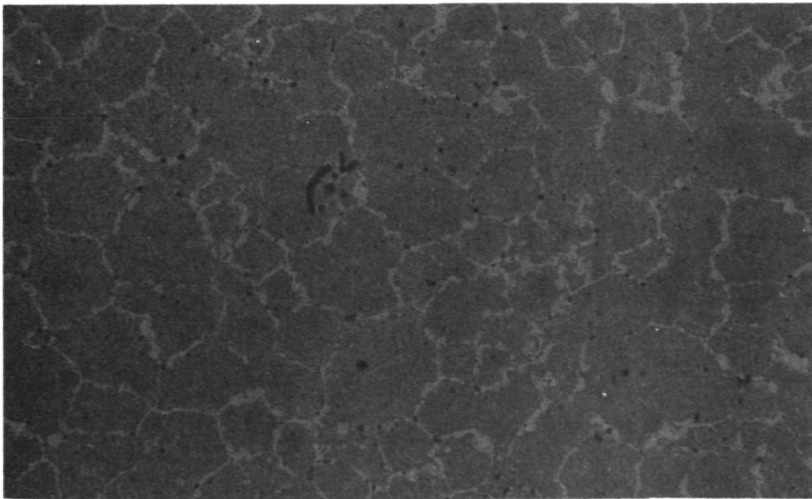


40x

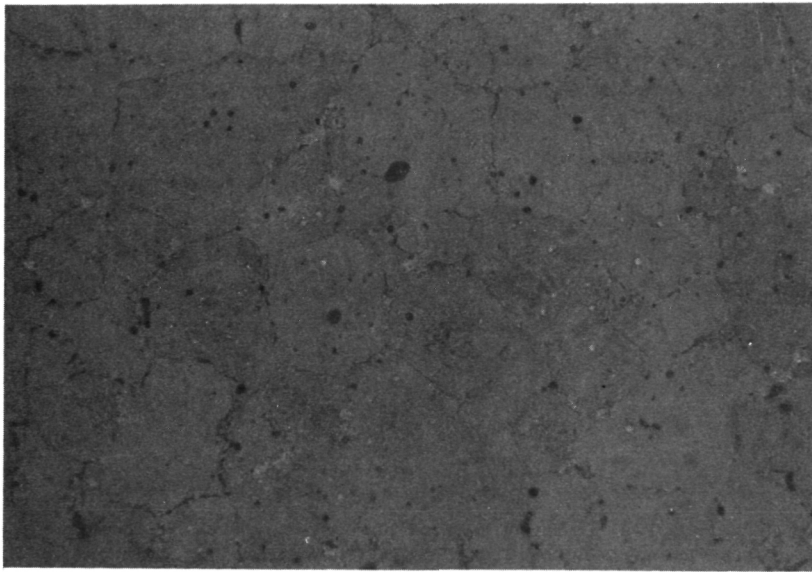


200x

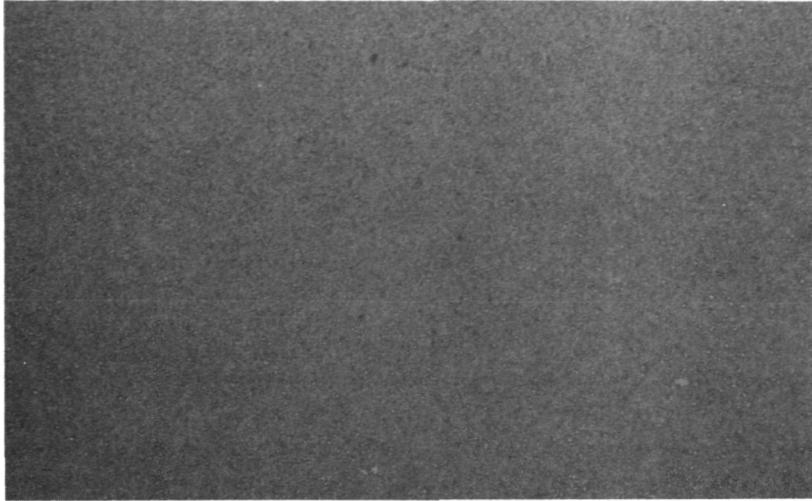
Figure 26. Feldmühle TTZ Baseline 12040C (22000F) Fracture Origin, Specimen 13812.



NILSEN



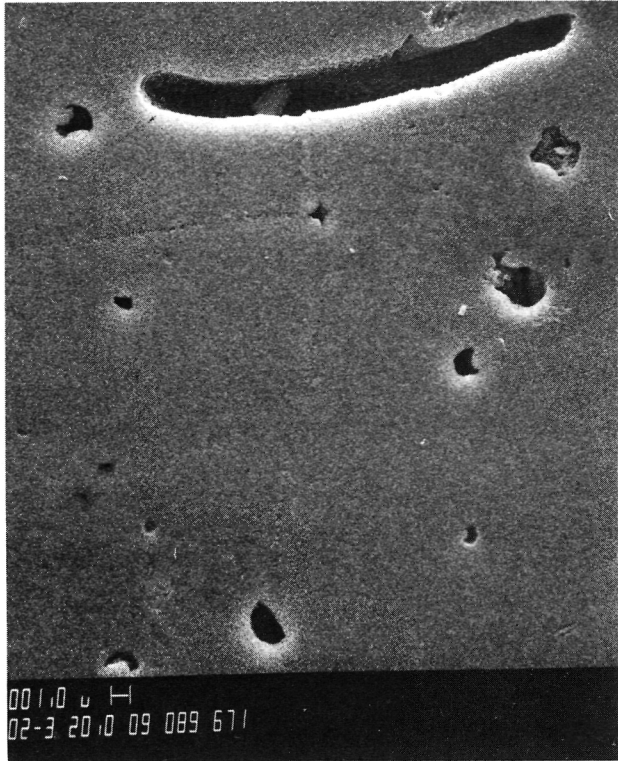
COORS



NGK

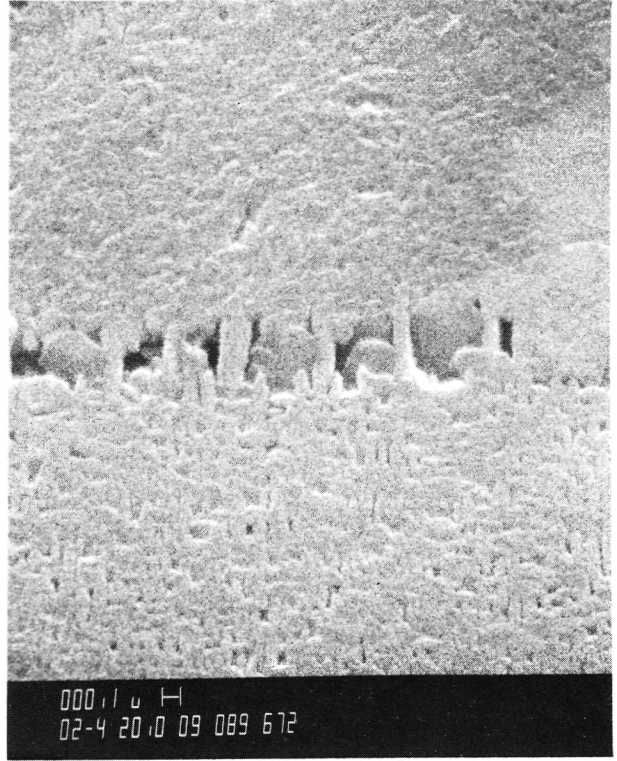
NOTE: ALL SAMPLES ETCHED IN 1.0-PERCENT HF IN HOT PHOSPHORIC ACID

Figure 27. Photomicrographs of Etched TTZ at 200X.



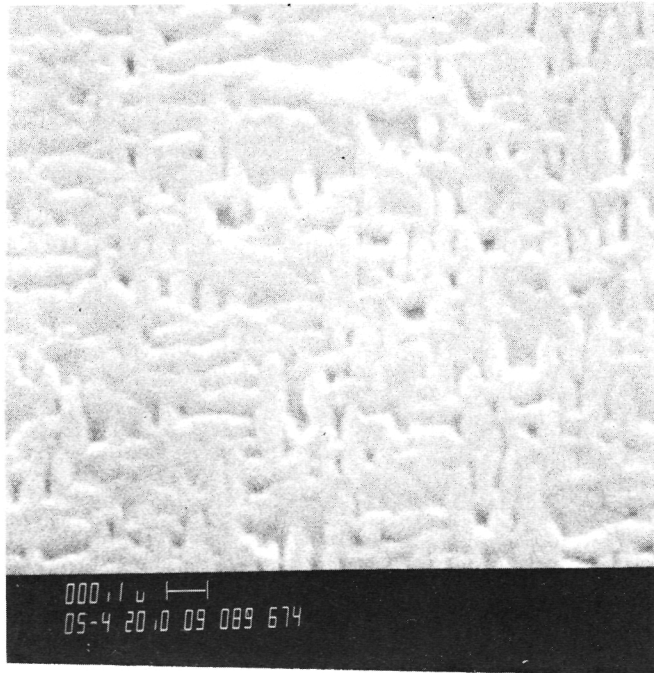
A

2000x



B

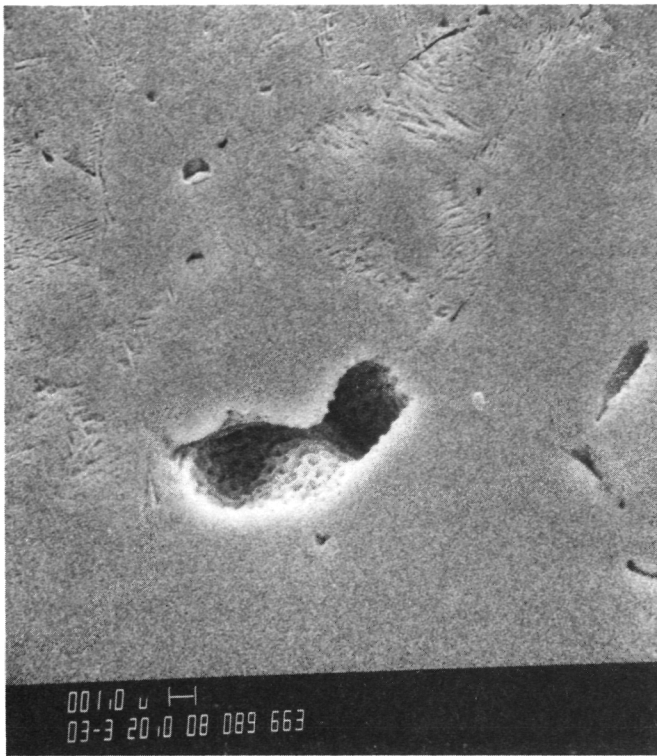
20,000x



C

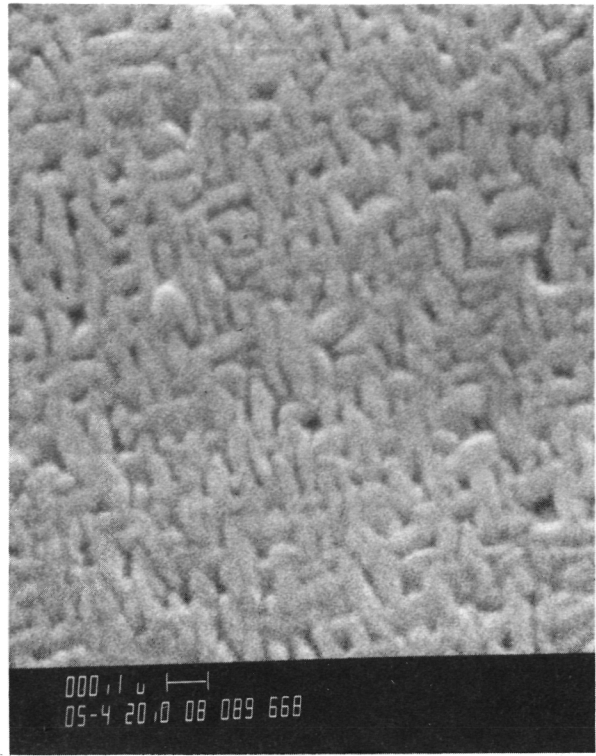
50,000x

Figure 28. Nilsen TTZ Microstructures.



A

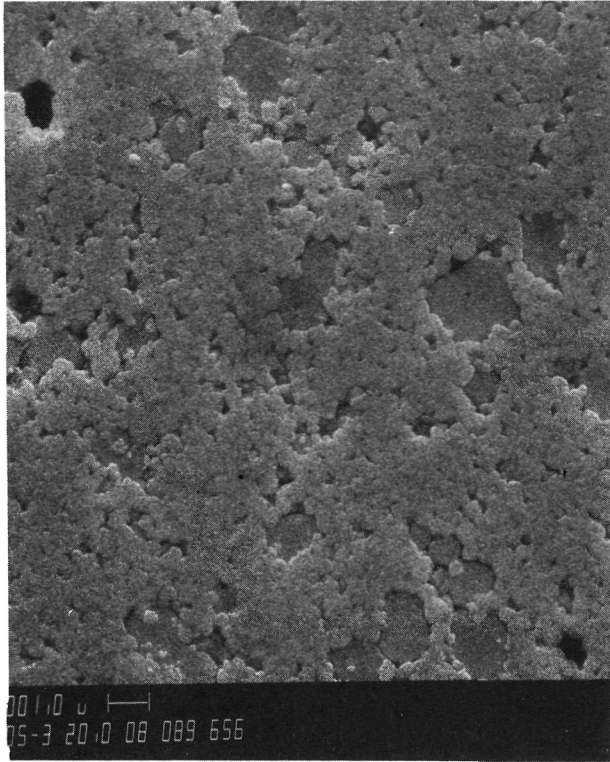
3000x



B

50,000x

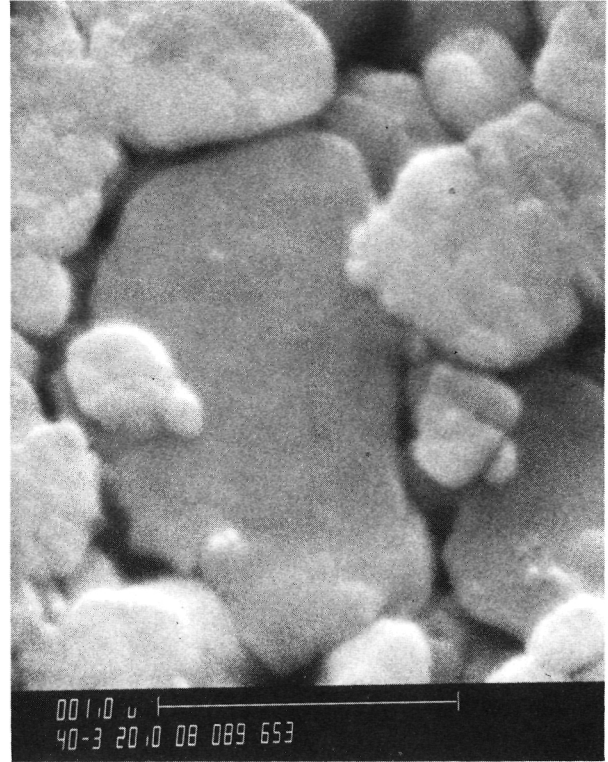
Figure 29. Coors TTZ Microstructure.



5000x

A

NGK



40,000x

B

NGK

Figure 30. NGK TTZ Microstructure.

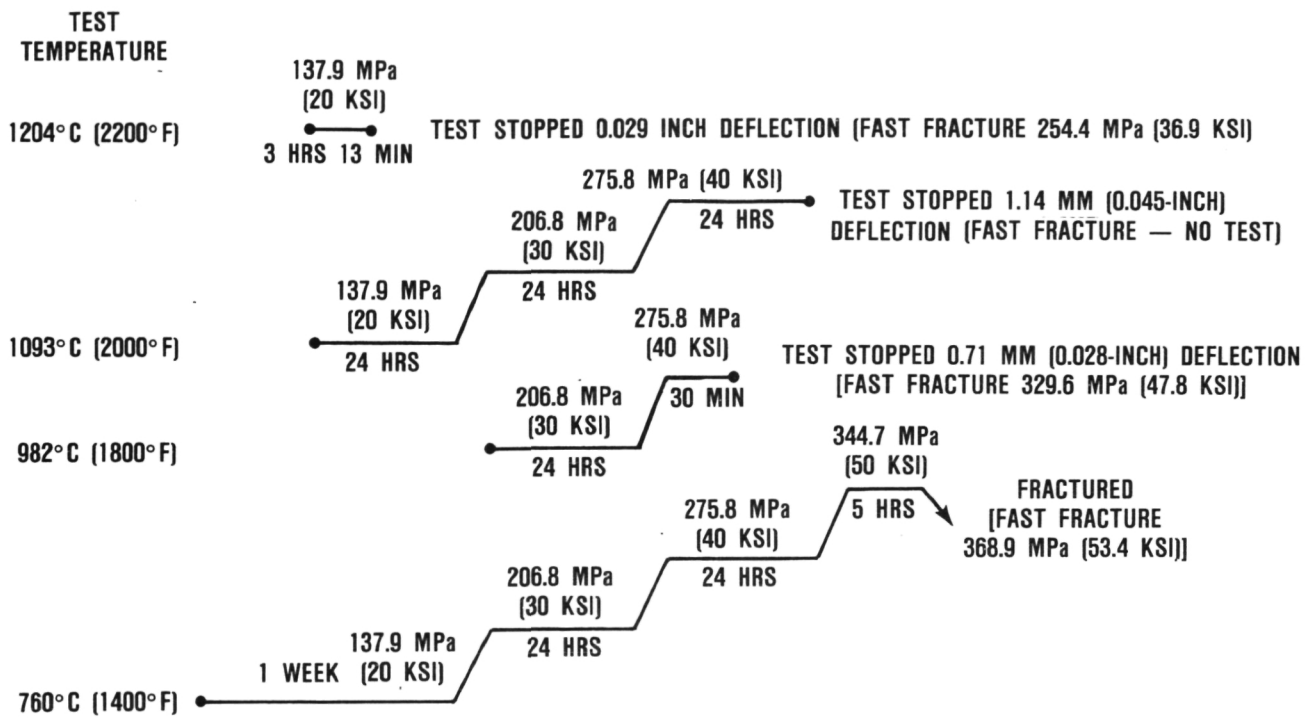


Figure 31. Nilsen TTZ Stepped Stress Rupture Tests.

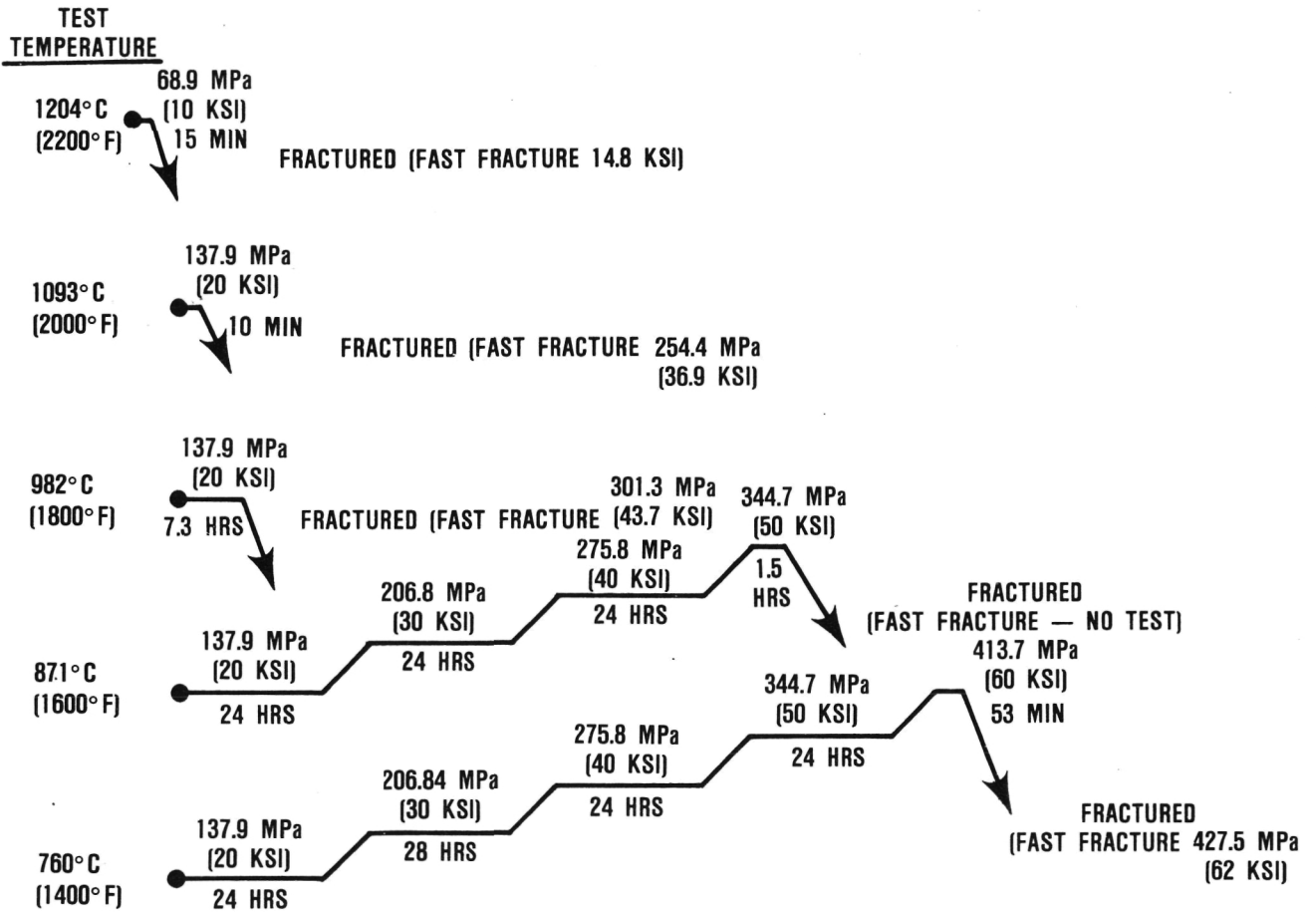


Figure 32. NGK TTZ Stepped Stress Rupture Tests.

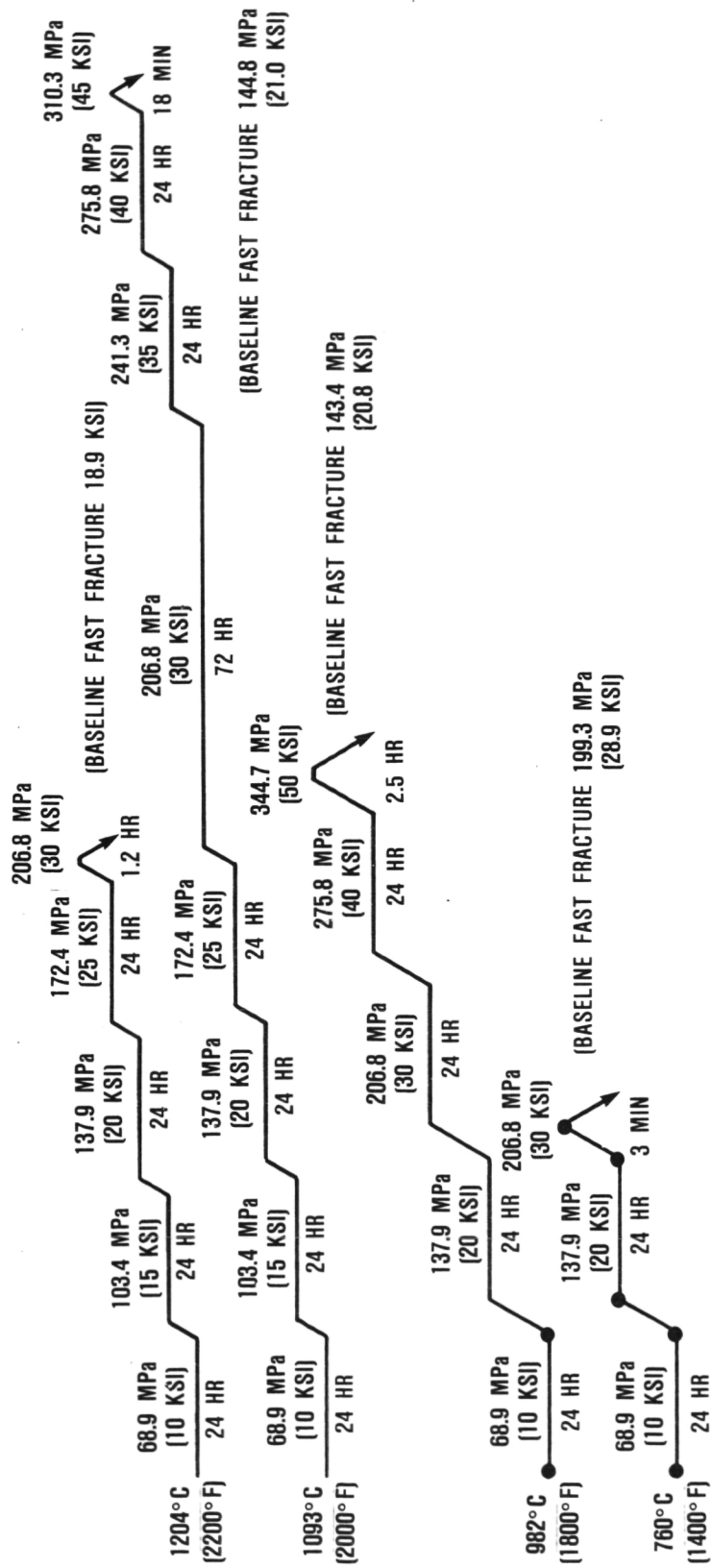


Figure 33. Coors TTZ Stepped Stress Rupture Tests.

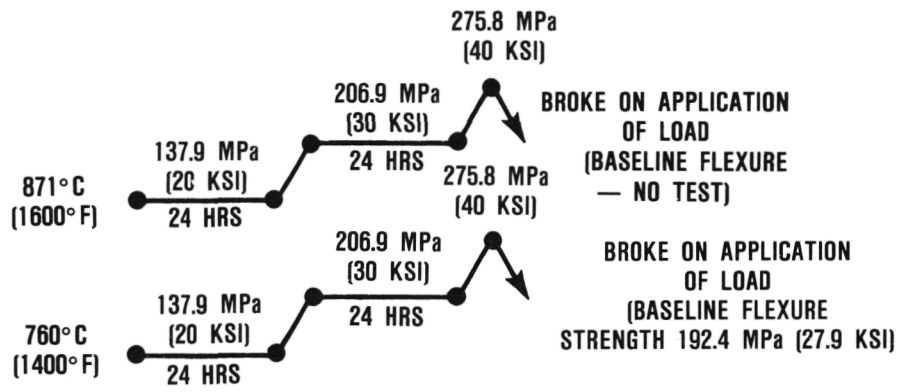


Figure 34. Stepped Stress Rupture of Feldmühle TTZ.

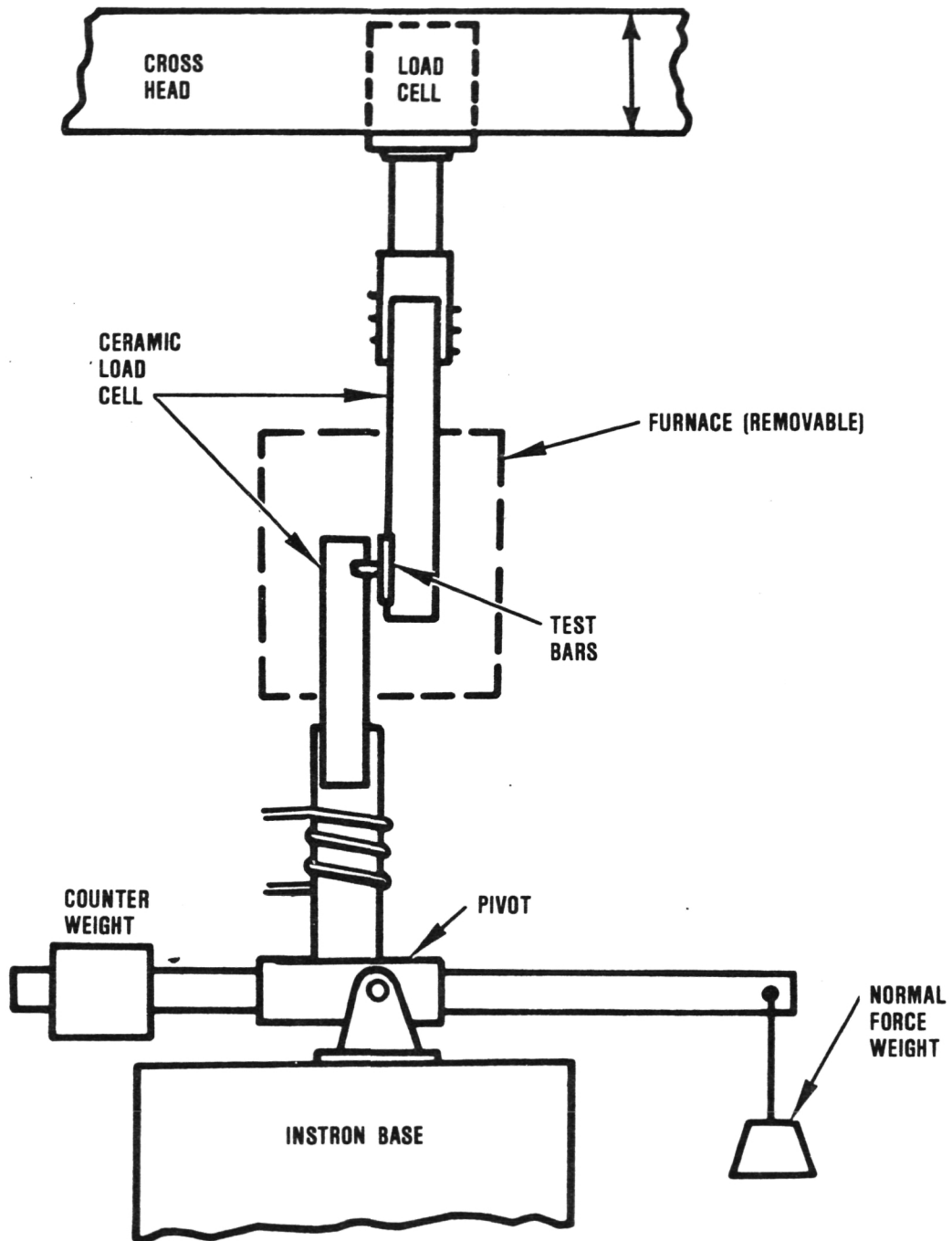
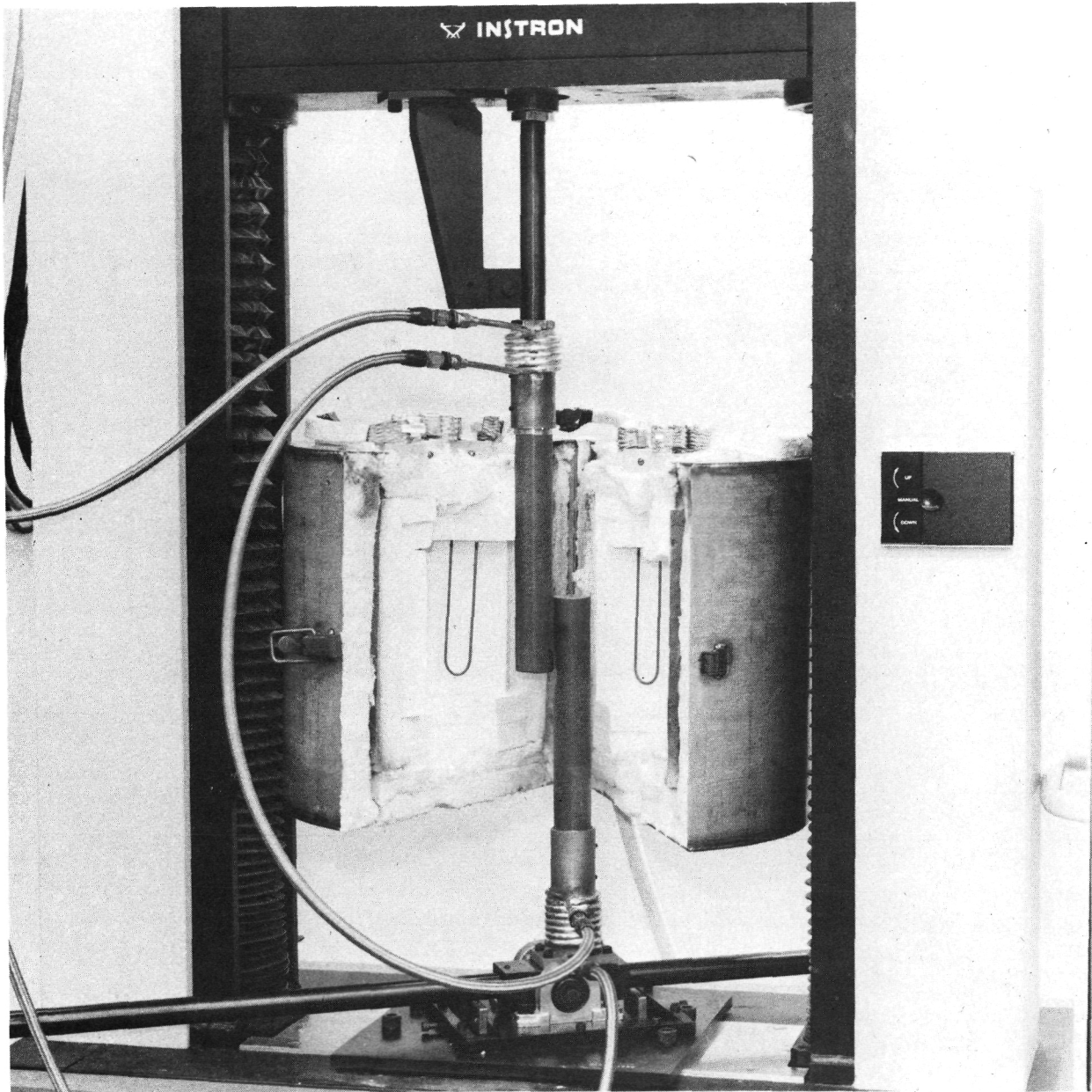


Figure 35. Contact Stress Test Apparatus Schematic.



78424-7

Figure 36. Contact Stress Test Apparatus.

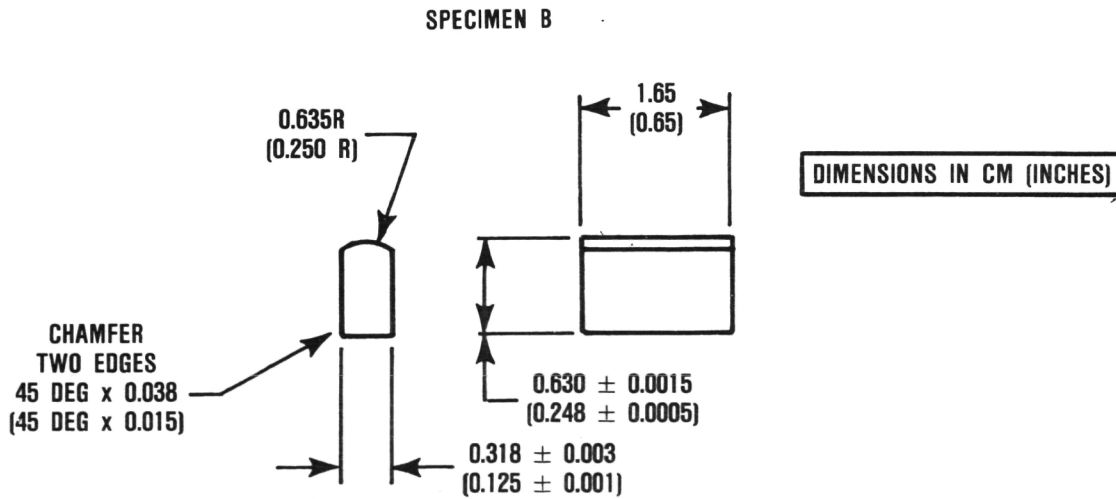
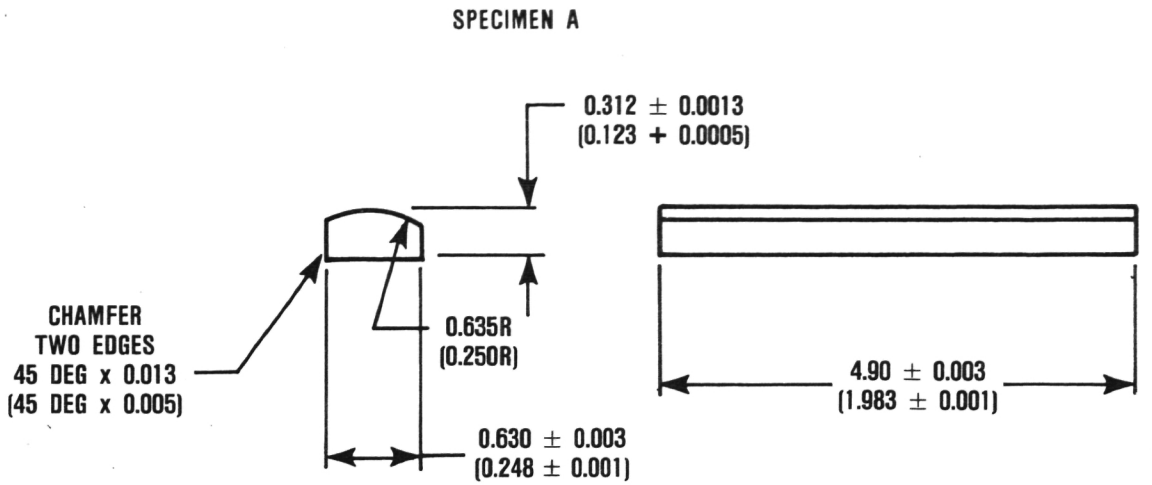


Figure 37. Contact Stress Test Specimens.

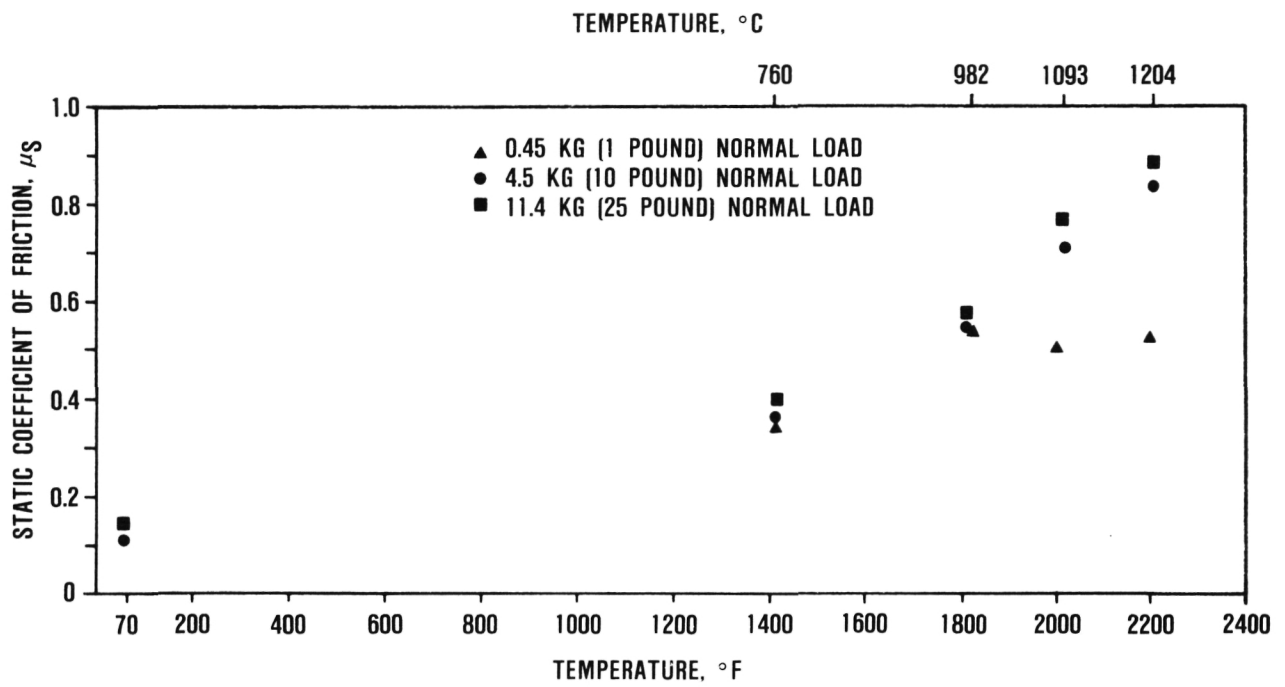


Figure 38. Nilsen TTZ Static Coefficient of Friction.

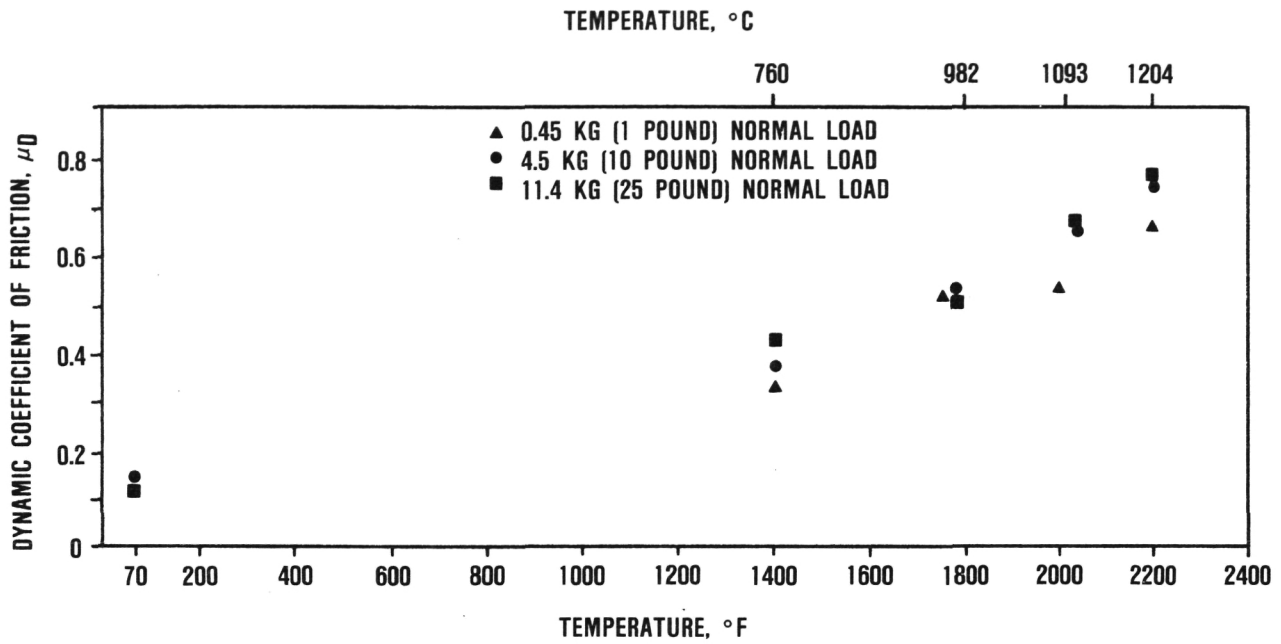
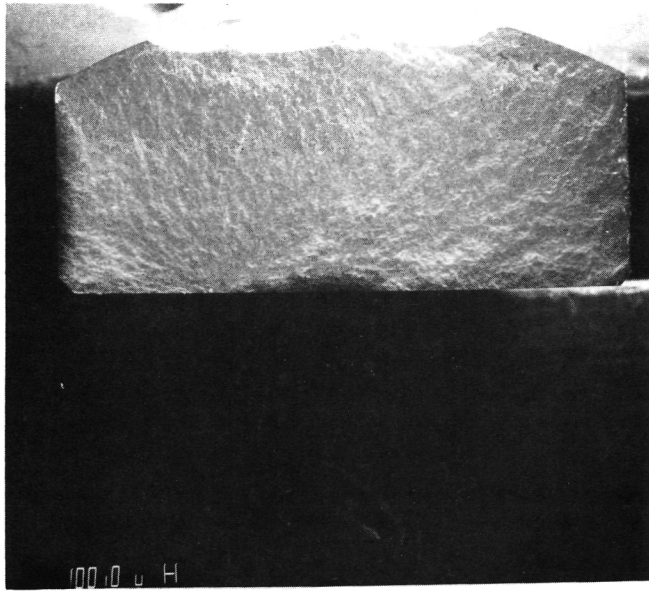


Figure 39. Nilsen TTZ Dynamic Coefficient of Friction.



10x



200x

Figure 40. Nilsen TTZ 760°C (1400°F) 11.4 kg (25-Pound) Normal Contact Load, Specimen 11927.

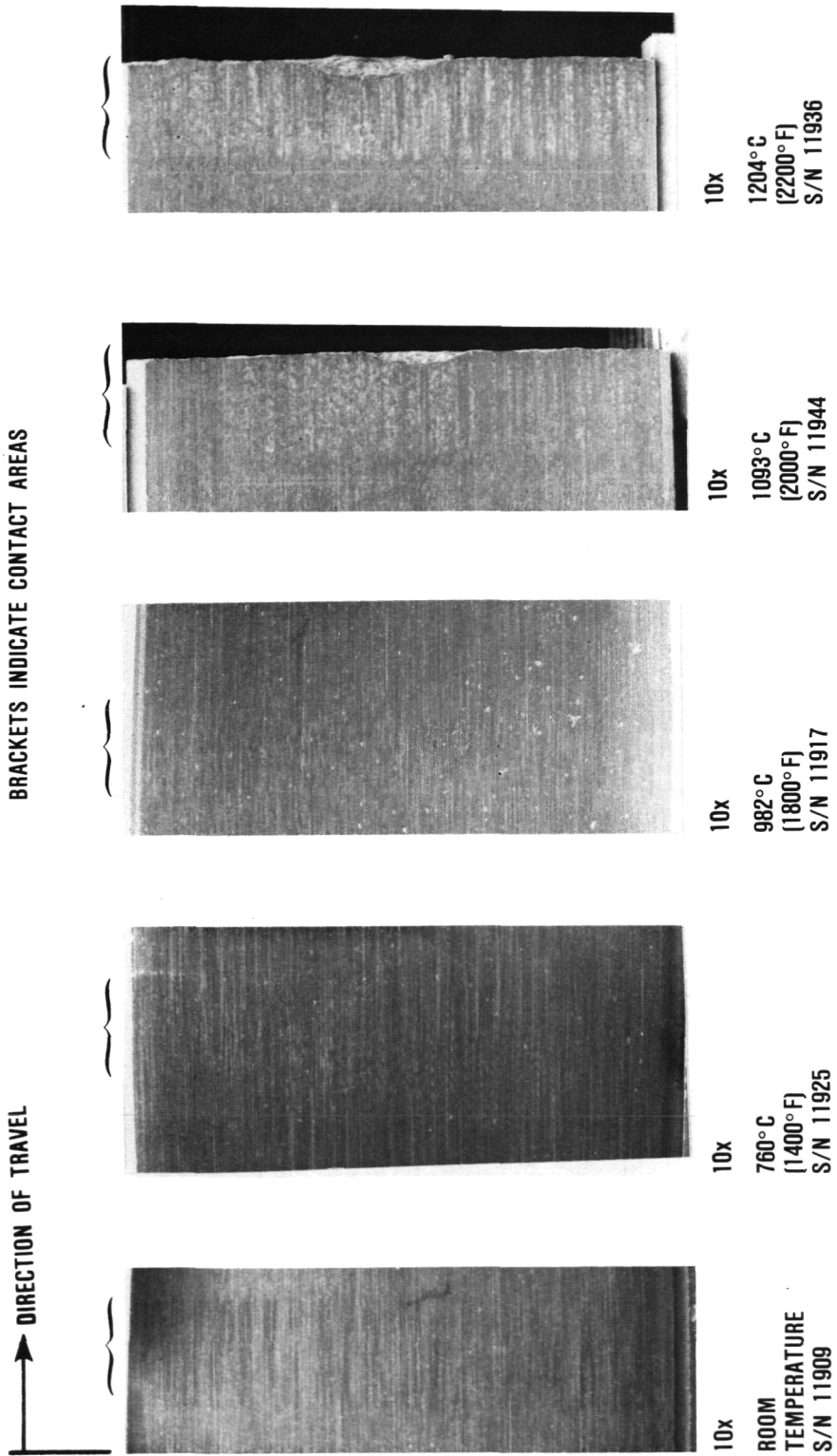


Figure 41. Nilsen TTZ Contact Areas, 11.4 kg (25-Pound) Normal Contact Load.

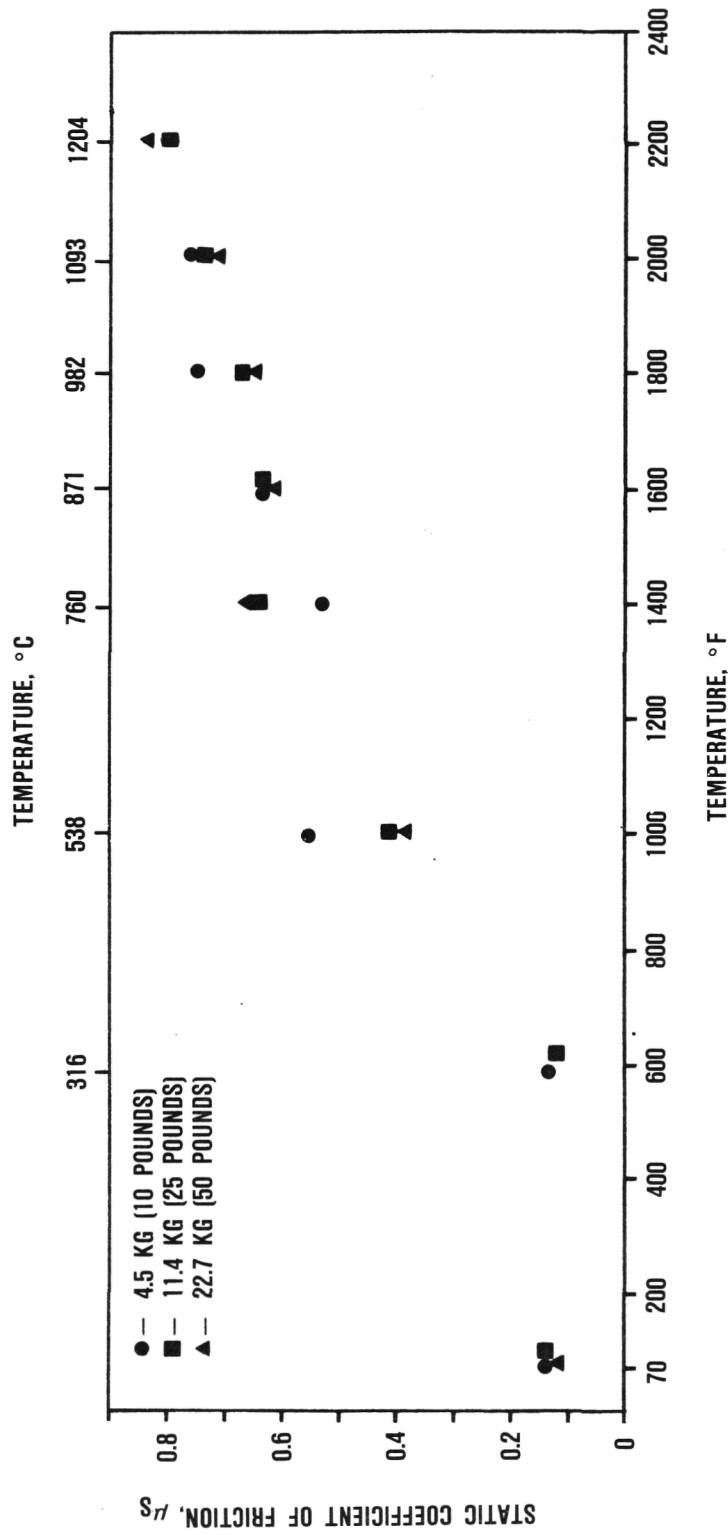


Figure 42. NGK TTZ Static Coefficient of Friction.

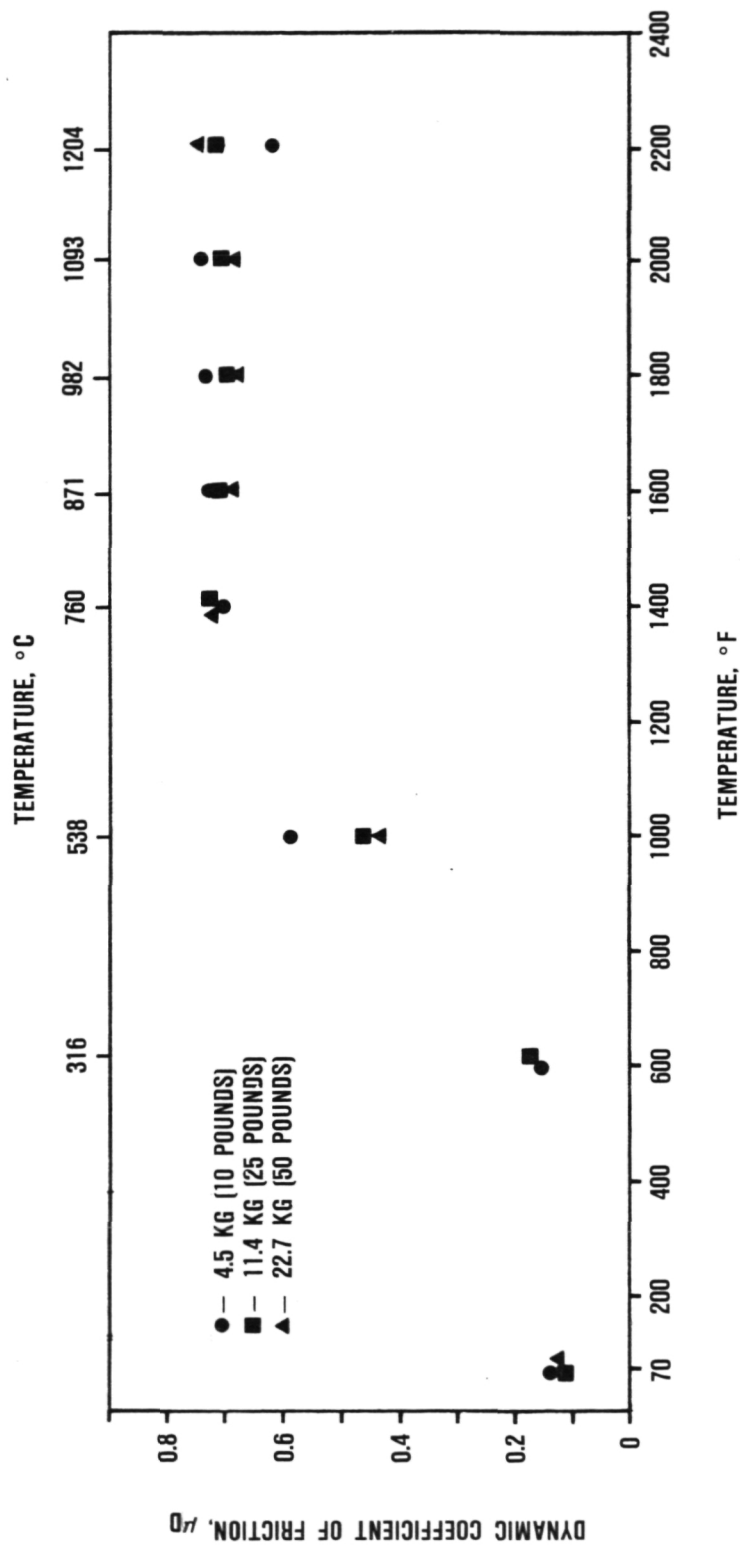


Figure 43. NGK TTZ Dynamic Coefficient of Friction.

MP-89064

DIRECTION OF TRAVEL
↓

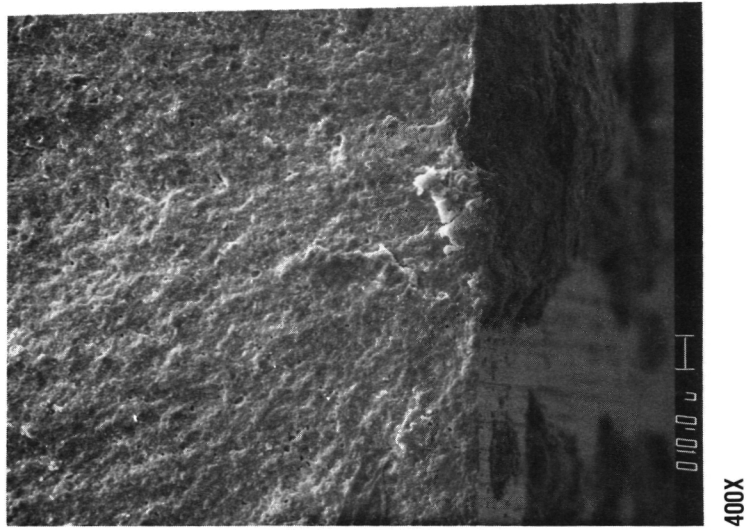
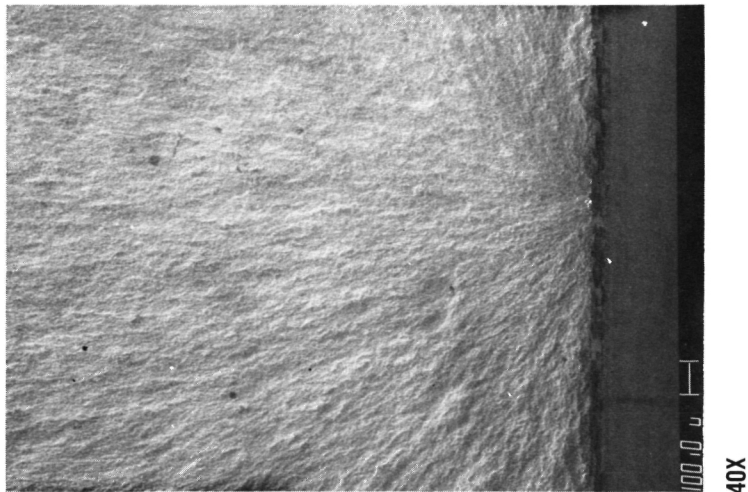
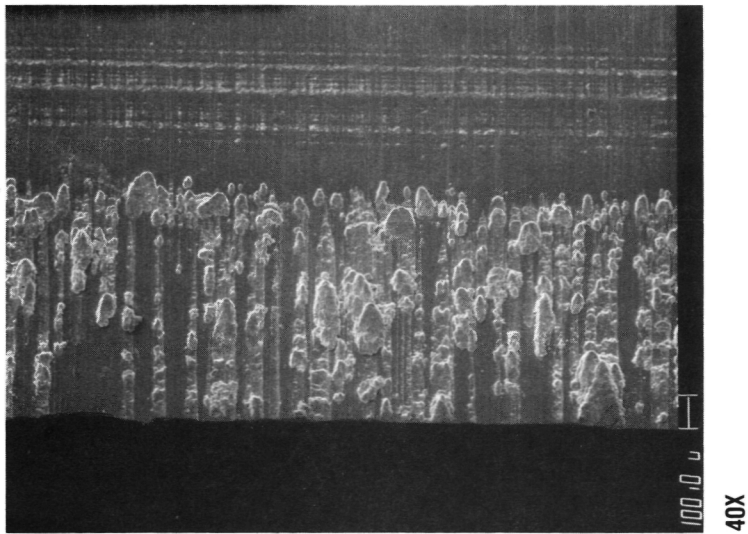


Figure 44. NGK TTZ 1093°C (2000°F) 22.7 kg (50-Pound) Normal Contact Load, Specimen 12365.

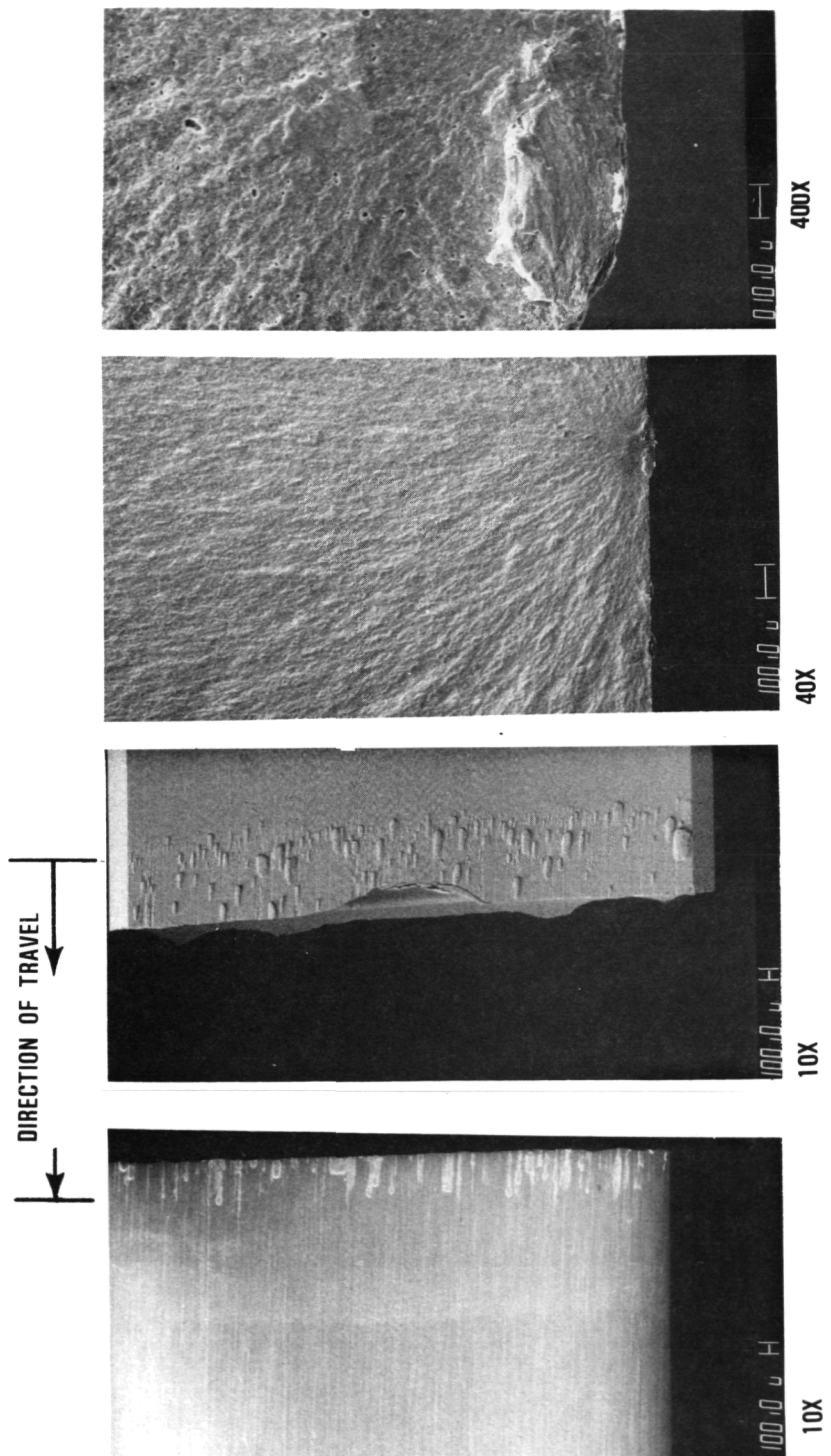
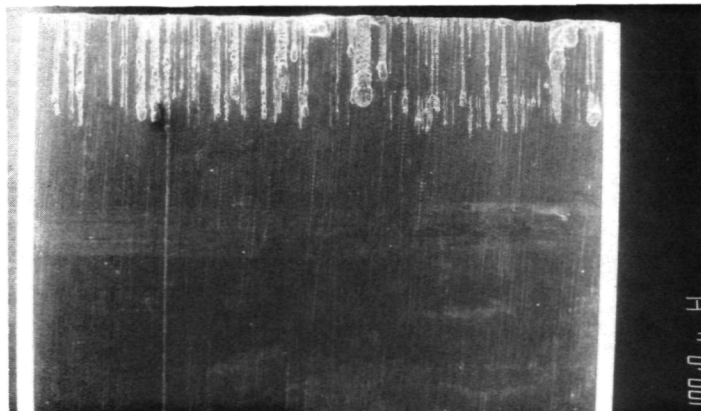


Figure 45. NGK TZ 871°C (1600°F) 22.7 kg (50-Pound) Normal Contact Load, Specimen 12347.

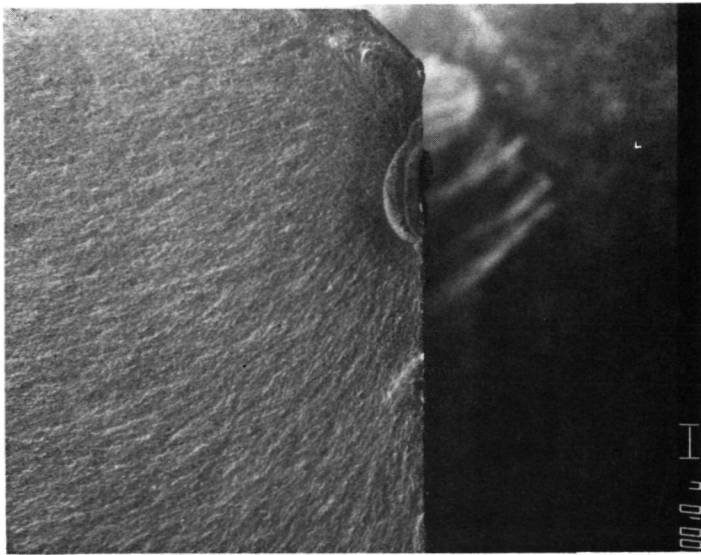
MP-89059

DIRECTION OF TRAVEL



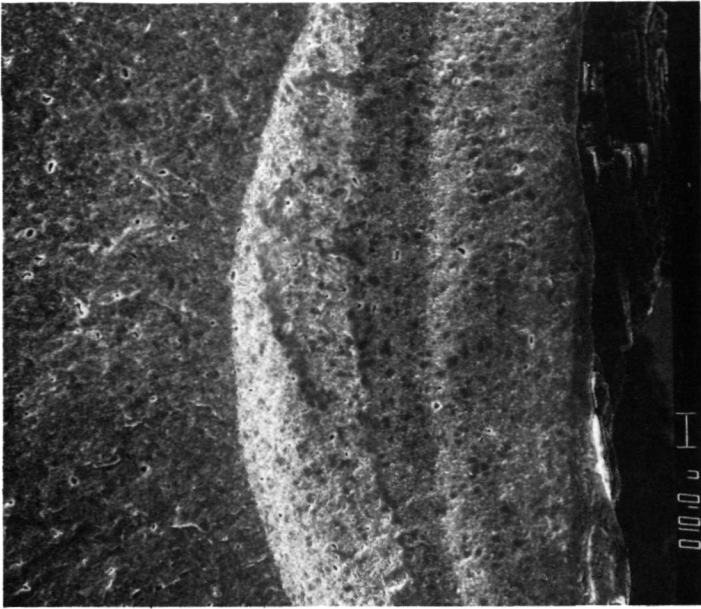
10X

CONTACT AREA



40X

FRACTURE ORIGIN CONTACT INDUCED



400X

Figure 46. NGK TTZ 760°C (1400°F) 22.7 kg (50-Pound) Normal Contact Load, Specimen 12338.

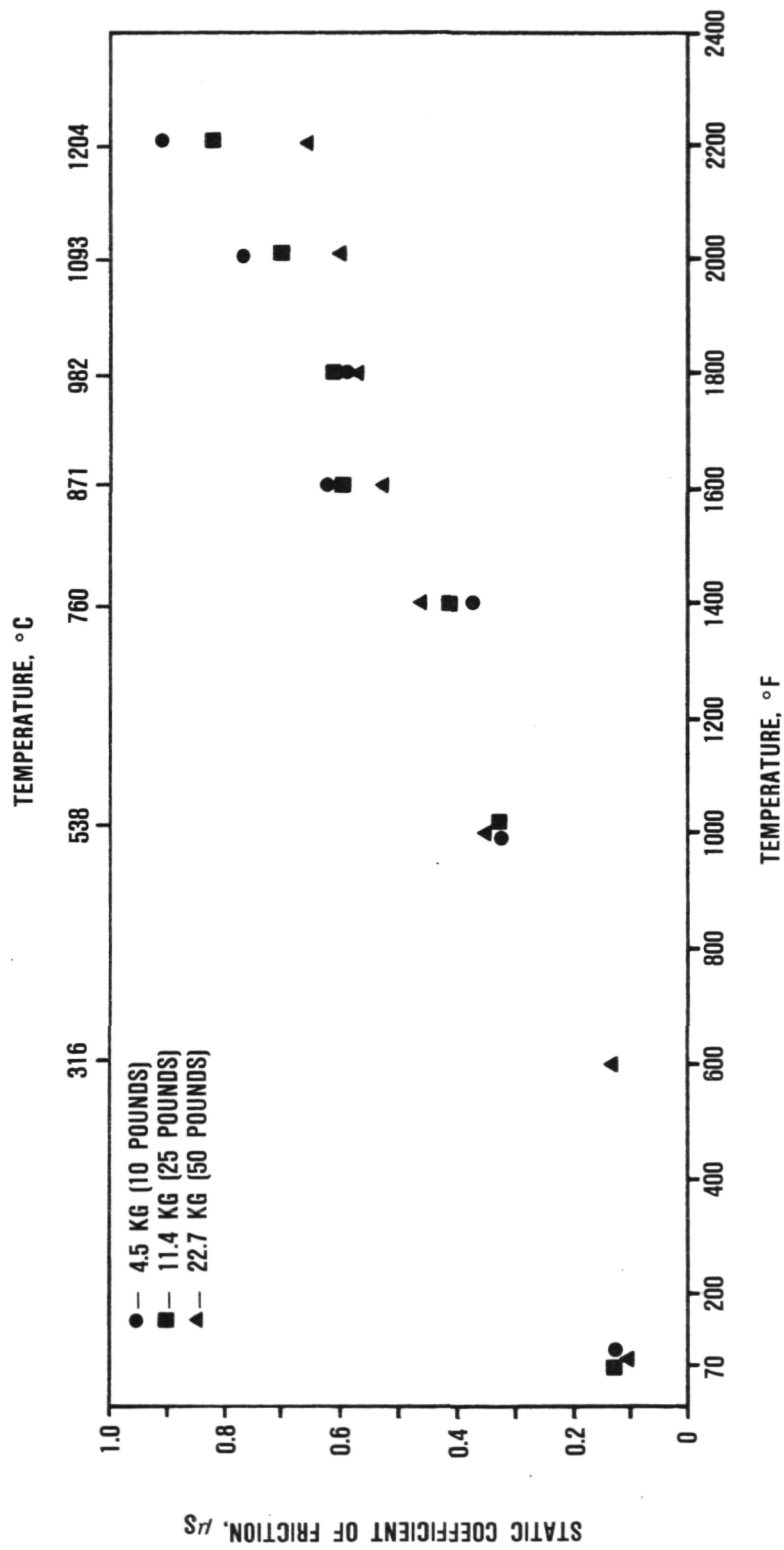


Figure 47. Coors TTZ Static Coefficient of Friction.

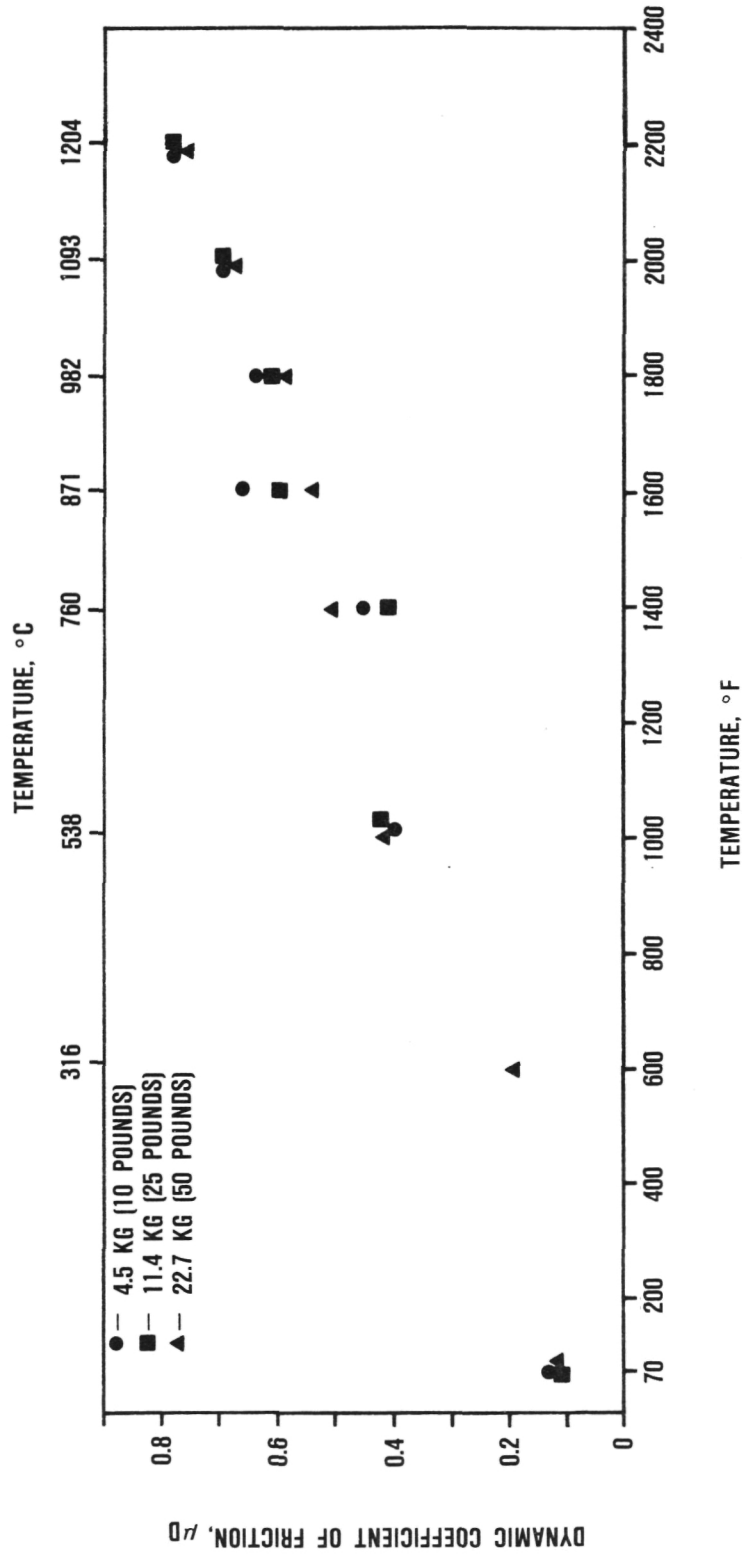


Figure 48. Coors TTZ Dynamic Coefficient of Friction.

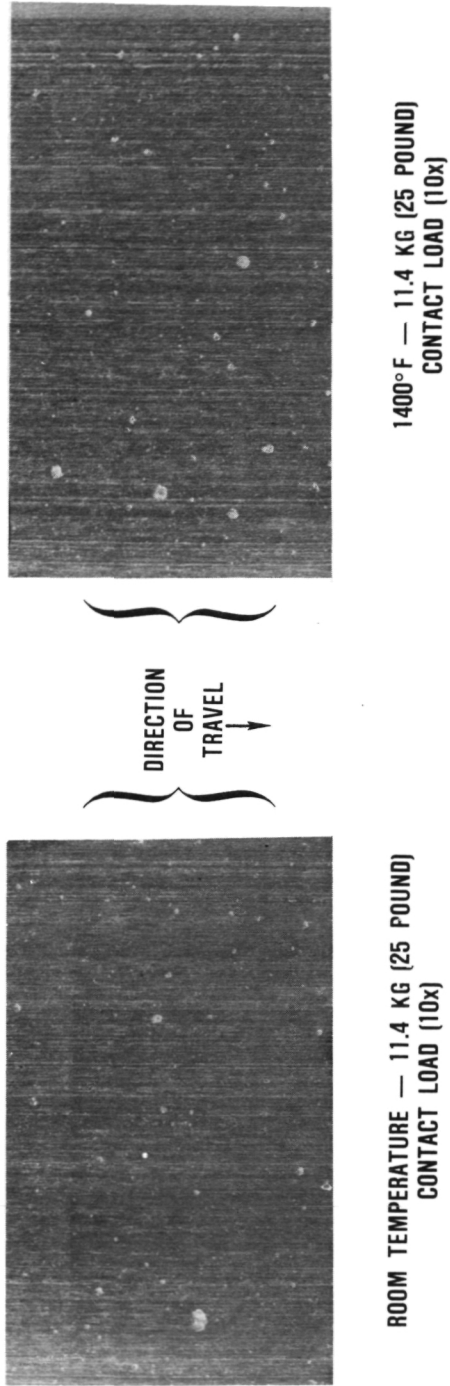
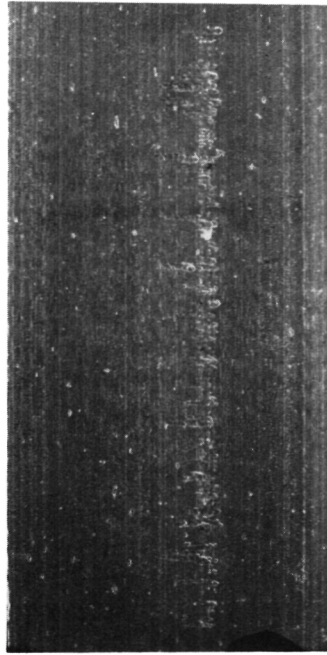
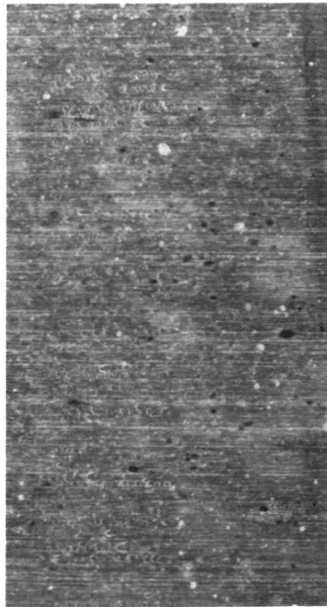


Figure 49. Coors TTZ Contact Area.

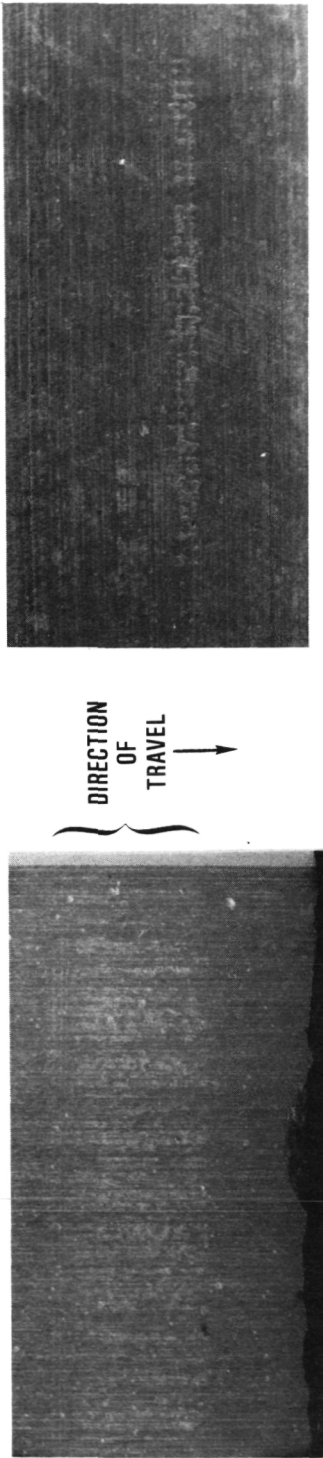


STATIONARY RADIUSED SPECIMEN
CONTACT AREA (10x)



FLAT MOVING SPECIMEN
(10x)

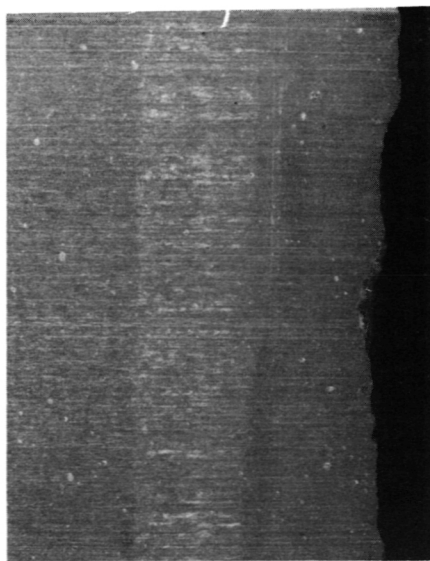
Figure 50. Coors TTZ 9820C (1800°F) 11.4 kg (25-Pound) Normal Contact Area.



FLAT MOVING SPECIMEN
(10x)

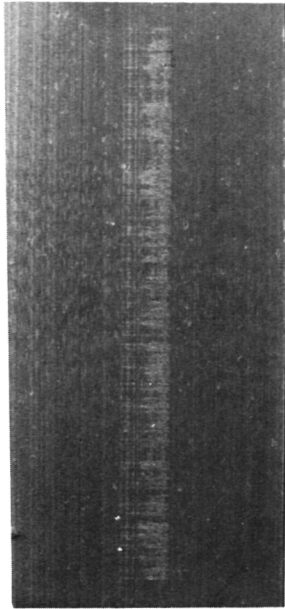
STATIONARY RADIUSED SPECIMEN
CONTACT AREA (10x)

Figure 51. Coors TTZ 10930C (2000°F) 11.4 kg (25-Pound) Normal Contact Area.



FLAT MOVING SPECIMEN
(10x)

}
DIRECTION
OF
TRAVEL
↓



STATIONARY RADIUSED SPECIMEN
CONTACT AREA (10x)

Figure 52. Coors TTZ 12040C (2200°F) 11.4 kg (25-Pound) Normal Contact Area.

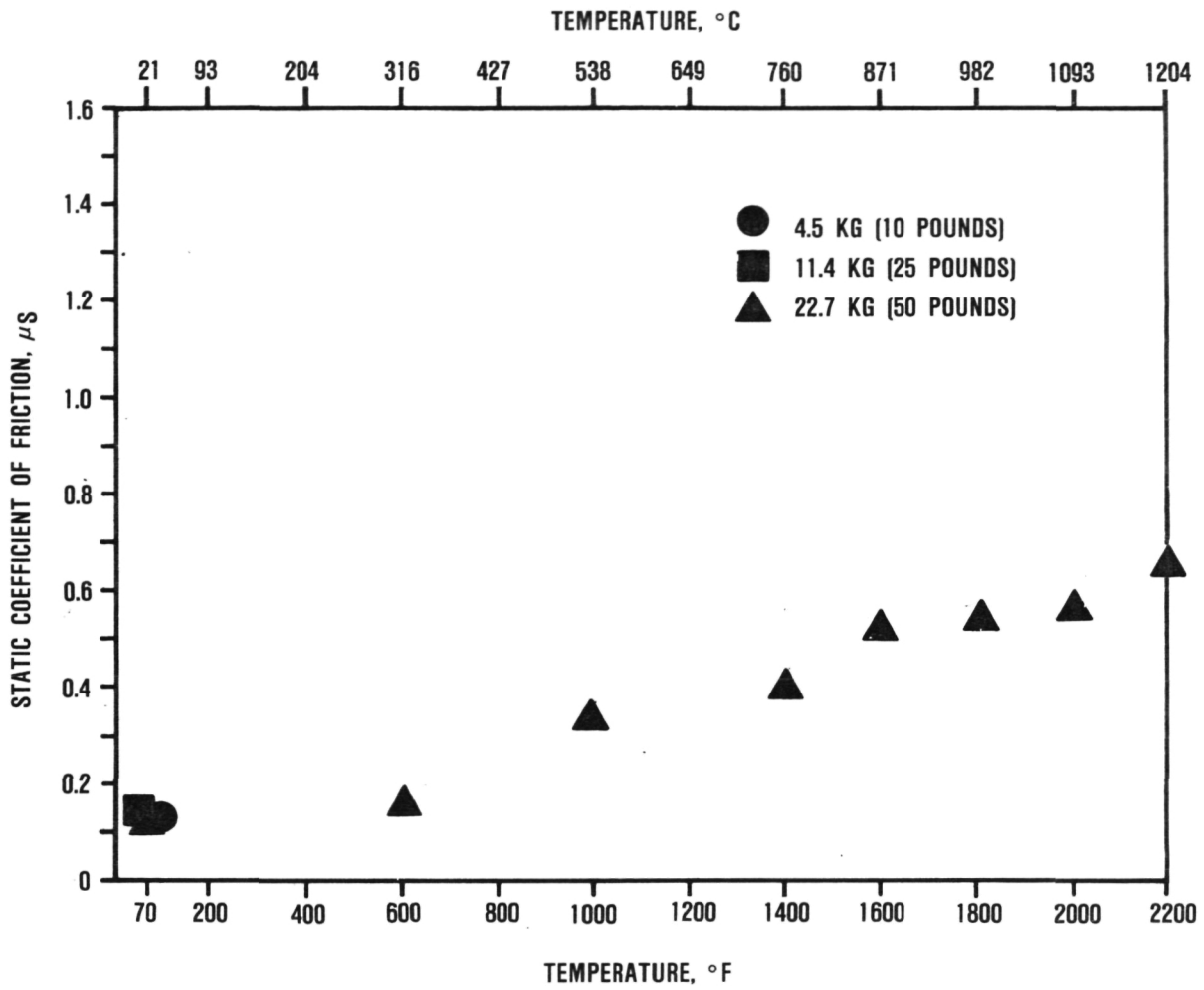


Figure 53. Feldmühle TTZ Static Coefficient of Friction.

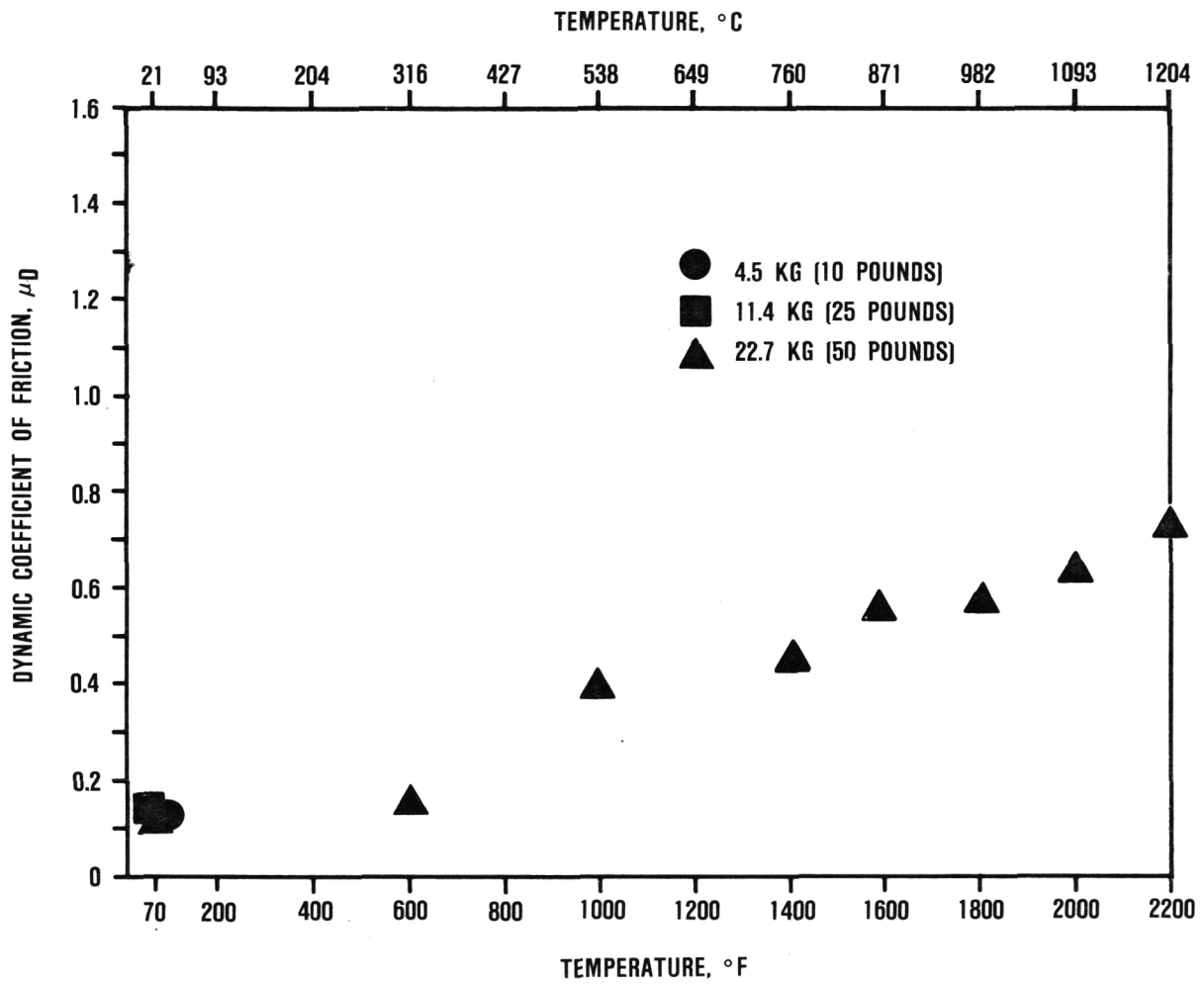


Figure 54. Feldmühle TTZ Dynamic Coefficient of Friction.

CONTACT AREAS AND DIRECTION OF TRAVEL

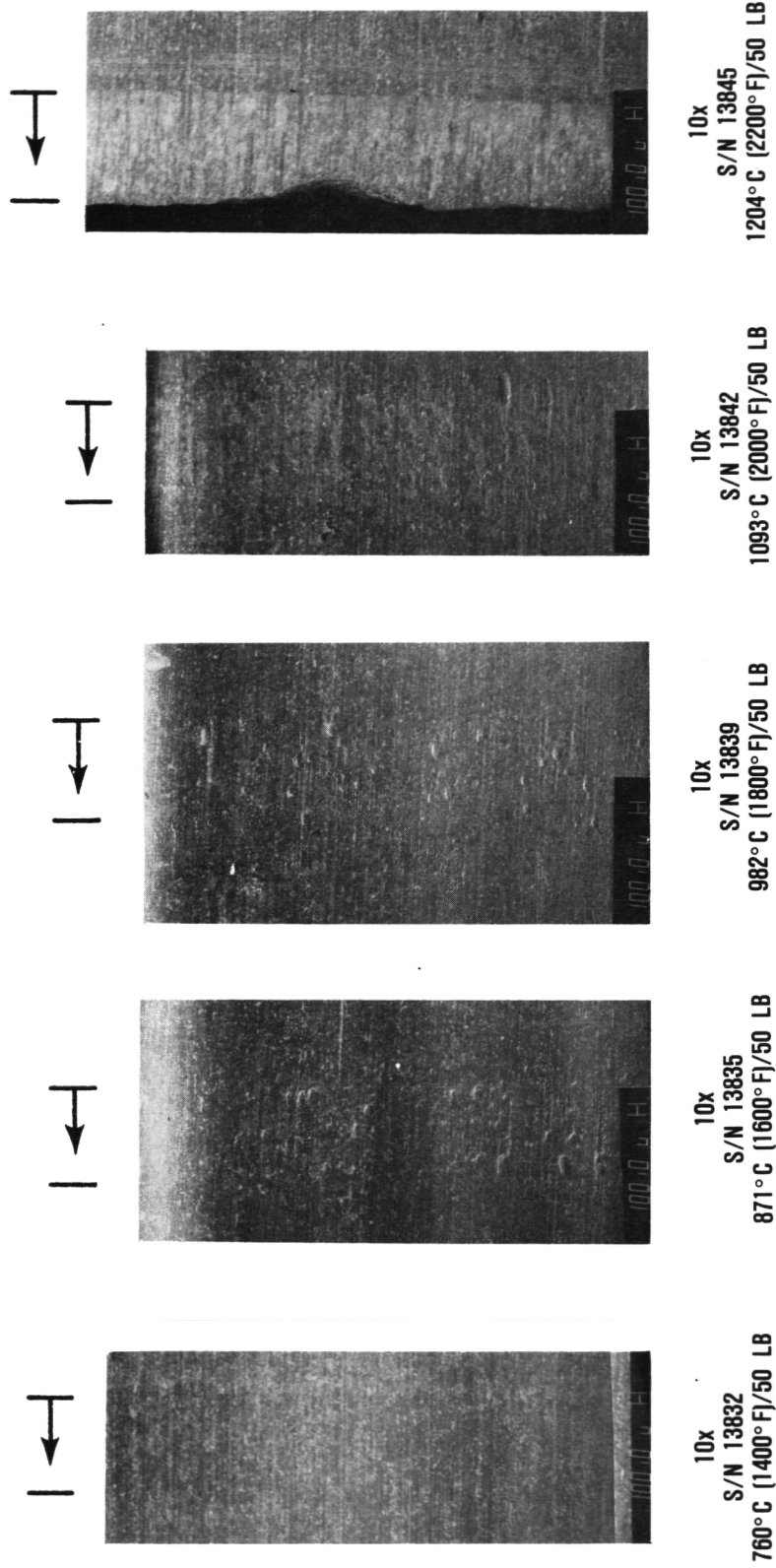
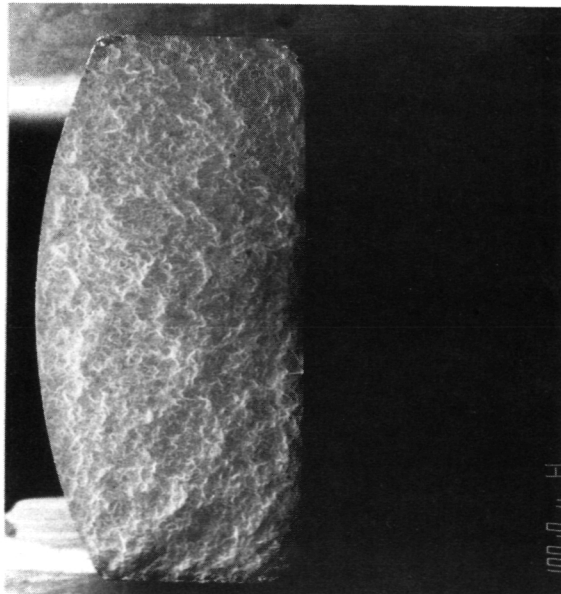
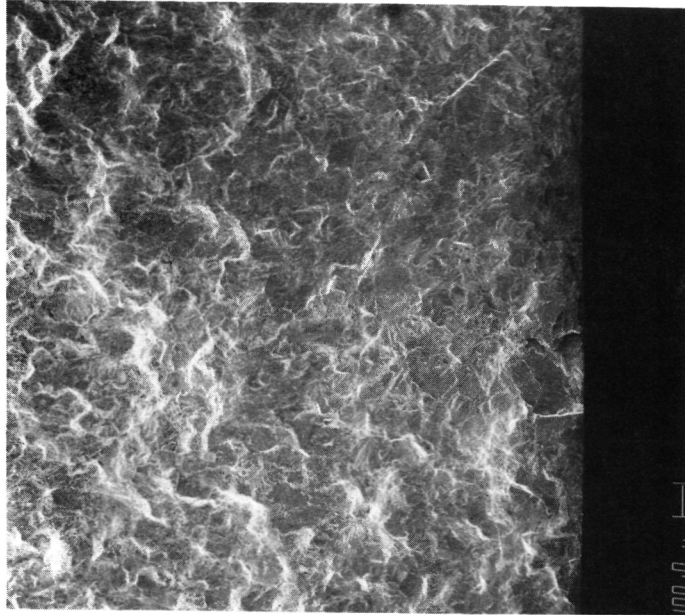


Figure 55. Feldmühle TTZ Contact Areas.



10x



40x

S/N 13845

Figure 56. Feldmühle TTZ Contact Stress Induced Fracture
Origin 1204°C (2200°F) 150-Pound Contact Load.

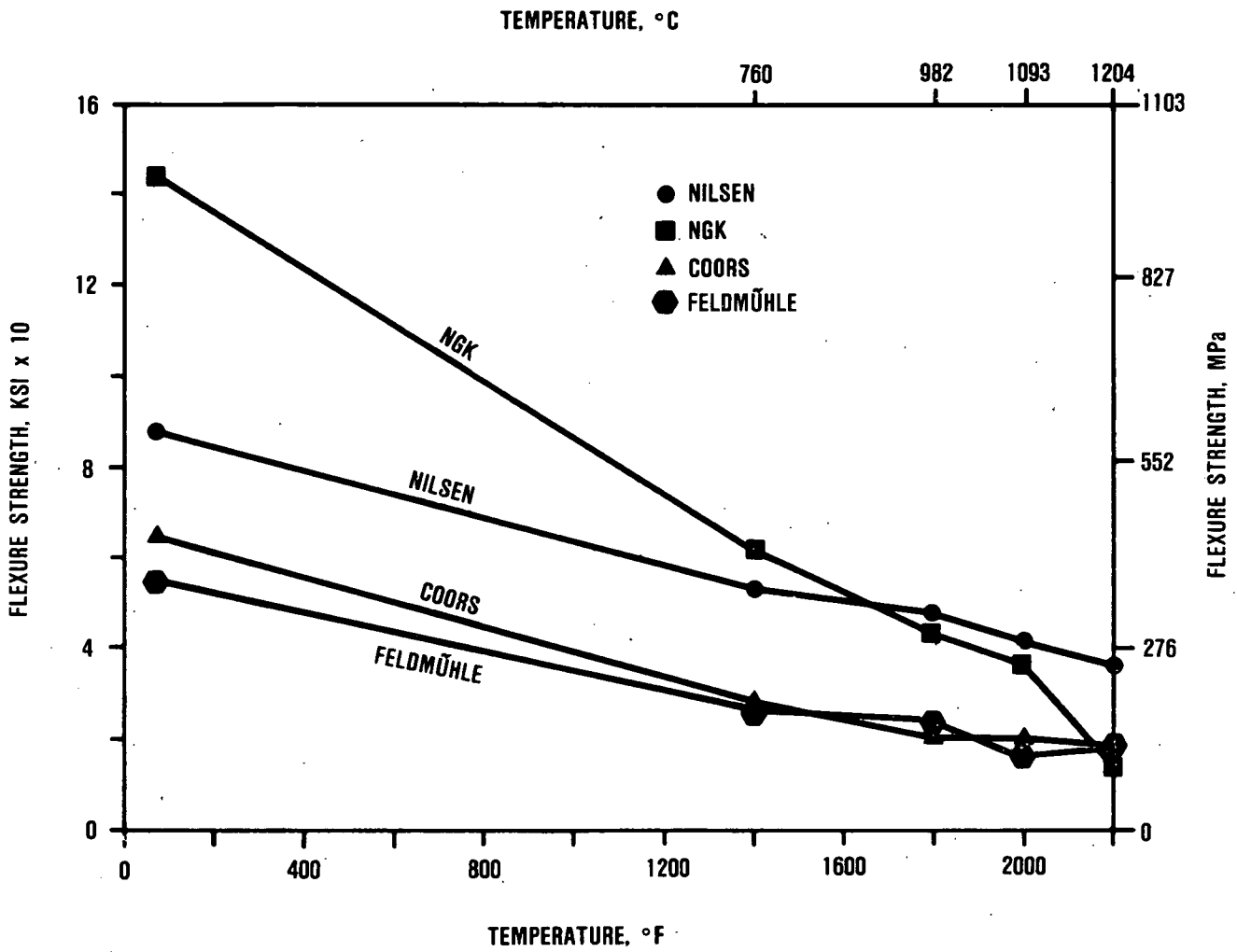


Figure 57. Comparison of Baseline TTZ Flexure Strength.

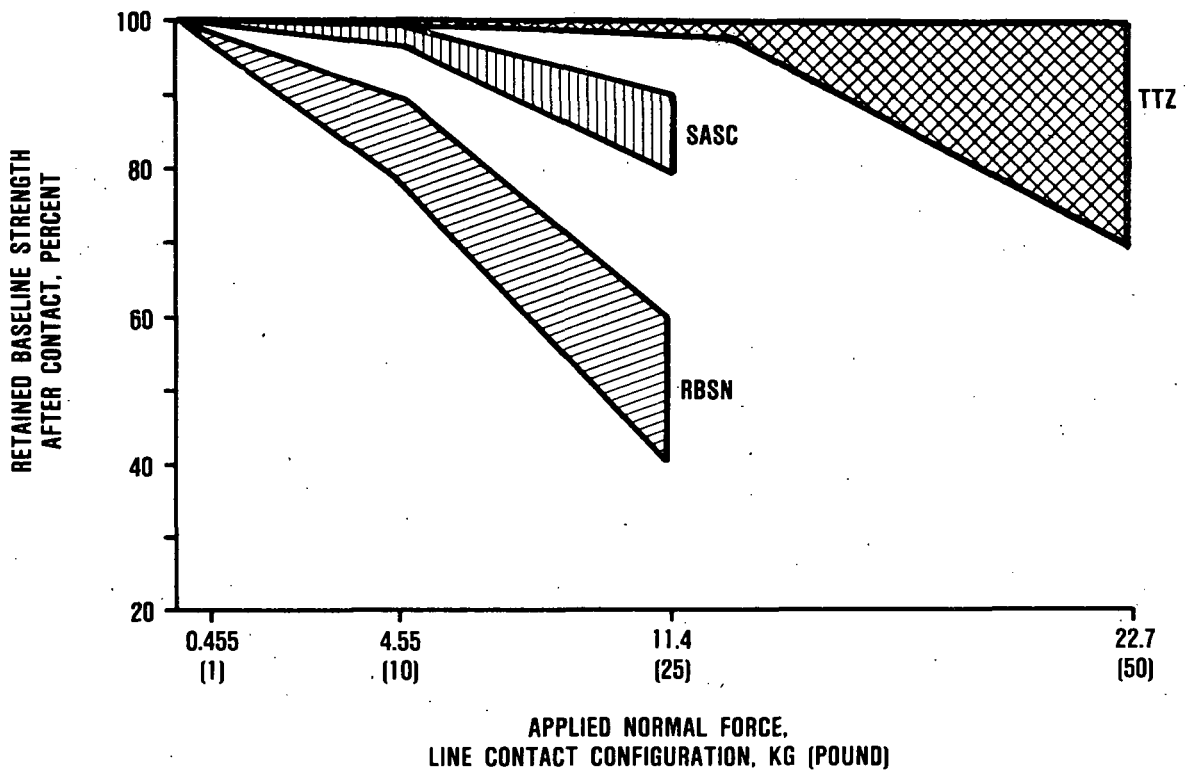


Figure 58. Relative Contact Stress Resistance of TTZ, SASC and RBSN.

REFERENCES

1. Marmach, M., D. Servent, R.H.J. Hannink, M.J. Murray, M.V. Swain: Toughened PSZ Ceramics - Their Role as Advanced Engine Components. SAE Technical Paper 830318, 1983.
2. Woods, M.E., I. Oda: PSZ Ceramics for Adiabatic Engine Components. SAE Technical Paper 820429, 1982.
3. Richerson, D.W., K.M. Johansen: Ceramic Gas Turbine Engine Demonstration Program. Final Report, DARPA Contract N00024-76-C-5352, May 1982.
4. Smyth, J.R.: Contact Stress Analysis of Elastic Visioelastic Interface Conditions. Final Report, ONR Contract N00014-80-C-00870, January 1984.
5. Finger, D.G.: Contact Stress Analysis of Ceramic-to-Metal Interfaces. Final Report, ONR Contract N00014-78-C-0547, 1979.
6. Smith, J.O., Chang Keng Liu: Stresses Due to Tangential and Normal Loads on an Elastic Solid with Application to Some Contact Stress Problems. J. Appl. Mech., 20 [2] 157-166 (1953).
7. Boresi, A.P., O.M. Sidebottom, F.B. Seely, J.O. Smith. pp. 581-627 in Advanced Mechanics of Materials, 3rd Ed., Wiley, New York, 1978.
8. Richerson, D.W., W.D. Carruthers, L.J. Lindberg: Contact Stress and Coefficient of Friction Effects on Ceramic Interfaces. pp. 661-76 in Surfaces and Interfaces in Ceramic and Ceramic-Metal Systems, (J. Pask and A. Evans, eds.) Plenum, New York, 1981.
9. Smyth, J.R., D.W. Richerson: High Temperature Dynamic-Contact Behavior of Sintered Alpha Silicon Carbide. Ceramic Engineering and Science Proceedings, 4 [7-8] (1983).
10. Richerson, D.W., L.J. Lindberg, W.D. Carruthers, J. Dahn: Contact Stress Effects on Si_3N_4 and SiC Interfaces. Ceramic Engineering and Science Proceedings, 2 [7-8] 578-588 (1981).
11. Smith, D.K., C.F. Cline: Verification of Existence of Cubic Zirconia at High Temperature. J. Am. Ceramic Soc., 45 [5] 249-50 (1962).
12. Teufer, G.: Crystal Structure of Tetragonal ZrO_2 . Acta Crystallogr., 15 [11] 1187 (1962).

13. McCullough J.D., K.N. Trueblood: Crystal Structure of Baddeleyite (Monoclinic ZrO_2). Acta Crystallogr., 12 [7] 507-11 (1959).
14. Smith, D.K., H.W. Newkirk: Crystal Structure of Baddeleyite (Monoclinic ZrO_2) and its Relation to the Ploymorphism of ZrO_2 . Acta Crystallogr., 18 [6] 983-91 (1965).
15. Ruff, O., F. Ebert: Refractory Ceramics: 1, The Forms of Zirconium Dioxide. Z. Anorg. Allg. Chem., 180 [1] 19-41 (1929).
16. Wolten, G.M.: Diffusionless Phase Transformations in Zirconia and Hafnia. J. Am. Ceramic Soc., 46 [9] 418-22 (1963).
17. Porter, D.L., A.H. Heuer: Microstructural Development in MgO - Partially Stabilized Zirconia (Mg-PSZ). J. Am. Ceramic Soc., 62 [5-6] 298-205 (1979).
18. Green, D.J., D.R. Maki, P.S. Nicholson: Microstructural Development in Partially Stabilized ZrO_2 in the System CaO- ZrO_2 . J. Am. Ceramic Soc., 57 [3] 136-39 (1974).
19. Garvie, R.C., P.S. Nicholson: Structure and Thermomechanical Properties of Partially Stabilized Zirconia in the CaO- ZrO_2 System. J. Am Ceramic Soc., 55 [3] 152-57 (1972).
20. Bansal, G.K., A.H. Heuer: Precipitation in Partially Stabilized Zirconia. J. Am. Ceramic Soc., 58 [5-6] 235-38 (1975).
21. Garvie, R.C., R.H. Hannink, R.T. Pascoe: Ceramic Steel? Nature (London), 258, [5537] 703-704 (1975).
22. Larsen, R.C., J.W. Adams: Long-Term Stability and Properties of Zirconia Ceramics for Heavy Duty Diesel Engine Components. Monthly Report, NASA Contract DEN3-305, January 1984.
23. Schioler, L.J., G.D. Quinn, R.N. Katz: Time-Temperature Dependence of the Strength of Commercial Zirconia Ceramics. Proceedings of the 21st Automotive Technology Development Contractors Coordination Meeting, Dearborn, MI, November 1983.
24. Kingery, W.D., H.K. Bowen, D.R. Uhlmann: pp 794-95 in Introduction to Ceramics, 2nd Ed., Wiley, New York, 1976.

1. Report No. NASA CR-174728		2. Government Accession No.		3. Recipient's Catalog No.	
4. Title and Subtitle HIGH TEMPERATURE CERAMIC INTERFACE STUDY				5. Report Date August 1984	
				6. Performing Organization Code	
7. Author(s) Laura J. Lindberg				8. Performing Organization Report No. 31-5738	
				10. Work Unit No.	
9. Performing Organization Name and Address Garrett Turbine Engine Company P.O. Box 5217 Phoenix, Arizona 85010				11. Contract or Grant No. DEN3-324	
				13. Type of Report and Period Covered Contractor Report	
12. Sponsoring Agency Name and Address U.S. Department of Energy Office of Vehicle and Engine R&D Washington, D.C. 20545				14. Sponsoring Agency Code DOE/NASA/0324-1	
15. Supplementary Notes Final Report. Prepared under Interagency Agreement DE-AI01-80CS50194. Project Manager, H. Davison, Energy Technology Division, NASA Lewis Research Center, Cleveland, Ohio 44135					
16. Abstract <p>Monolithic SiC and Si₃N₄ are susceptible to contact stress damage at static and sliding interfaces. Transformation-toughened zirconia (TTZ) was evaluated under sliding contact conditions to determine if the higher material fracture toughness would reduce the susceptibility to contact stress damage.</p> <p>Contact stress tests were conducted on four commercially available TTZ materials at normal loads ranging from 0.455 to 22.7 kg (1 to 50 pounds) at temperatures ranging from room temperature to 1204°C (2200°F). Static and dynamic friction were measured as a function of temperature.</p> <p>Flexural strength measurements after these tests determined that the contact stress exposure did not reduce the strength of TTZ at contact loads of 0.455, 4.55, and 11.3 kg (1, 10, and 25 pounds). Prior testing with the lower toughness SiC and Si₃N₄ materials resulted in a substantial strength reduction at loads of only 4.55 and 11.3 kg (10 and 25 pounds). An increase in material toughness appears to improve ceramic material resistance to contact stress damage.</p> <p>Baseline material flexure strength was established and the stress rupture capability of TTZ was evaluated. Stress rupture tests have determined that TTZ materials are susceptible to deformation due to creep and that aging of TTZ materials at elevated temperatures results in a reduction of material strength.</p>					
17. Key Words (Suggested by Author(s)) Heavy duty diesel engine; Ceramic materials; Ceramic components			18. Distribution Statement Unclassified - Unlimited STAR Category 85 DOE Category UC-96		
19. Security Classif. (of this report) Unclassified		20. Security Classif. (of this page) Unclassified		21. No. of pages 113	22. Price*